PROSPECTS OF GRAVITATIONAL-WAVE ASTEROSEISMOLOGY WITH BINARY NEUTRON STAR MERGERS

NIKOLAOS STERGIOULAS

DEPARTMENT OF PHYSICS
ARISTOTLE UNIVERSITY OF THESSALONIKI

Funded by the Horizon 2020 Framework Programme
of the European Union

Hirschegg, January 14, 2020

GW170817 Binary Neutron Star (BNS) merger

GW + EM follow up

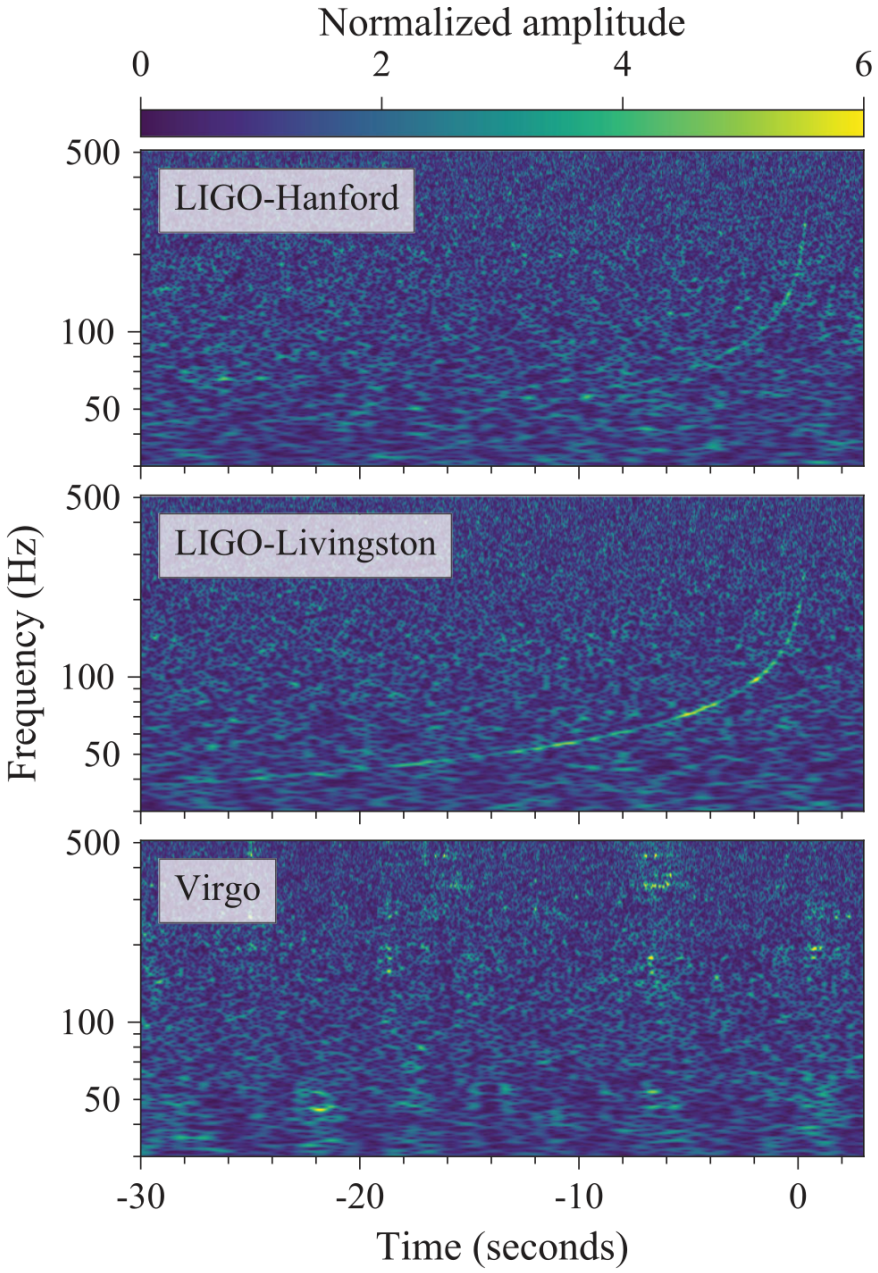

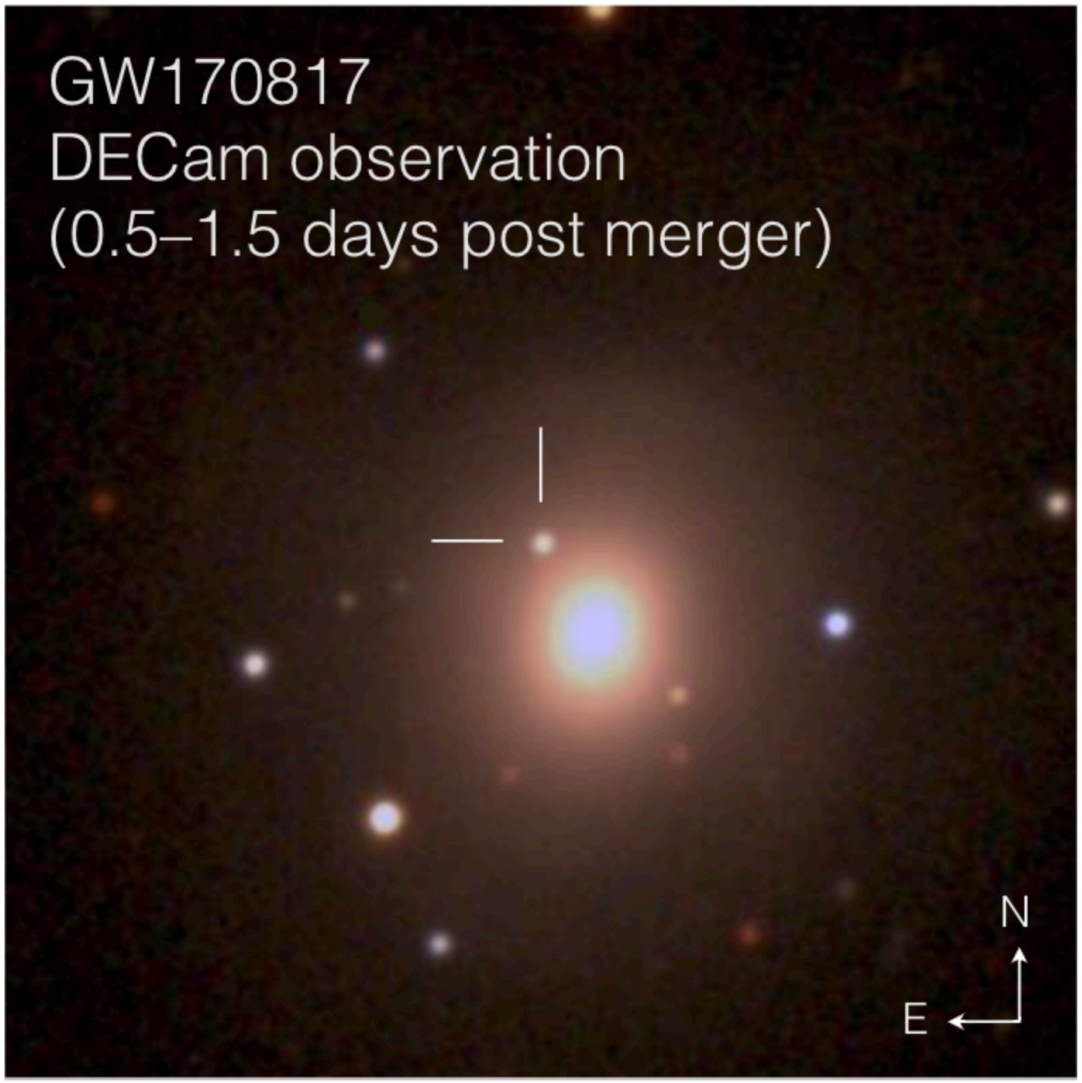

EOS Constraints through BNS mergers

1) GW @ inspiral (already achieved with GW170817)

2) GW @ post-merger (expected with A+ and 3G detectors)

3) EM emission (e.g. first results by NICER)

4) GW + EM (multimessenger) (minimum radius constraint)

5) all of the above + laboratory experiments

Λ through GW @ Inspiral

For NS binaries with individual masses around $1.4M_\odot$, the dimensionless tidal deformability Λ could be realistically determined with about **10% accuracy** by combining information from about 20 – 100 sources.

Additional effects (may become relevant for next-generation detectors)

1) tidal excitations of *resonant modes*

2) gravitomagnetic excitations of resonant modes

3) resonant shattering of the NS crust by tides

4) nonlinear tidal effects

BNS Mergers in O3 LVC Run

So far: 1 detection + 4 candidate events

S191213g	BNS (77%), Terrestrial (23%)	Dec. 13, 2019 04:34:08 UTC	GCN Circulars Notices | VOE	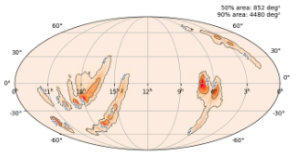	1.1197 per year
S190910h	BNS (61%), Terrestrial (39%)	Sept. 10, 2019 08:29:58 UTC	GCN Circulars Notices | VOE	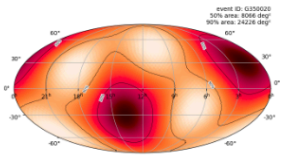	1.1312 per year
S190901ap	BNS (86%), Terrestrial (14%)	Sept. 1, 2019 23:31:01 UTC	GCN Circulars Notices | VOE	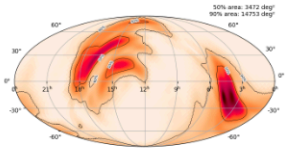	1 per 4.5093 years
S190426c	BNS (49%), MassGap (24%), Terrestrial (14%), NSBH (13%)	April 26, 2019 15:21:55 UTC	GCN Circulars Notices | VOE	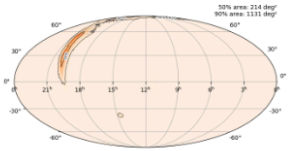	1 per 1.6276 years
GW190425	BNS (>99%)	April 25, 2019 08:18:05 UTC	GCN Circulars Notices | VOE	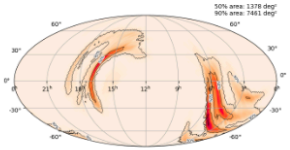	1 per 69834 years

Constraints from the inspiral of GW170817

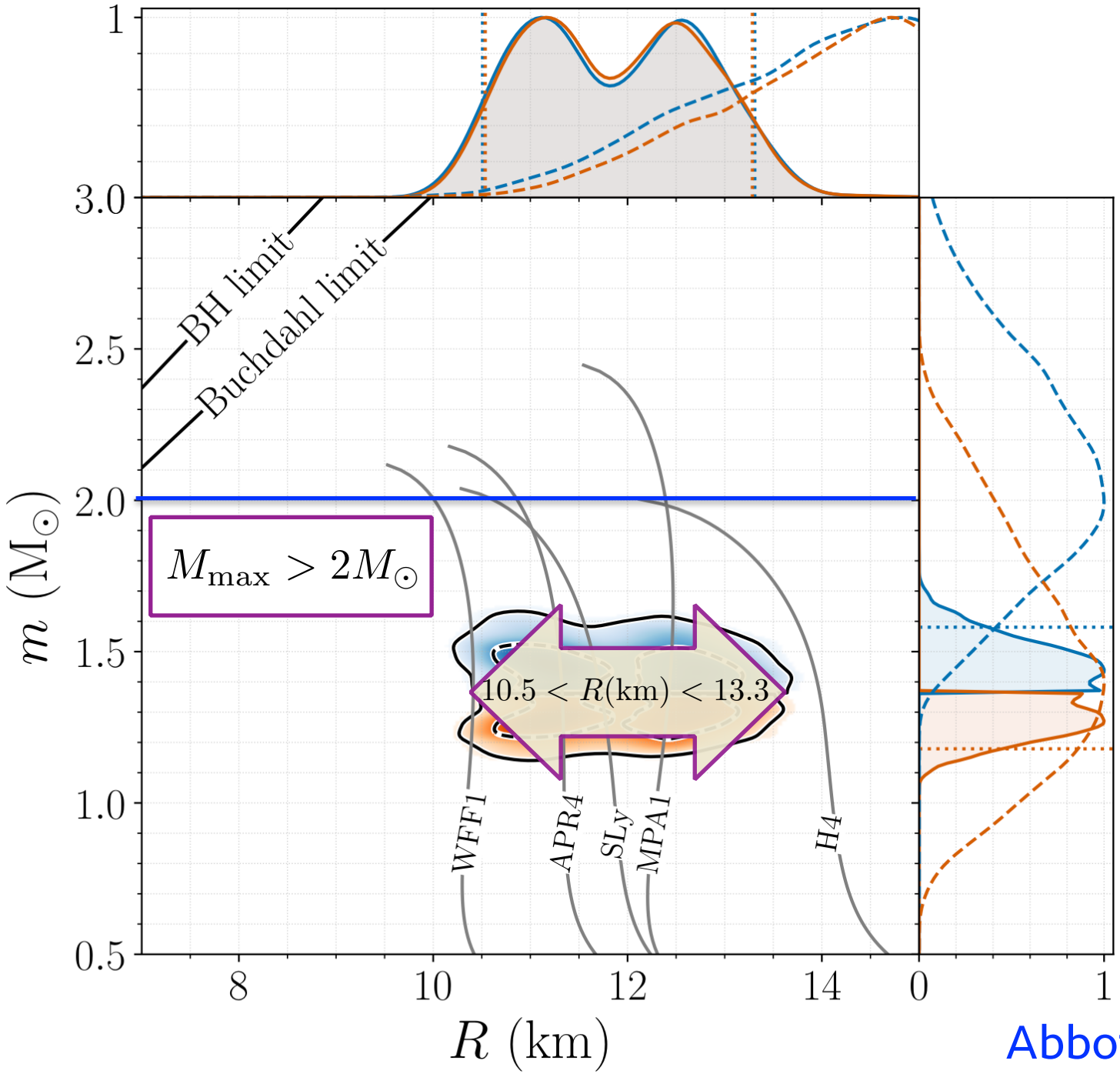

Abbot et al. (2018)

Constraints from the inspiral of GW170817

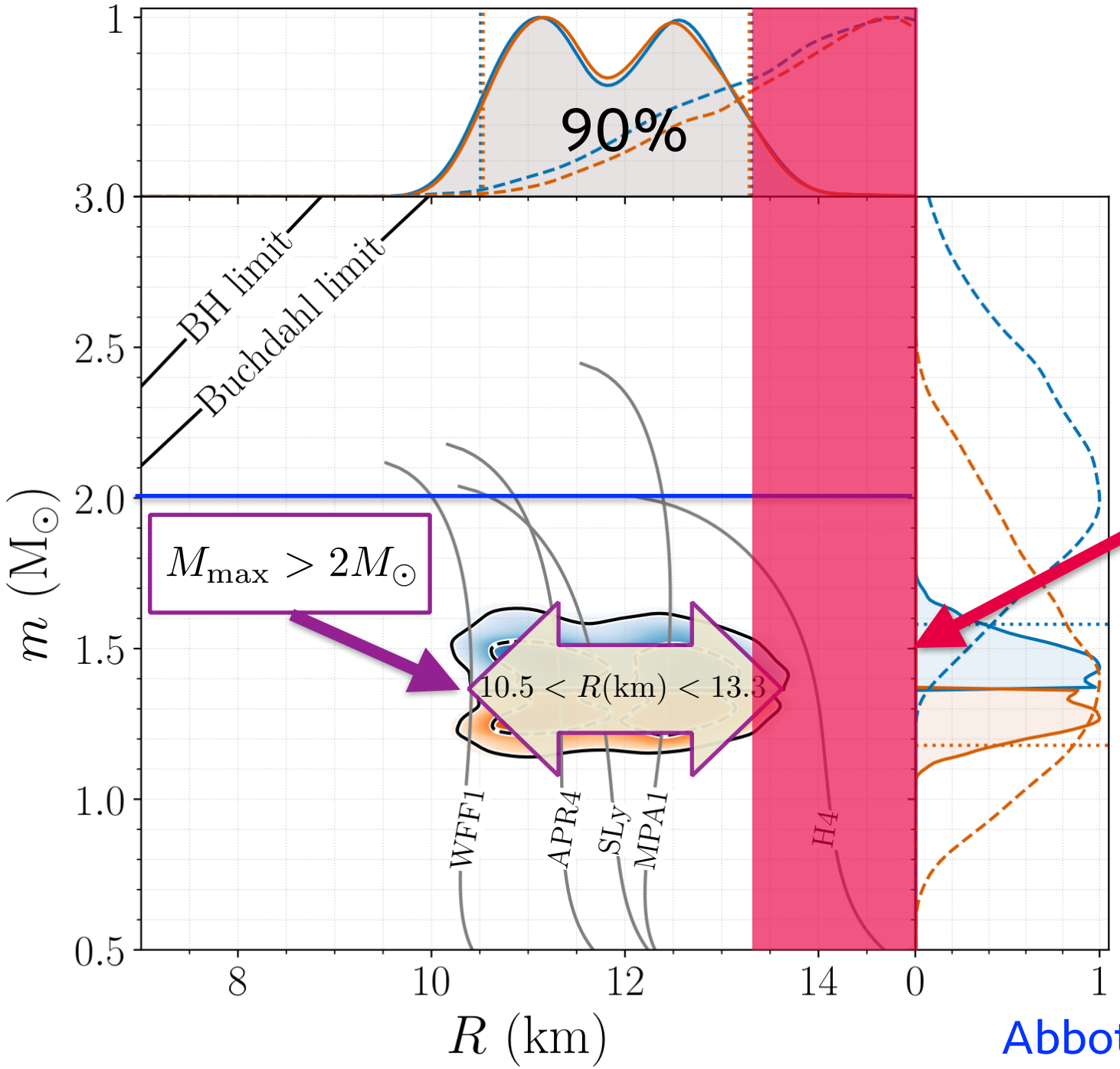

Abbot et al. (2018)

From Effective Λ to Radius

$$\tilde{\Lambda} = \frac{16}{13}\frac{(1+12q)\Lambda_A + (12+q)q^4\Lambda_B}{(1+q)^5}$$

$$q \equiv m_B/m_A (\leq 1)$$

$$\mathcal{M}_c = \frac{(m_1 m_2)^{3/5}}{(m_1+m_2)^{1/5}} = m_1 \frac{q^{3/5}}{(1+q)^{1/5}}$$

for GW170817:

$$= 1.188^{+0.004}_{-0.002}\ M_\odot$$

For fixed M_c ->
nearly mass-independent
empirical relation

Raithel, Oezel
& Psaltis (2018)

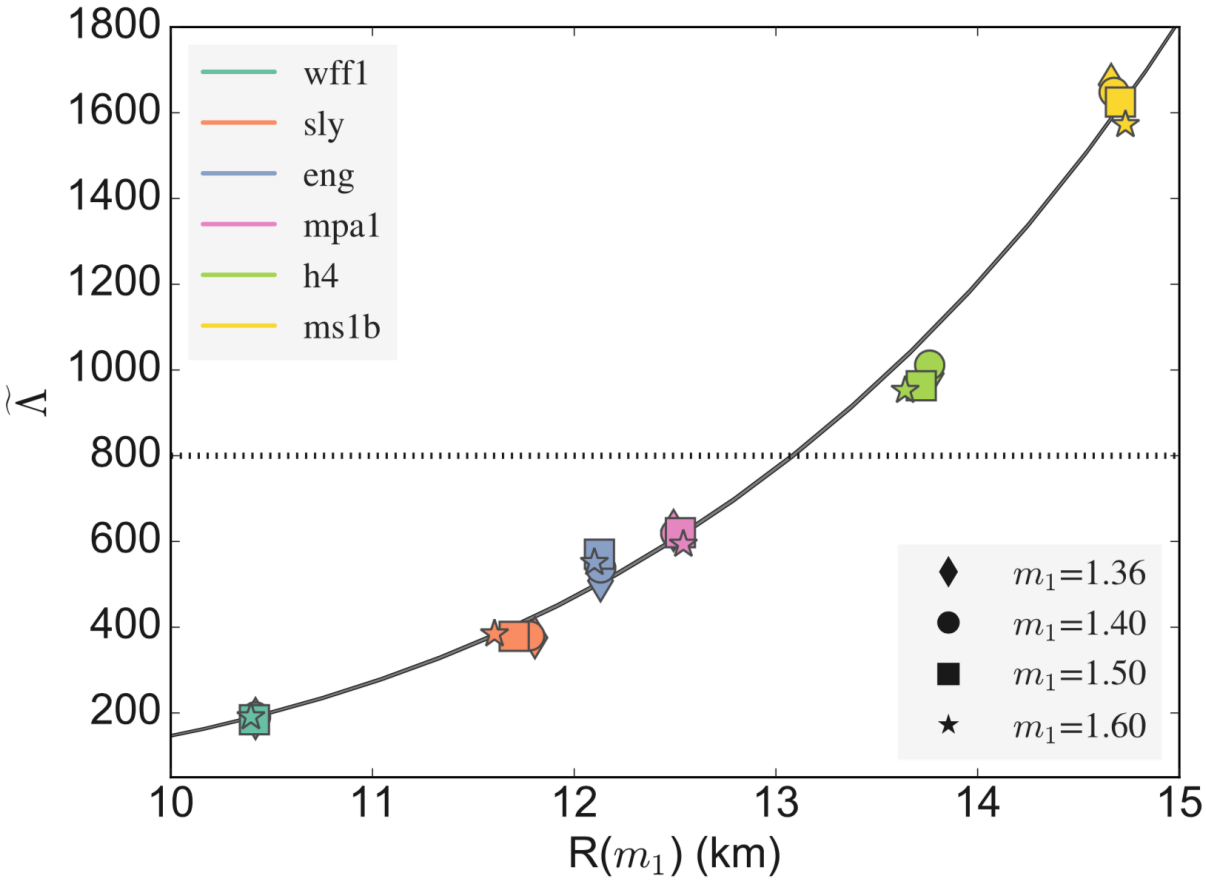

Various Radius Constraints based on GW170817

Montana et al. (2018)

Reference	R_i [km]
Without a phase transition	
Bauswein et al. [42]	$10.68^{+0.15}_{-0.03} \leq R_{1.6}$
Most et al. [51]	$12.00 \leq R_{1.4} \leq 13.45$
Burgio et al. [54]	$11.8 \leq R_{1.5} \leq 13.1$
Tews et al. [55]	$11.3 \leq R_{1.4} \leq 13.6$
De et al. [56]	$8.9 \leq R_{1.4} \leq 13.2$
LIGO/Virgo [57]	$10.5 \leq R_{1.4} \leq 13.3$
With a phase transition	
Annala et al. [46]	$R_{1.4} \leq 13.6$
Most et al. [51]	$8.53 \leq R_{1.4} \leq 13.74$
Burgio et al. [54]	$R_{1.5} = 10.7$
Tews et al. [55]	$9.0 \leq R_{1.4} \leq 13.6$
This work	
NS	$R_{1.4} = 13.11$
HS `Model-2`	$12.9 \leq R_{1.4} \leq 13.11$
HS_T `Model-1`	$10.1 \leq R_{1.4} \leq 12.9$
HS_T `Model-2`	$10.4 \leq R_{1.4} \leq 11.9$

Various Radius Constraints based on GW170817

Montana et al. (2018)

Reference	R_i [km]
Without a phase transition	
Bauswein et al. [42]	$10.68^{+0.15}_{-0.03} \leq R_{1.6}$
Most et al. [51]	$12.00 \leq R_{1.4} \leq 13.45$
Burgio et al. [54]	$11.8 \leq R_{1.5} \leq 13.1$
Tews et al. [55]	$11.3 \leq R_{1.4} \leq 13.6$
De et al. [56]	$8.9 \leq R_{1.4} \leq 13.2$
LIGO/Virgo [57]	$10.5 \leq R_{1.4} \leq 13.3$
With a phase transition	
Annala et al. [46]	$R_{1.4} \leq 13.6$
Most et al. [51]	$8.53 \leq R_{1.4} \leq 13.74$
Burgio et al. [54]	$R_{1.5} = 10.7$
Tews et al. [55]	$9.0 \leq R_{1.4} \leq 13.6$
This work	
NS	$R_{1.4} = 13.11$
HS `Model-2`	$12.9 \leq R_{1.4} \leq 13.11$
HS_T `Model-1`	$10.1 \leq R_{1.4} \leq 12.9$
HS_T `Model-2`	$10.4 \leq R_{1.4} \leq 11.9$

A Minimal Set of Assumptions

Bauswein, Just, Janka, NS (2017)

1) GR is valid.

2) There was no prompt collapse in the GW170817 merger event (to explain inferred mass of ejecta)

3) Causality holds $(v_s < c)$

and use the total mass derived from the inspiral GW signal

$$M_{\rm tot}^{\rm GW170817} = 2.74^{+0.04}_{-0.01}\, M_\odot$$

Differentially Rotating Models

(Bauswein & NS 2017)

hypermassive stars

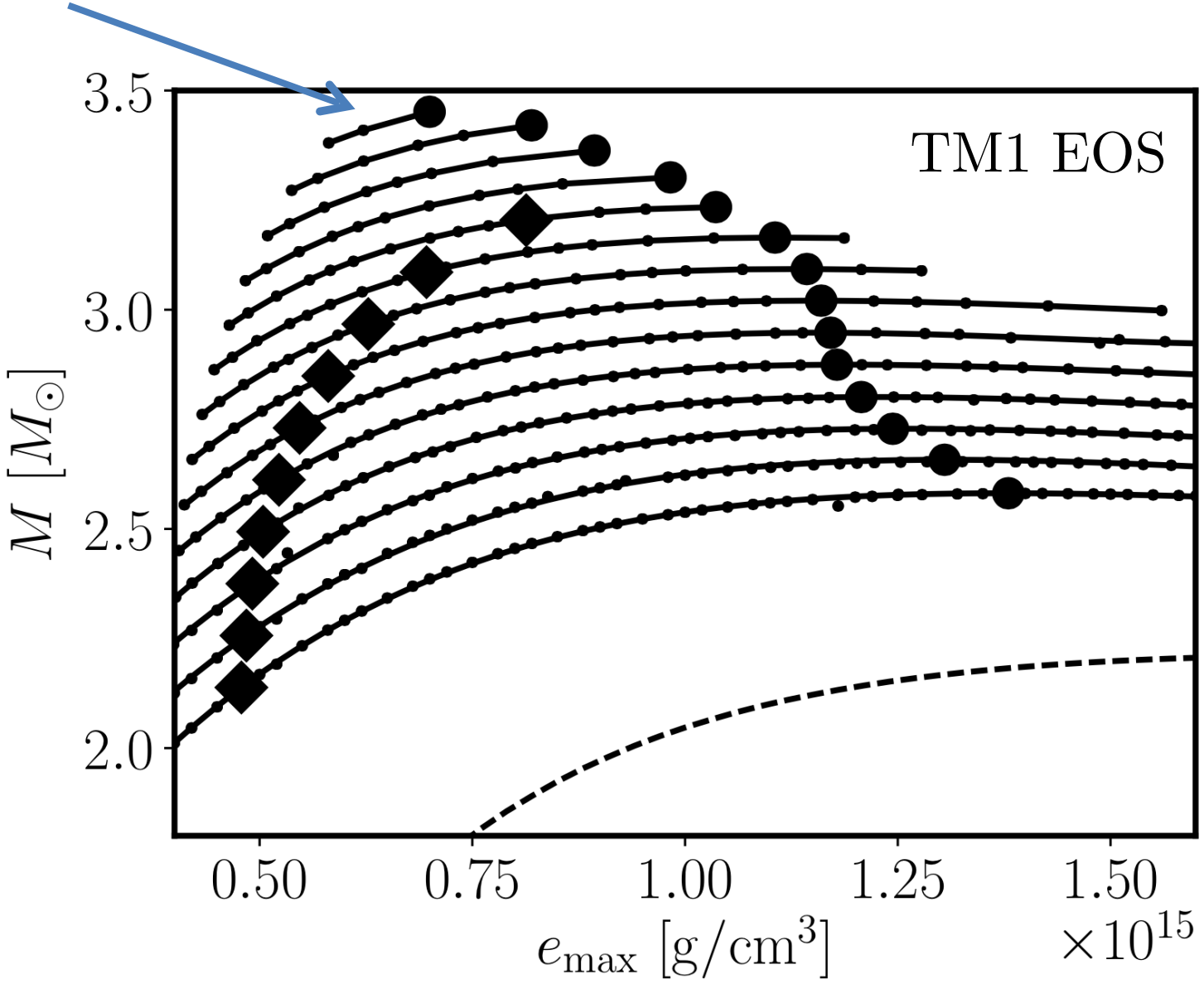

Differentially Rotating Models

(Bauswein & NS 2017)

hypermassive stars

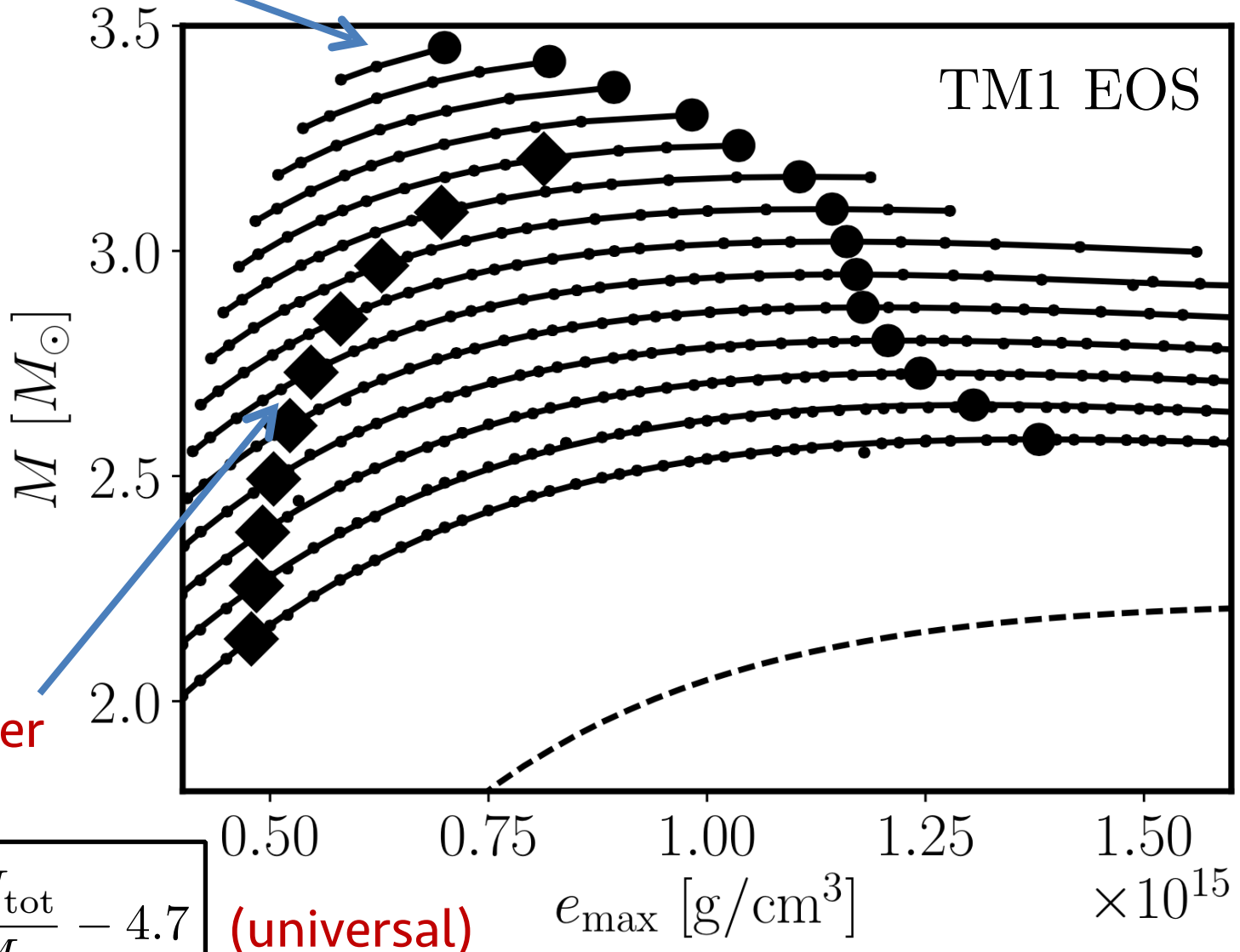

BNS merger remnants

$$\frac{cJ}{M_\odot^2} \simeq 4\frac{M_{\rm tot}}{M_\odot} - 4.7$$

(universal)

Differentially Rotating Models

(Bauswein & NS 2017)

hypermassive stars

Threshold mass

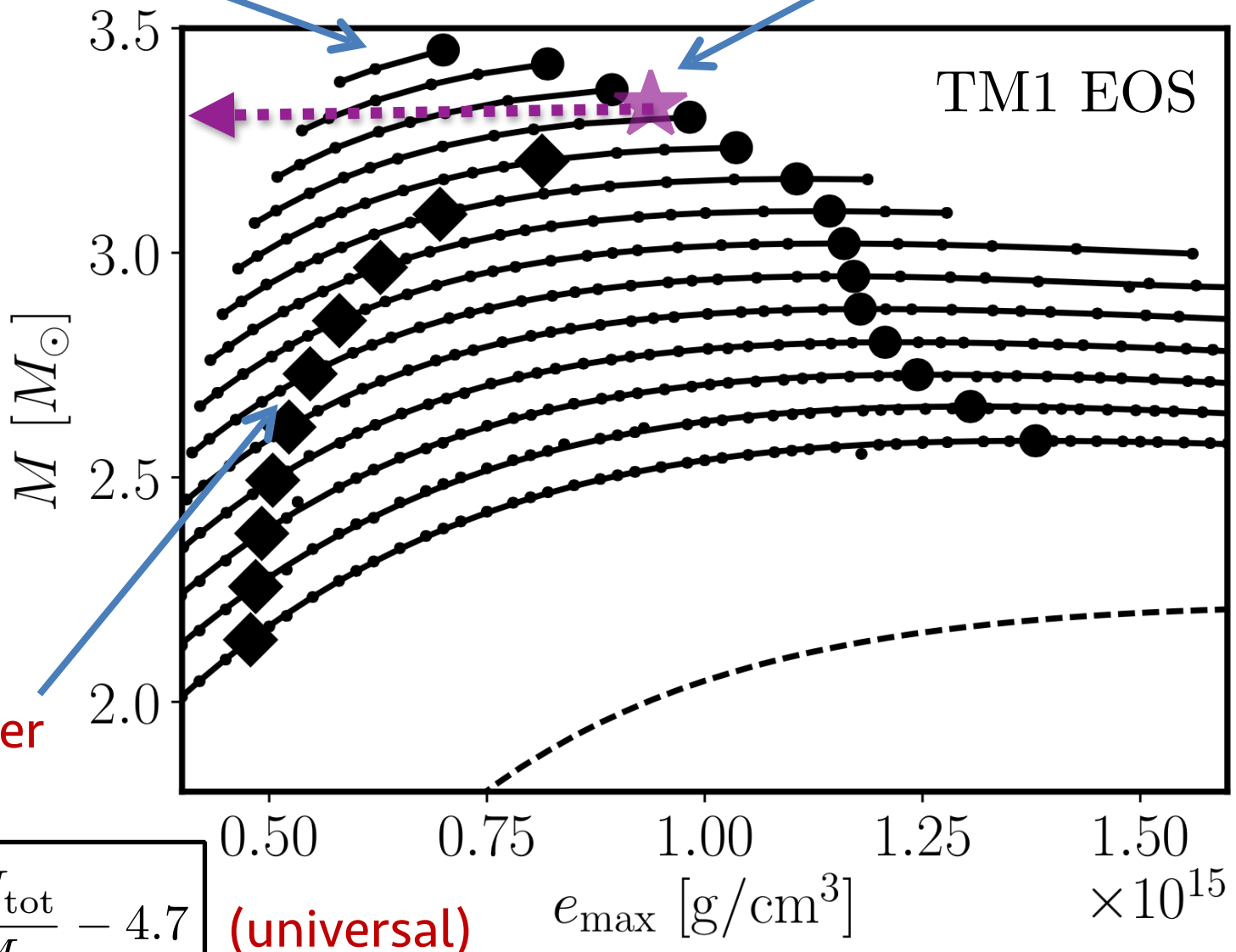

BNS merger remnants

$$\frac{cJ}{M_\odot^2} \simeq 4\frac{M_{\rm tot}}{M_\odot} - 4.7$$

(universal)

Differentially Rotating Models

(Bauswein & NS 2017)

hypermassive stars

Threshold mass

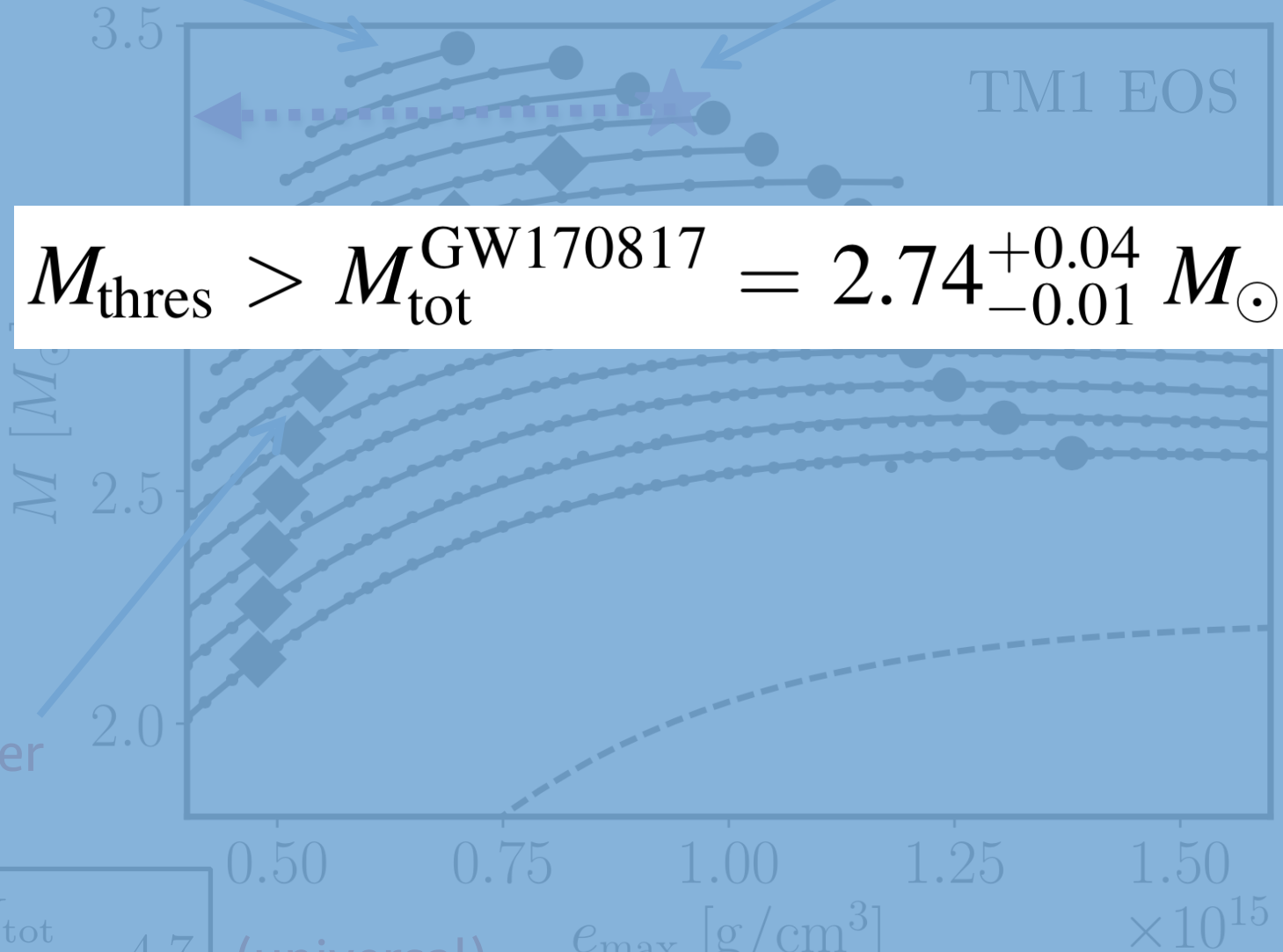

$$M_{\rm thres} > M_{\rm tot}^{\rm GW170817} = 2.74^{+0.04}_{-0.01}\, M_\odot$$

BNS merger remnants

$$\frac{cJ}{M_\odot^2} \simeq 4\frac{M_{\rm tot}}{M_\odot} - 4.7$$

(universal)

M_thres vs. M_max correlation

Bauswein, Baumgarte, Janka PRL (2013)

The threshold mass is related to the maximum TOV mass as

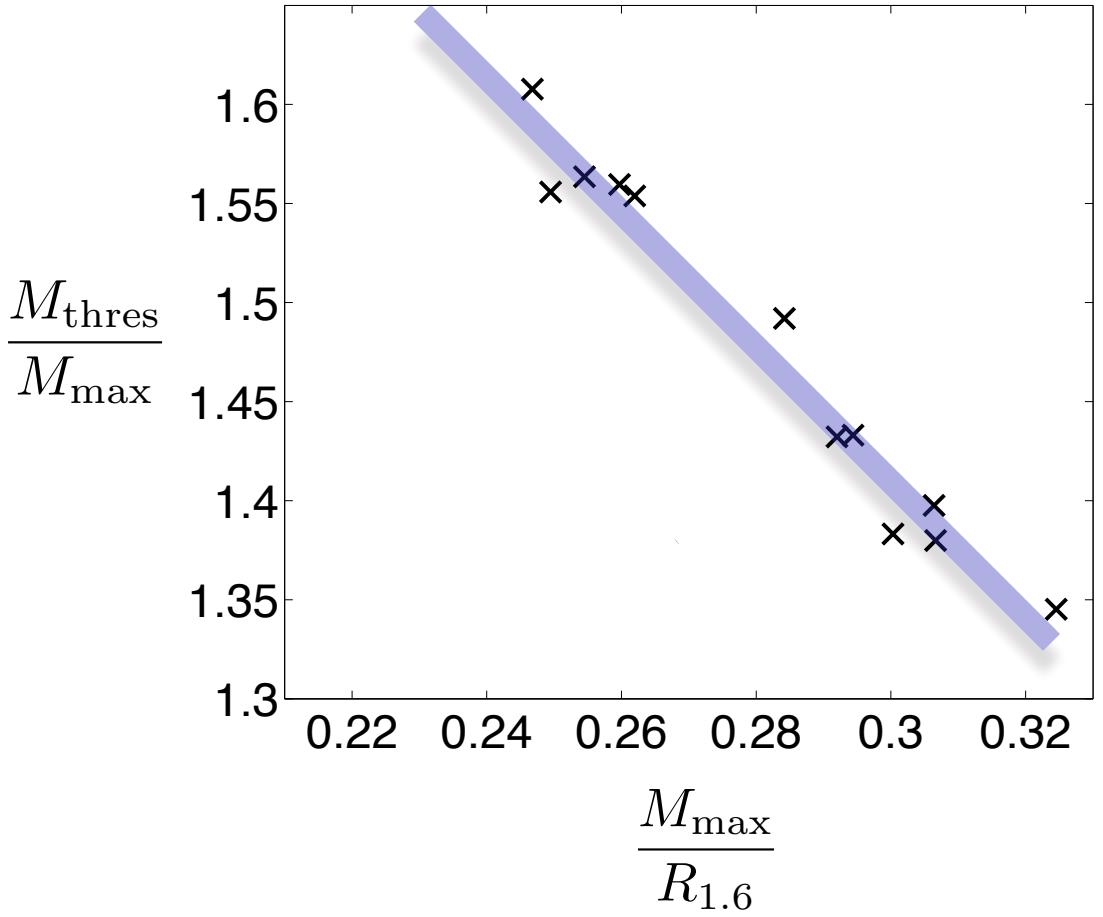

$$M_{\rm thres} = \left(-3.606 \frac{G M_{\rm max}}{c^2 R_{1.6}} + 2.38 \right) \cdot M_{\rm max} \; > 2.74 M_\odot$$

Maximally Compact EOS

Maximal compactness $\Leftrightarrow$ Maximally stiff core + maximally soft crust

Koranda, NS & Friedman (1997)

If whole star is at the causal limit

$$v_s = c$$

$$M_{\max} \leq \frac{1}{2.82} \frac{c^2 R_{\max}}{G}$$

(Lattimer & Prakash)

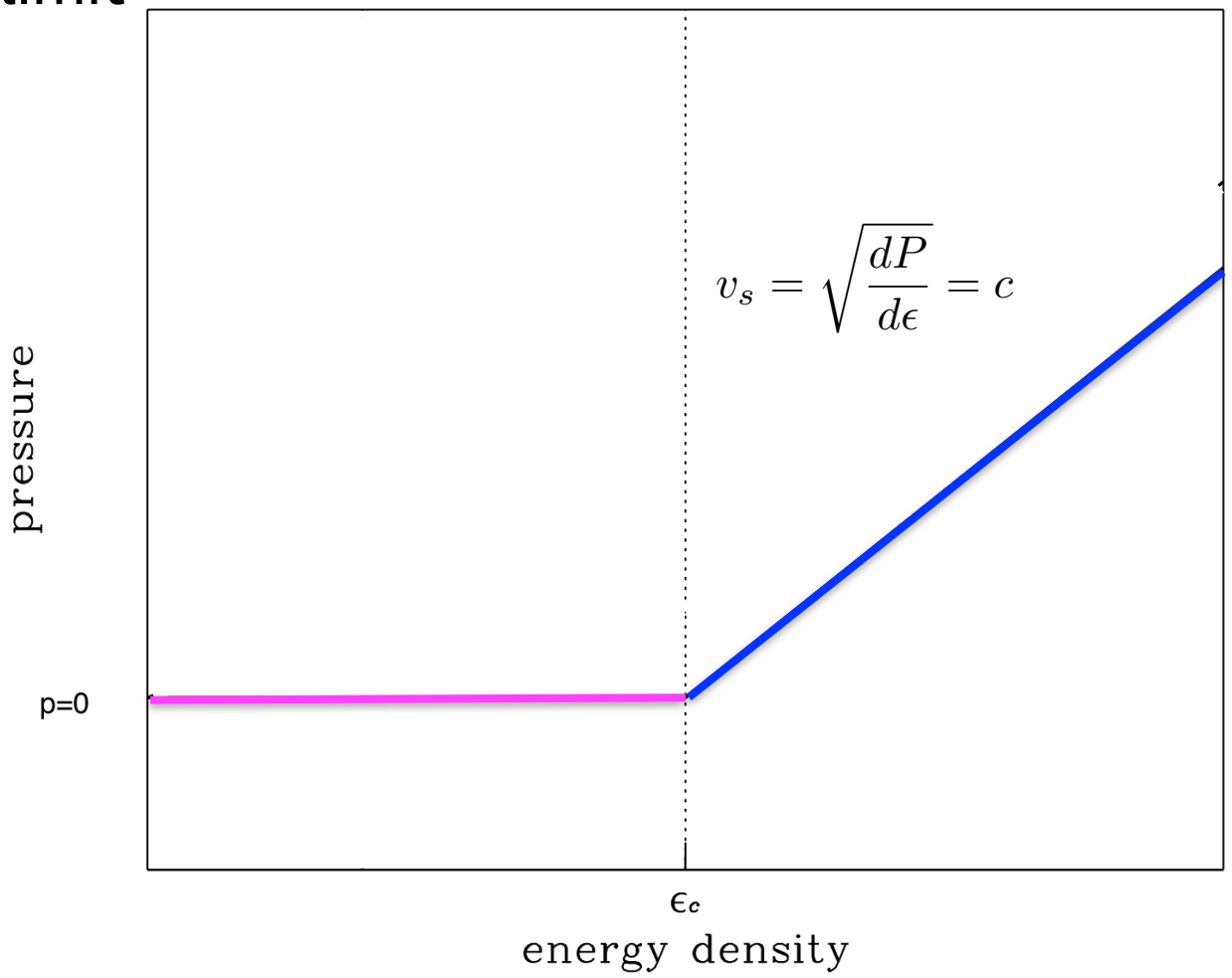

Maximally Compact EOS

Maximal compactness $\Leftrightarrow$ Maximally stiff core + maximally soft crust

Assume causal limit above

$$M > 1.6 M_\odot$$

for each EOS

$$M_{\rm max} \leq \frac{1}{3.10} \frac{c^2 R_{1.6}}{G}$$

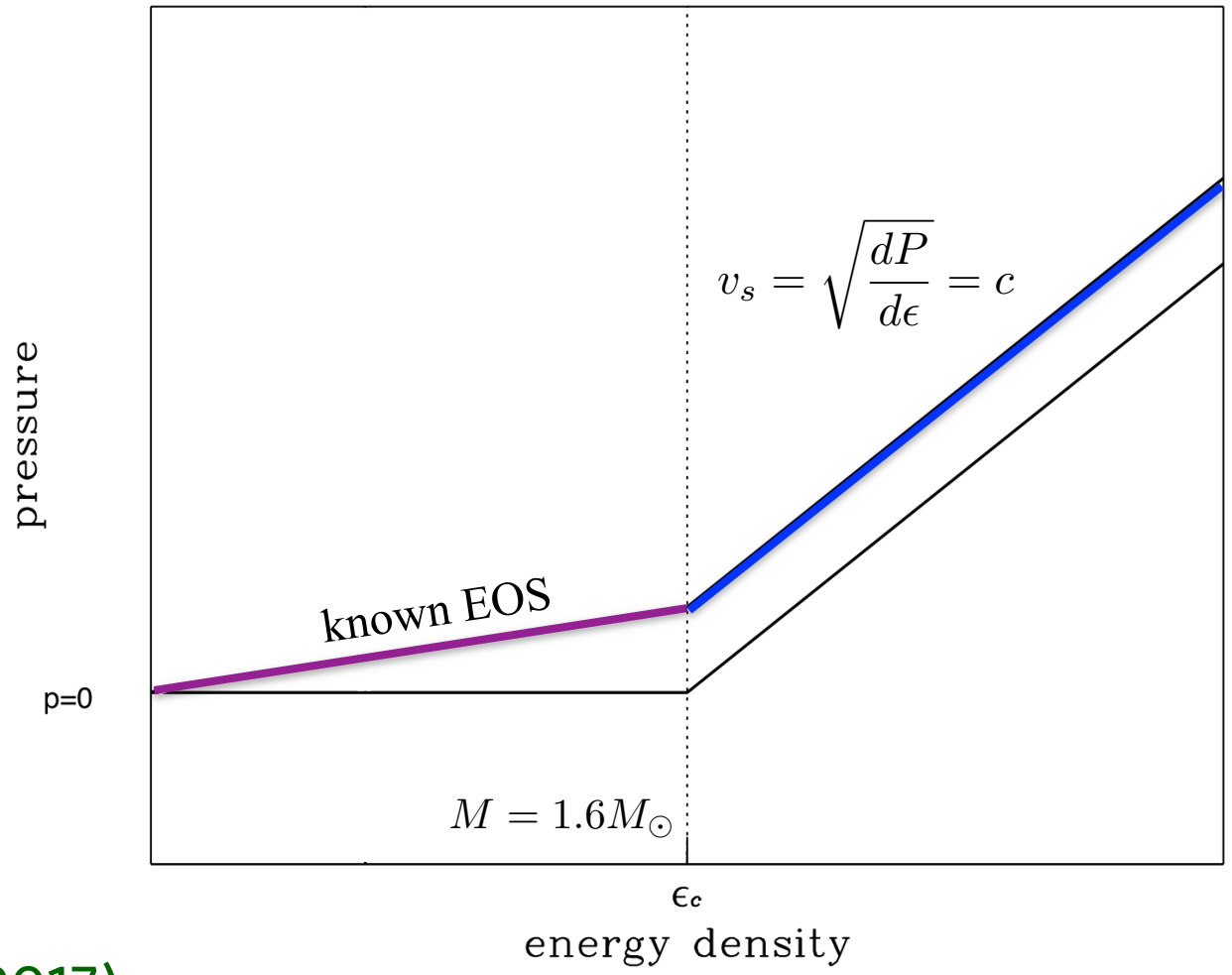

Bauswein, Just, Janka & NS (2017)

Radius Constraints from Minimal Assumptions

Bauswein, Just, Janka & NS (2017)

The combination of the minimal set of assumptions leads to a strict constraint on the radius:

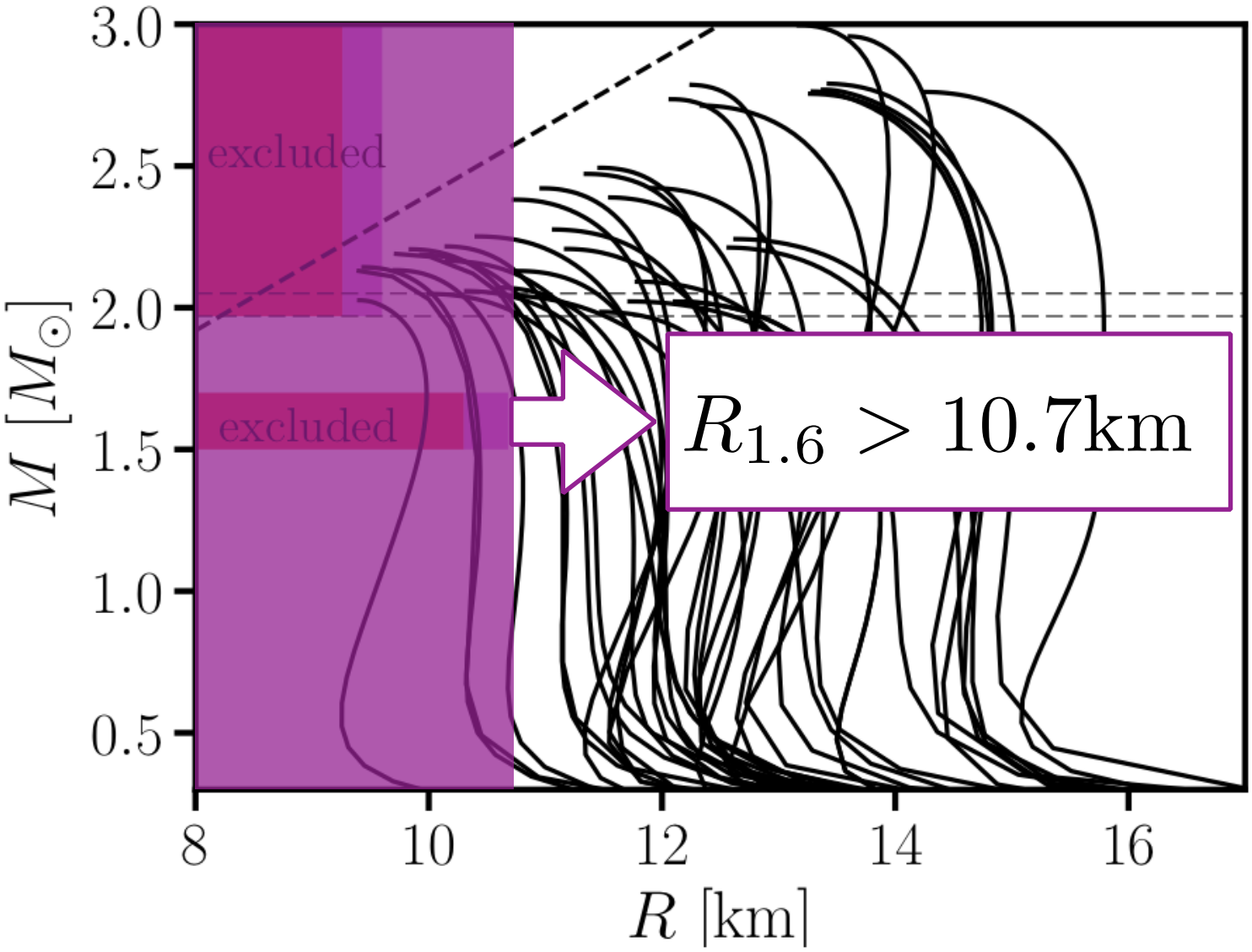

Comparison to Abbot et al. (2018)

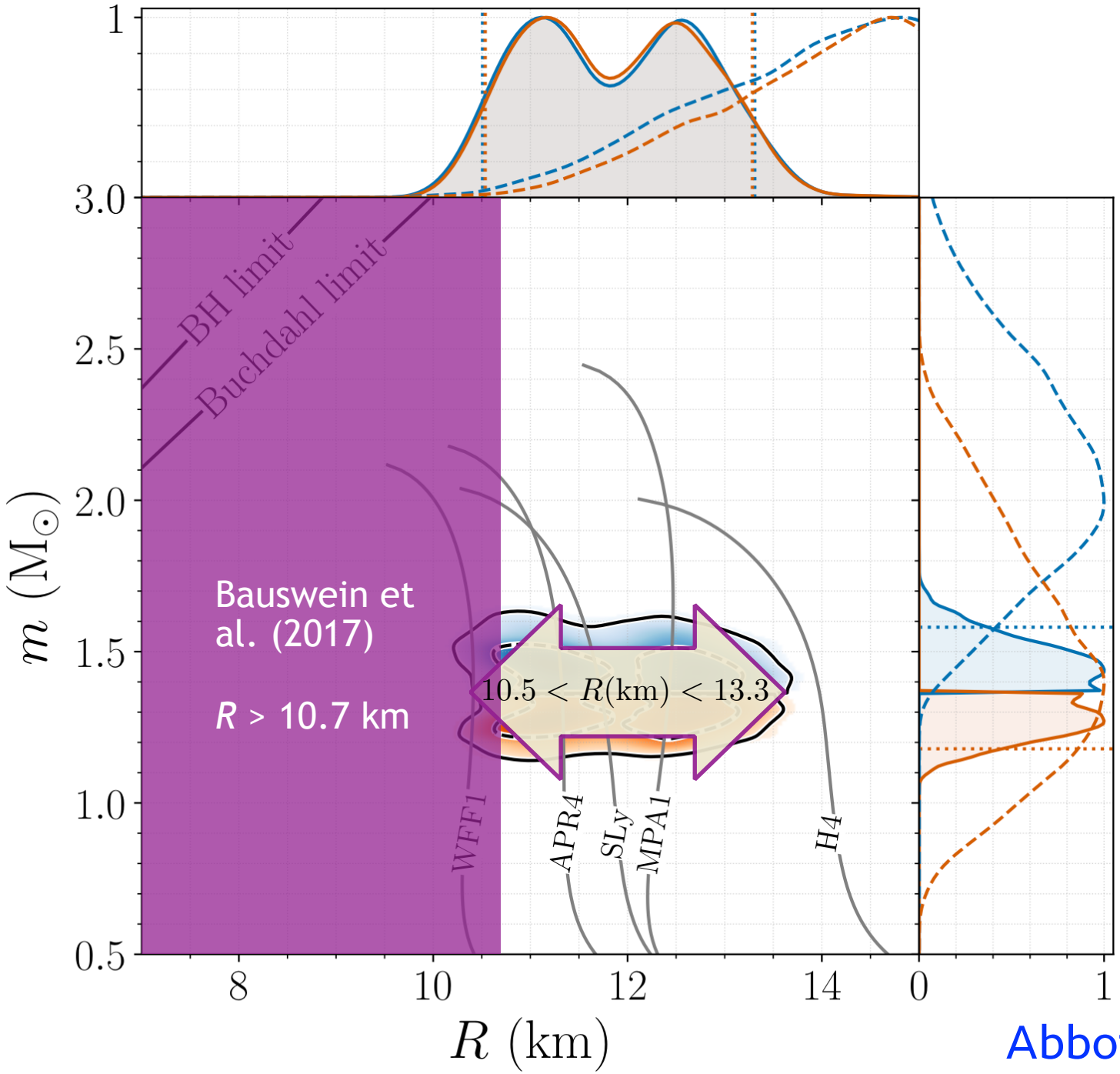

Abbot et al. (2018)

Constraints on M-R Relation

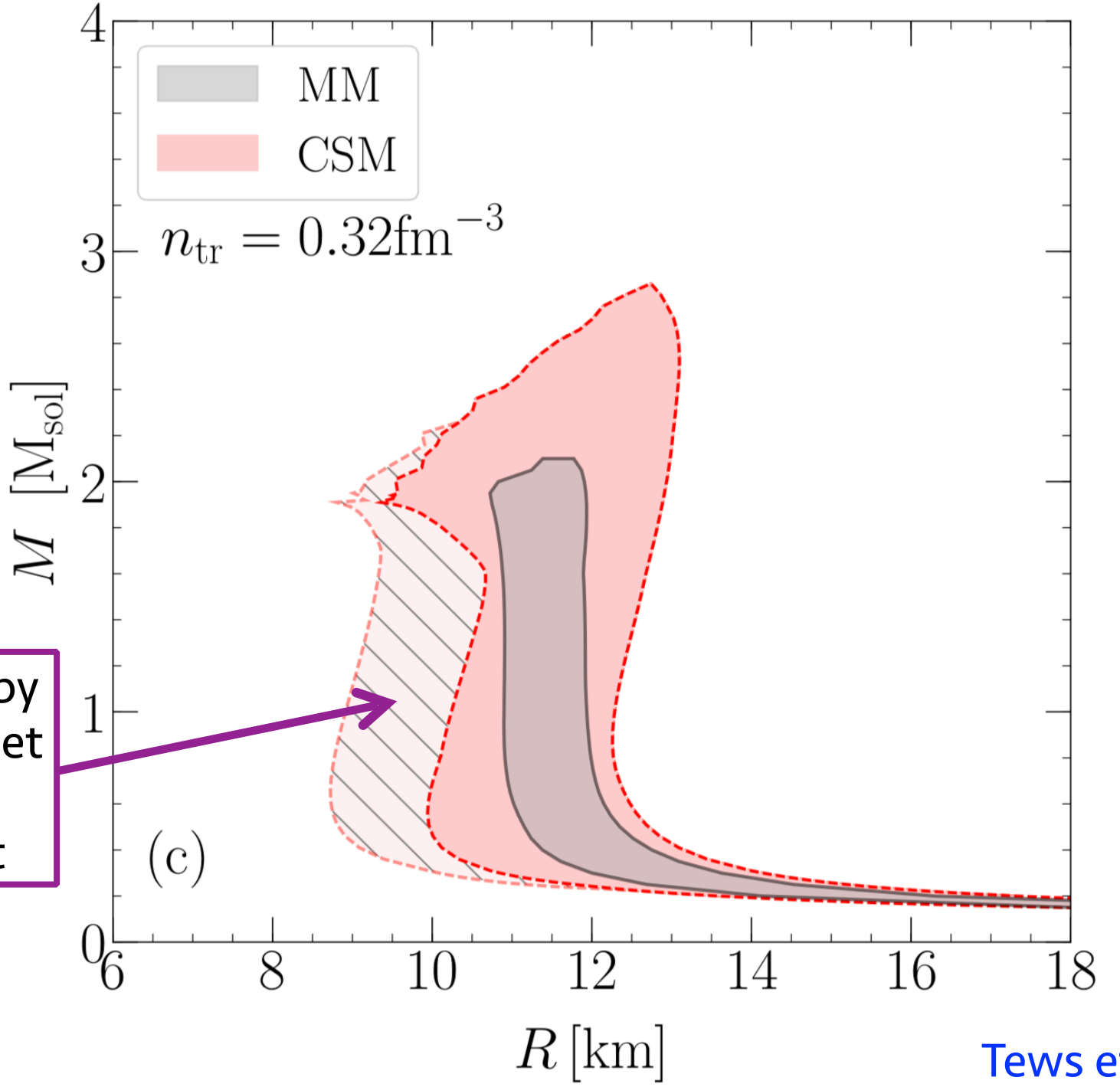

Excluded by Bauswein et al. (2017) constraint

Tews et al. (2019)

Constraints on EOS

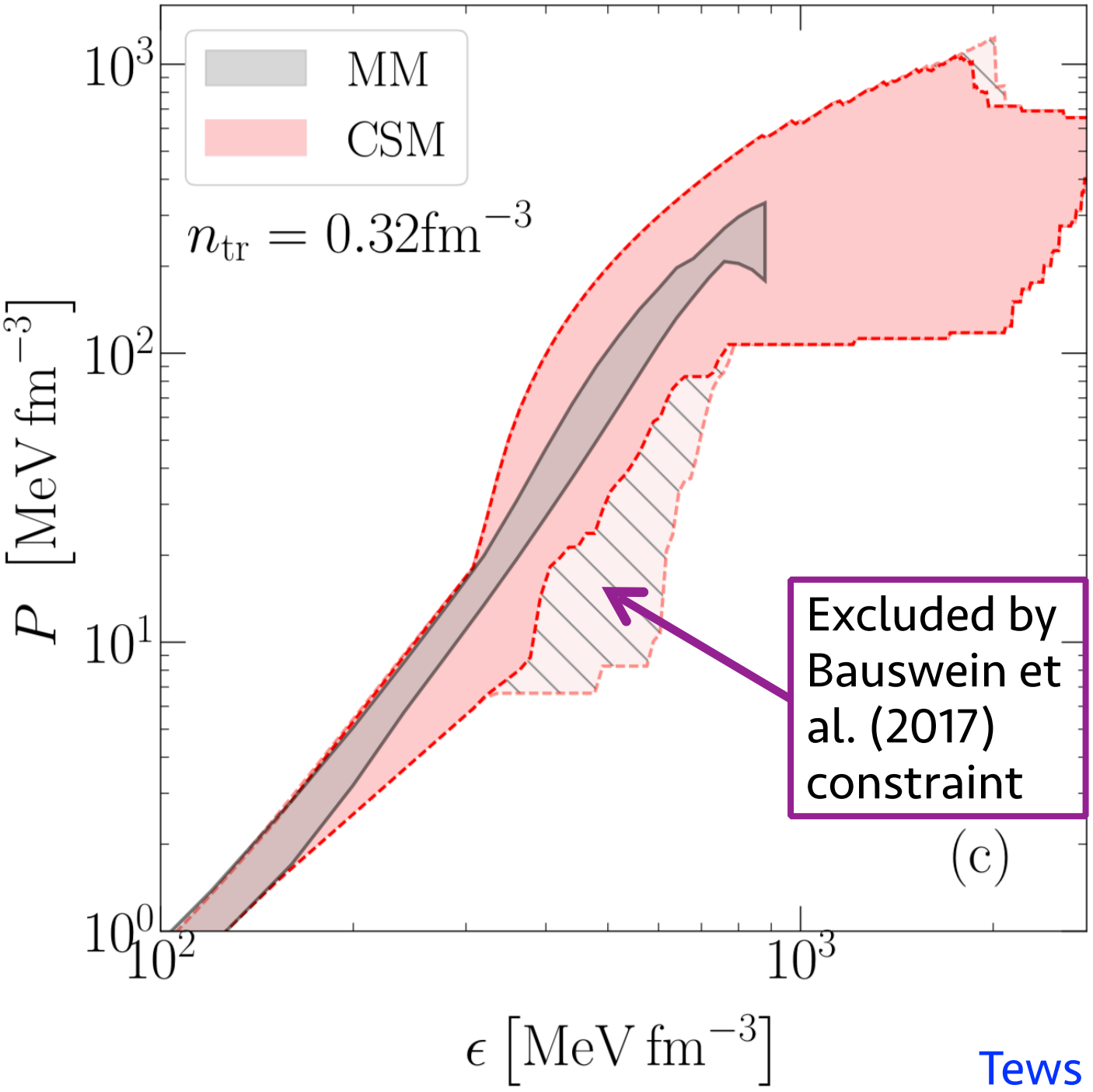

Tews et al. (2019)

Multimessenger Constraints on EOS

Campano, Tews, ..., Reddy et al. (2019)

GW170817 + no prompt collapse
+ larger EOS sample

$$M_{\text{thres}} = \left(-3.606 \frac{G M_{\text{max}}}{c^2 R_{1.6}} + 2.38 \right) \cdot M_{\text{max}}$$

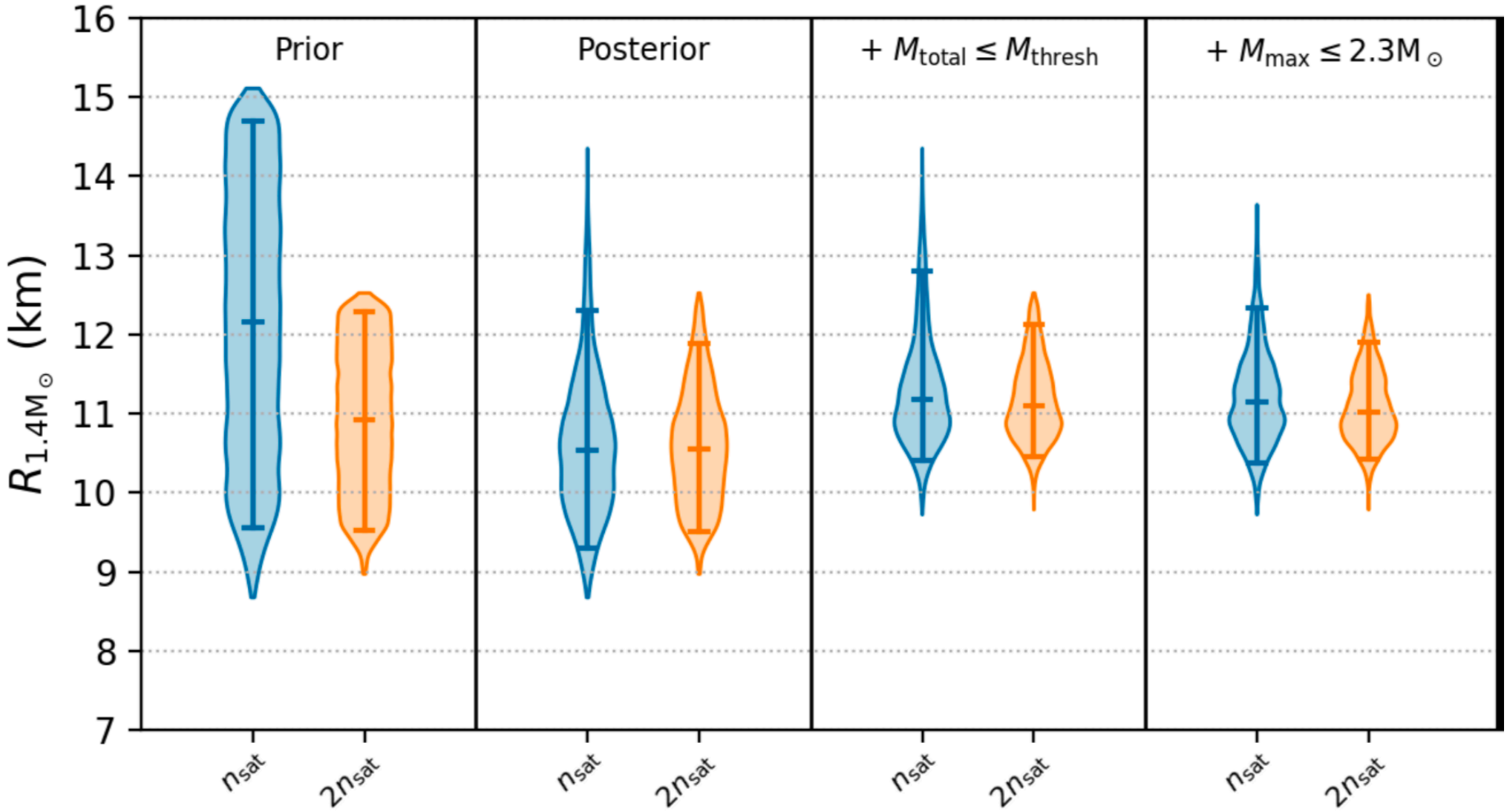

Constraints From Future Detections

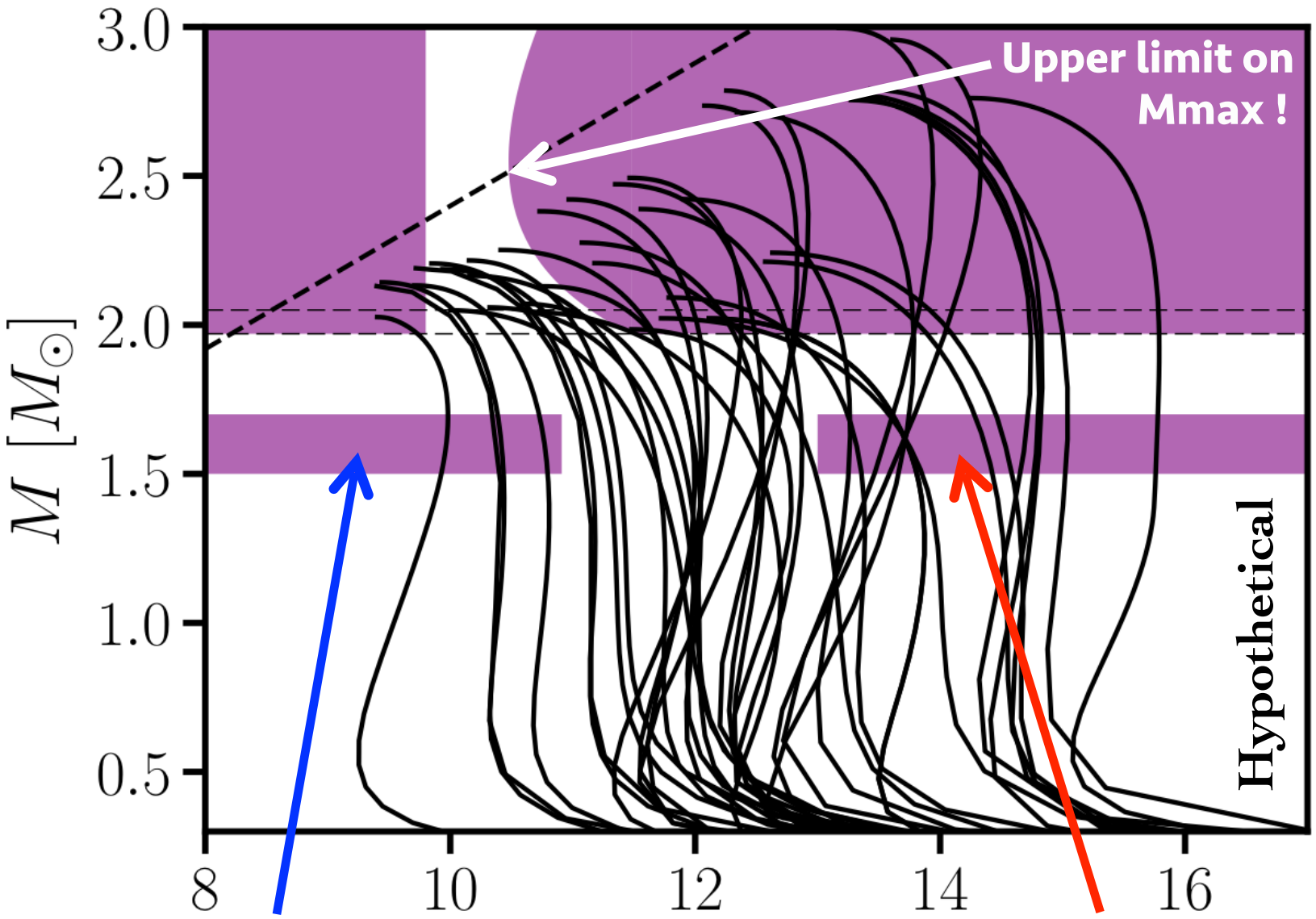

No collapse with

$M_{\mathrm{tot}} = 2.9 M_\odot$

Collapse with

$M_{\mathrm{tot}} = 3.1 M_\odot$

IF GW190425 WAS A PROMPT COLLAPSE

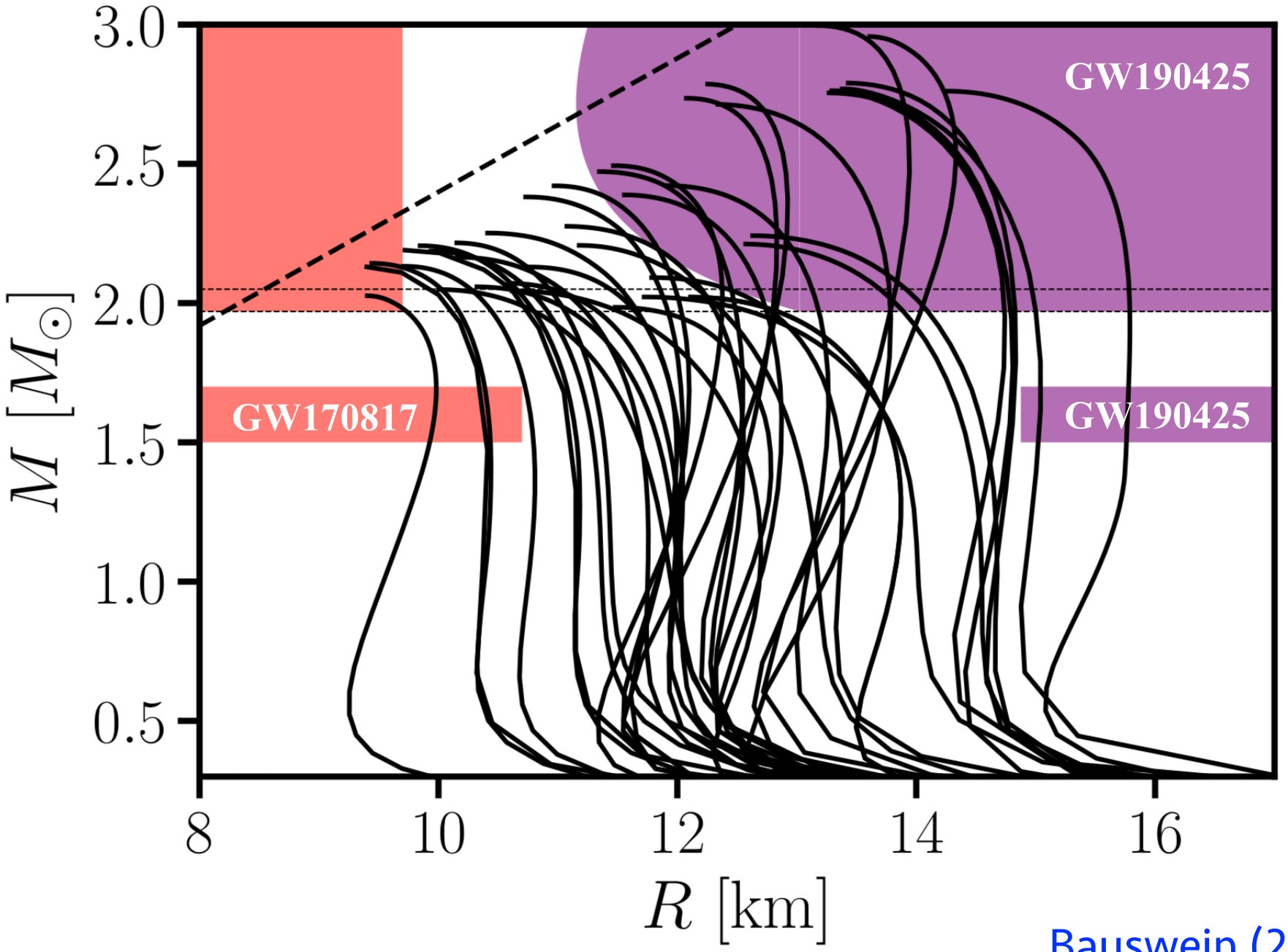

Bauswein (2020)

IF GW190425 WAS A PROMPT COLLAPSE

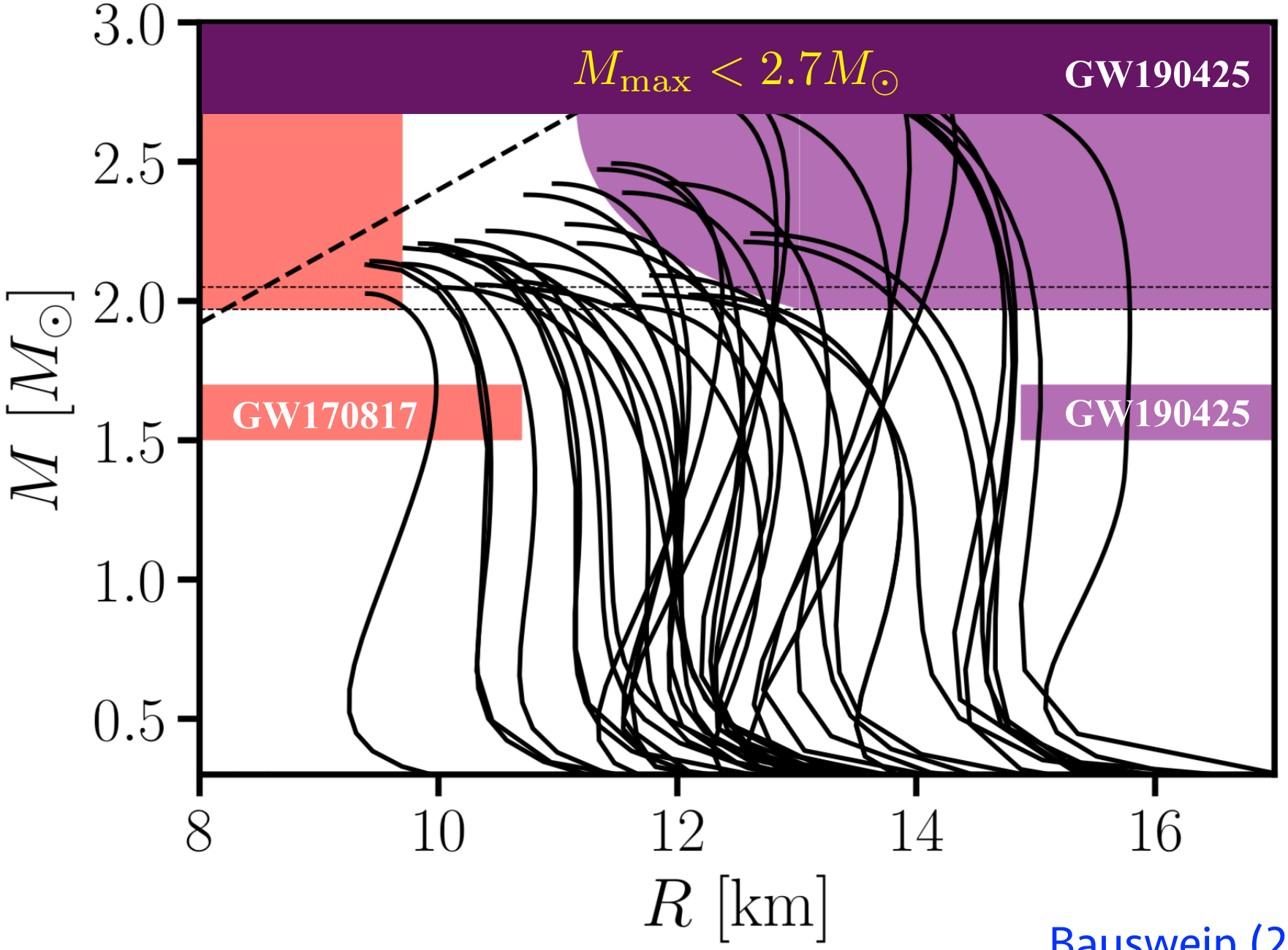

Bauswein (2020)

Limitations of Constraints from Inspiral

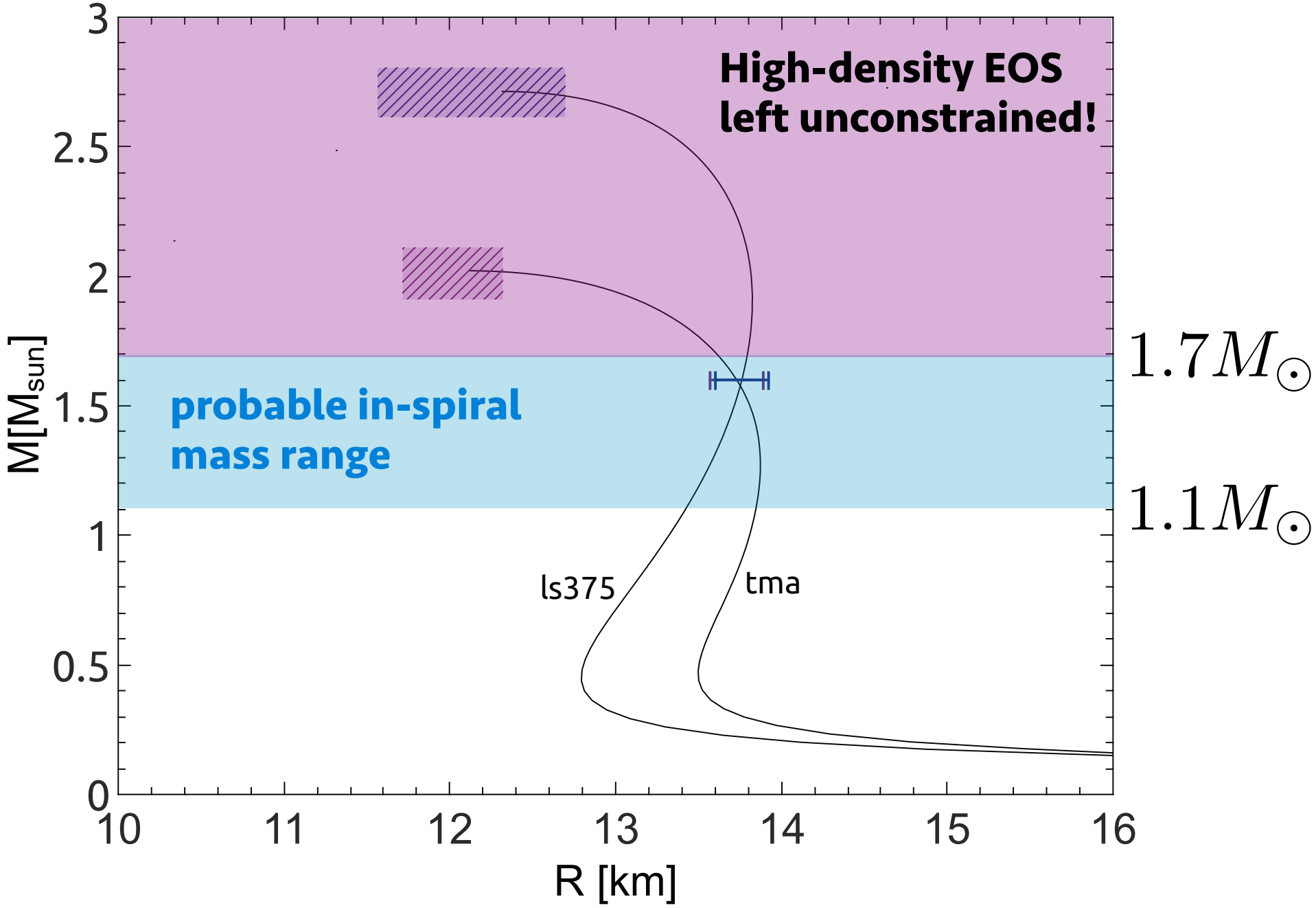

New Generations of GW Detectors

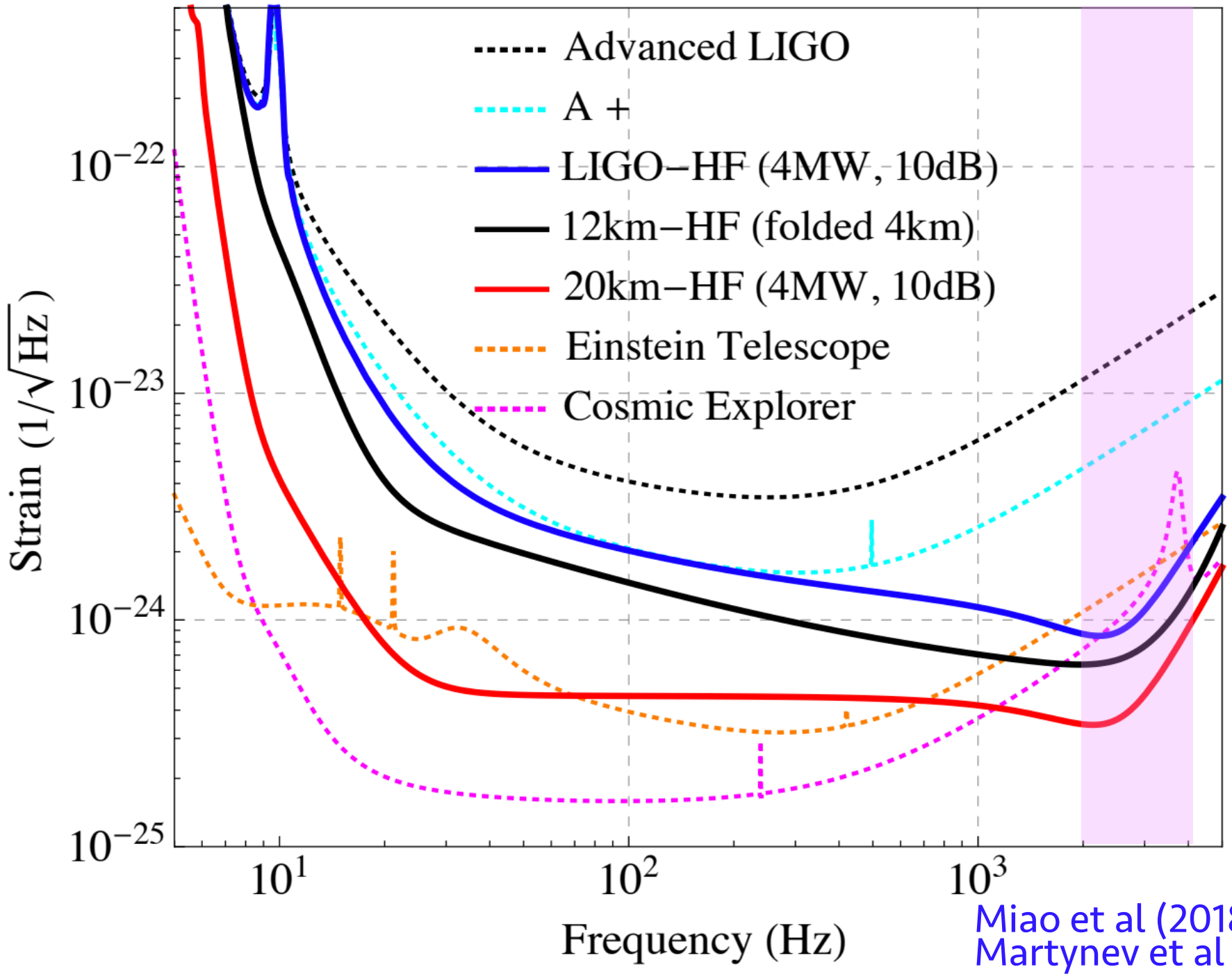

2G

2+G

3G

Miao et al (2018)
Martynev et al (2019)

OzHF 2km High-Frequency GW Detector

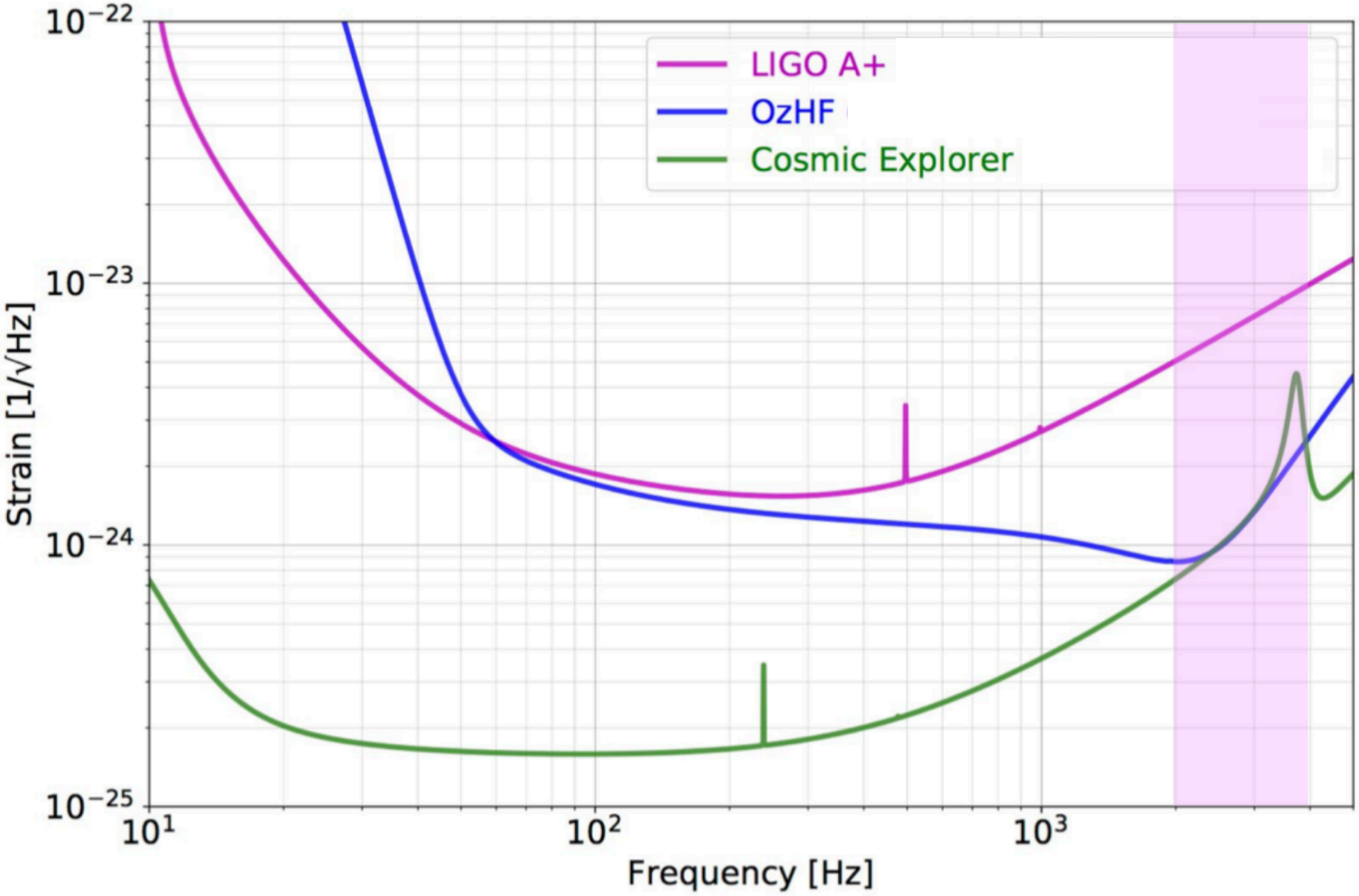

Lasky et al (2019)

Oscillations of Neutron Stars

$$\boldsymbol{\xi}(r,\theta,\phi) = \sum_{l=0}^{\infty} \sum_{m=-l}^{l} [U_l^m(r) Y_l^m(\theta,\phi)\hat{\boldsymbol{e}}_r + V_l^m(r)\nabla Y_l^m(\theta,\phi) + W_l^m(r)\hat{\boldsymbol{e}}_r \times \nabla Y_l^m(\theta,\phi)]$$

Main oscillation modes:

1. *f*-modes / *p*-modes

   fluid modes restored by pressure

2. *g*-modes

   restored by gravity/buoyancy

3. inertial modes (*r*-modes)

   restored by the Coriolis force in *rotating* stars

4. *w*-modes

   spacetime modes (similar to black hole modes)

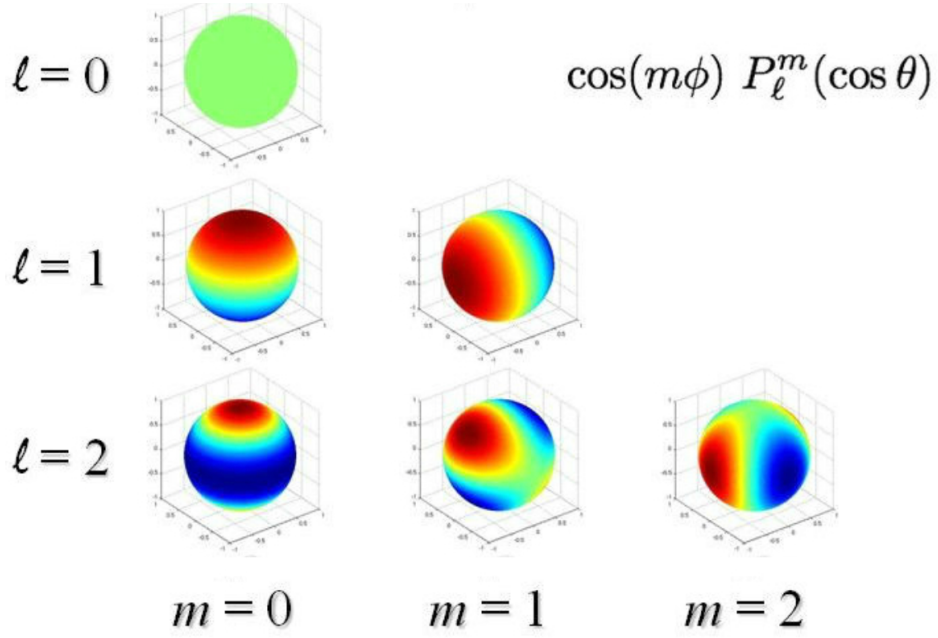

GW-detection: *f*-modes: stable oscillations

f-mode / *r*-mode *CFS*-instabilities

Post-Merger Gravitational Waves

The GW signal can be divided into three distinct phases: *inspiral*, *merger* and *post-merger ringdown*.

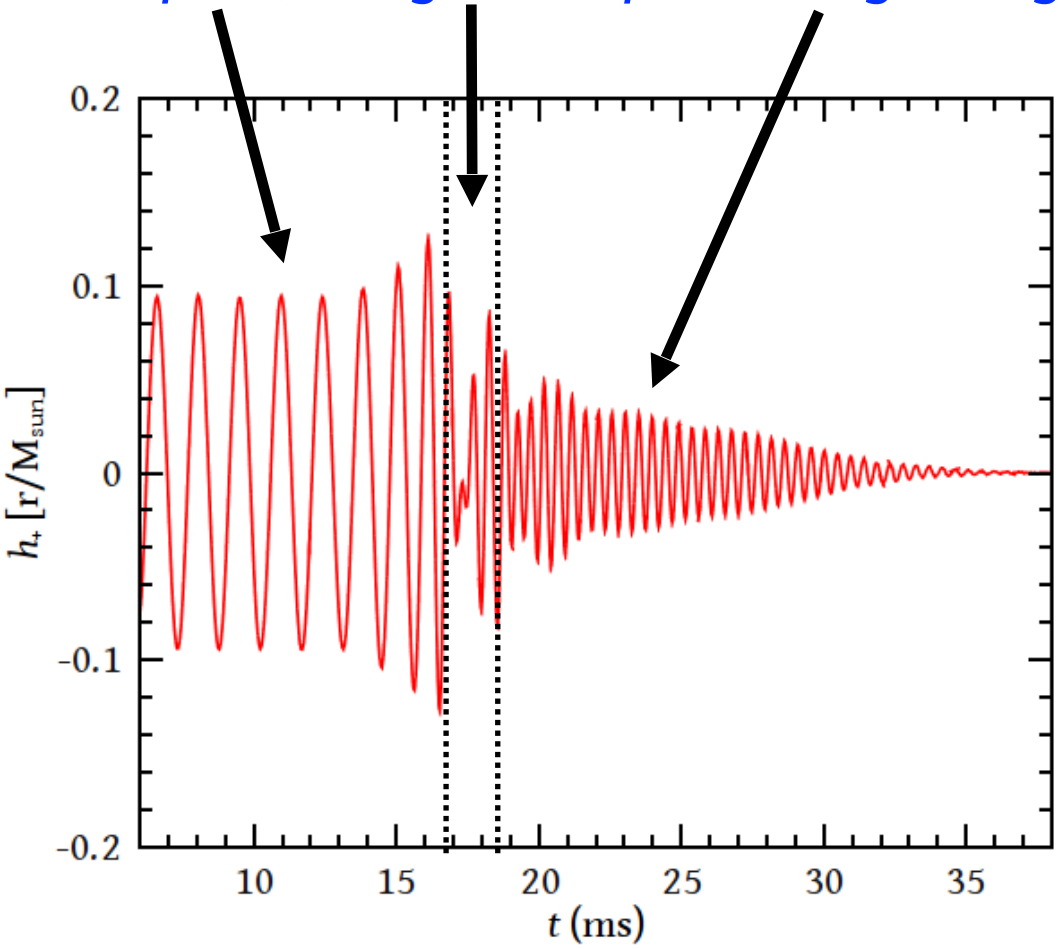

Post-Merger Gravitational Waves

The GW signal can be divided into three distinct phases:
inspiral, *merger* and *post-merger ringdown*.

Stergioulas et al. (2011)

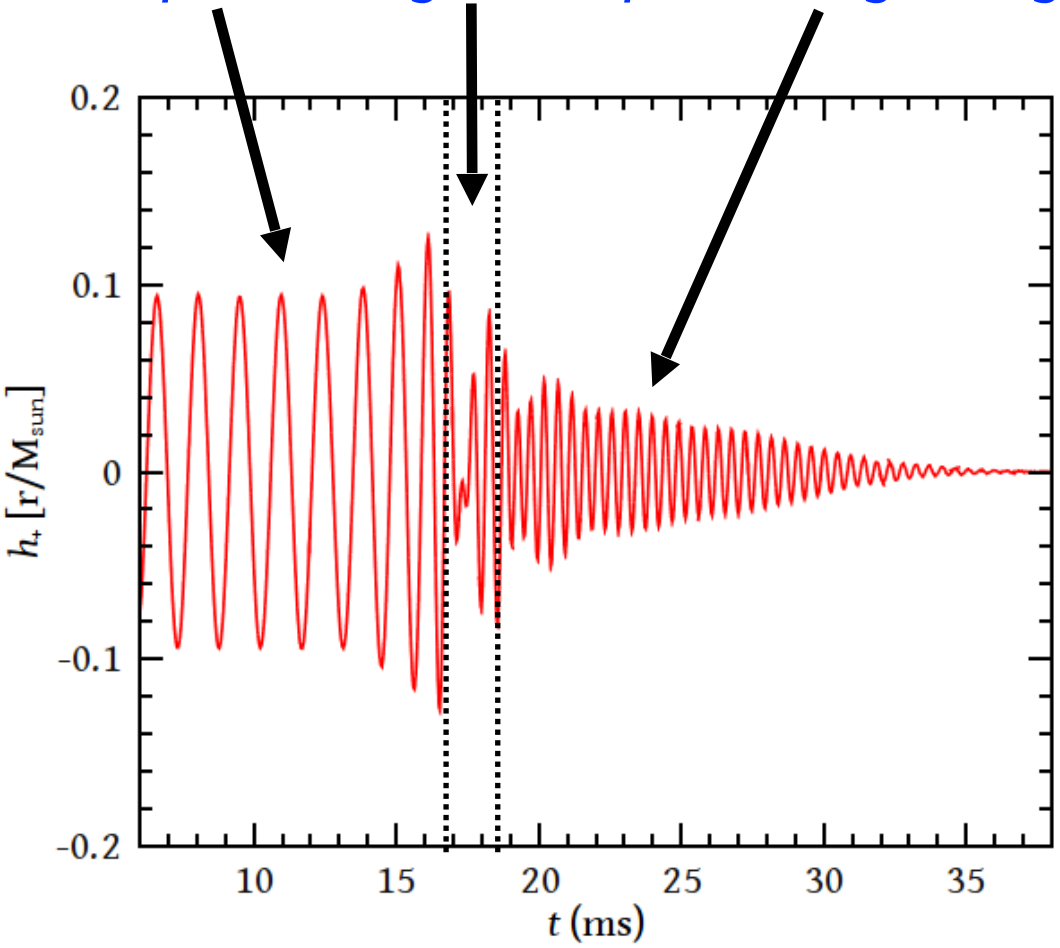

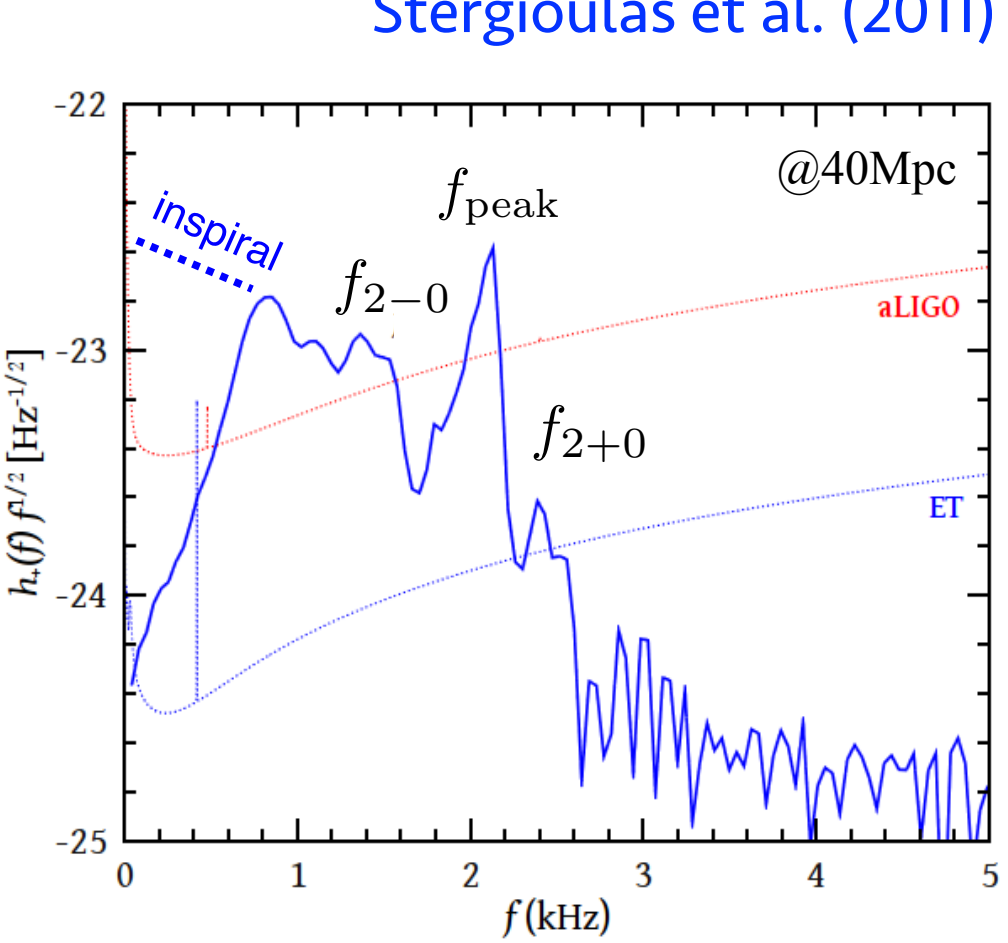

Post-Merger Gravitational Waves

The GW signal can be divided into three distinct phases:
inspiral, *merger* and *post-merger ringdown*.

Stergioulas et al. (2011)

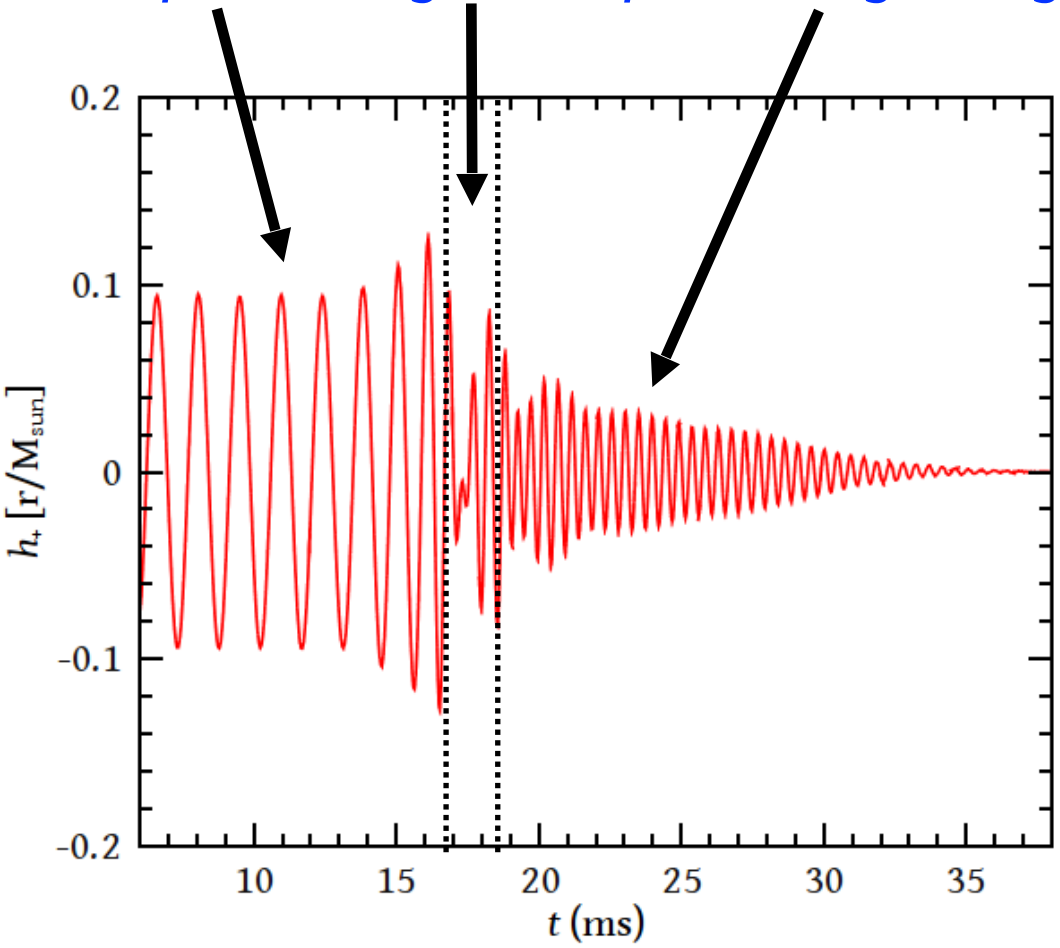

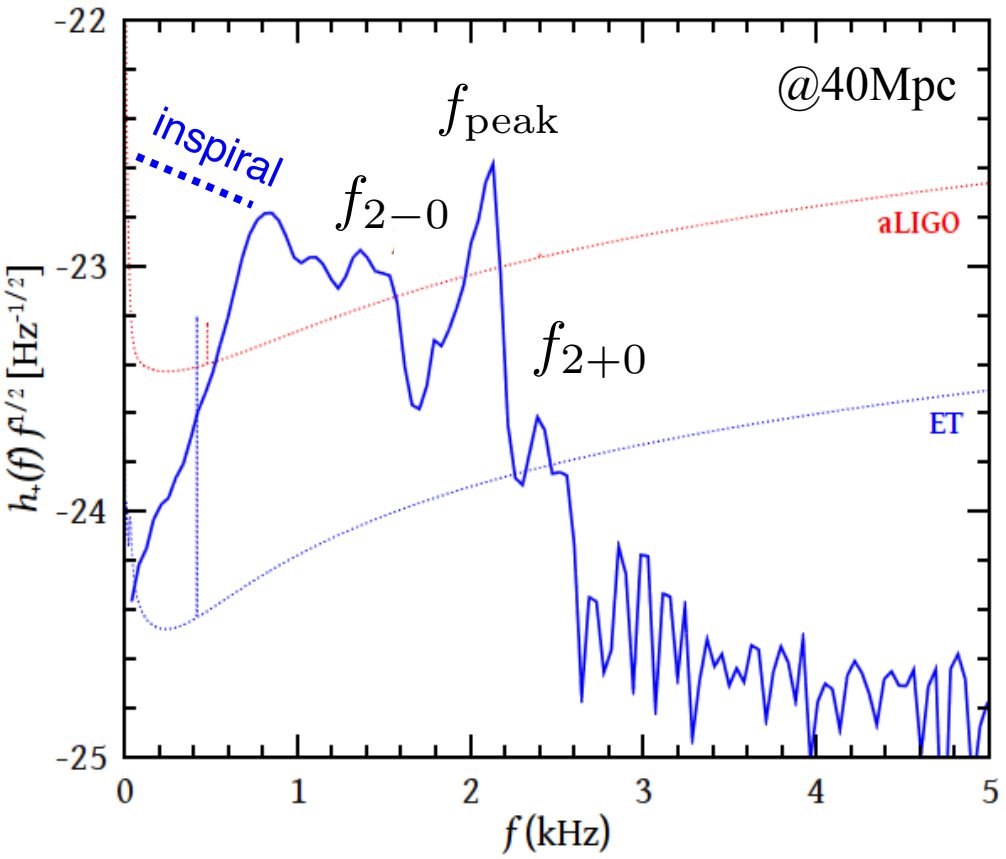

$$f_{\rm peak} = f_2$$

is due to the fundamental *l=m=2 f*-mode oscillation

$$f_{2-0} = f_2 - f_0$$
$$f_{2+0} = f_2 + f_0$$

are quasi-linear combination tones -> (Tartini tones)

Sorge (1745), Tartini (1754)

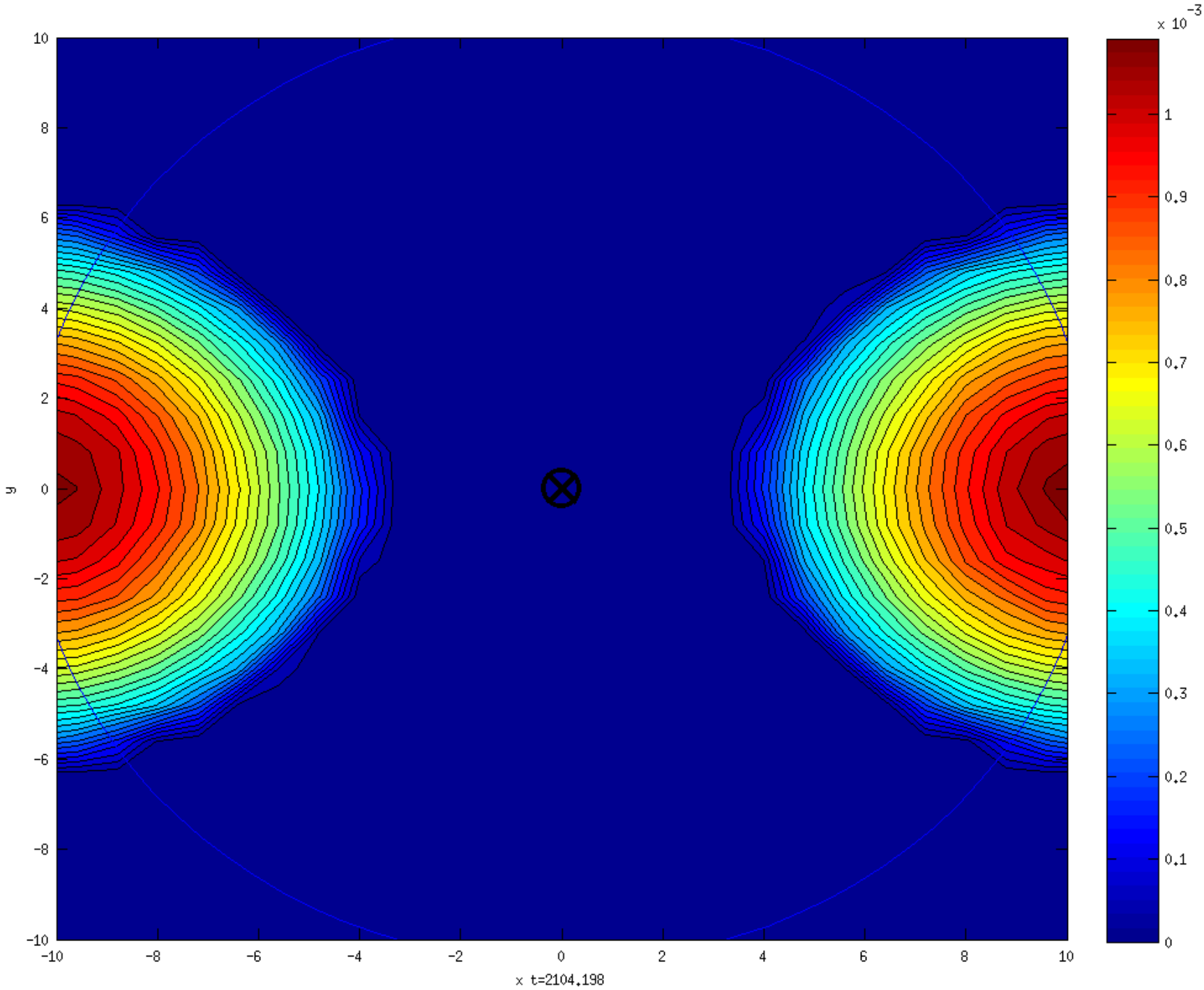
x 10^-3
1
0.9
0.8
0.7
0.6
0.5
0.4
0.3
0.2
0.1
0
10
8
6
4
2
0
-2
-4
-6
-8
-10
y
-10
-8
-6
-4
-2
0
2
4
6
8
10
x t=2104.198

Time-Frequency Analysis

Clark, Bauswein, NS, Shoemaker (2016)

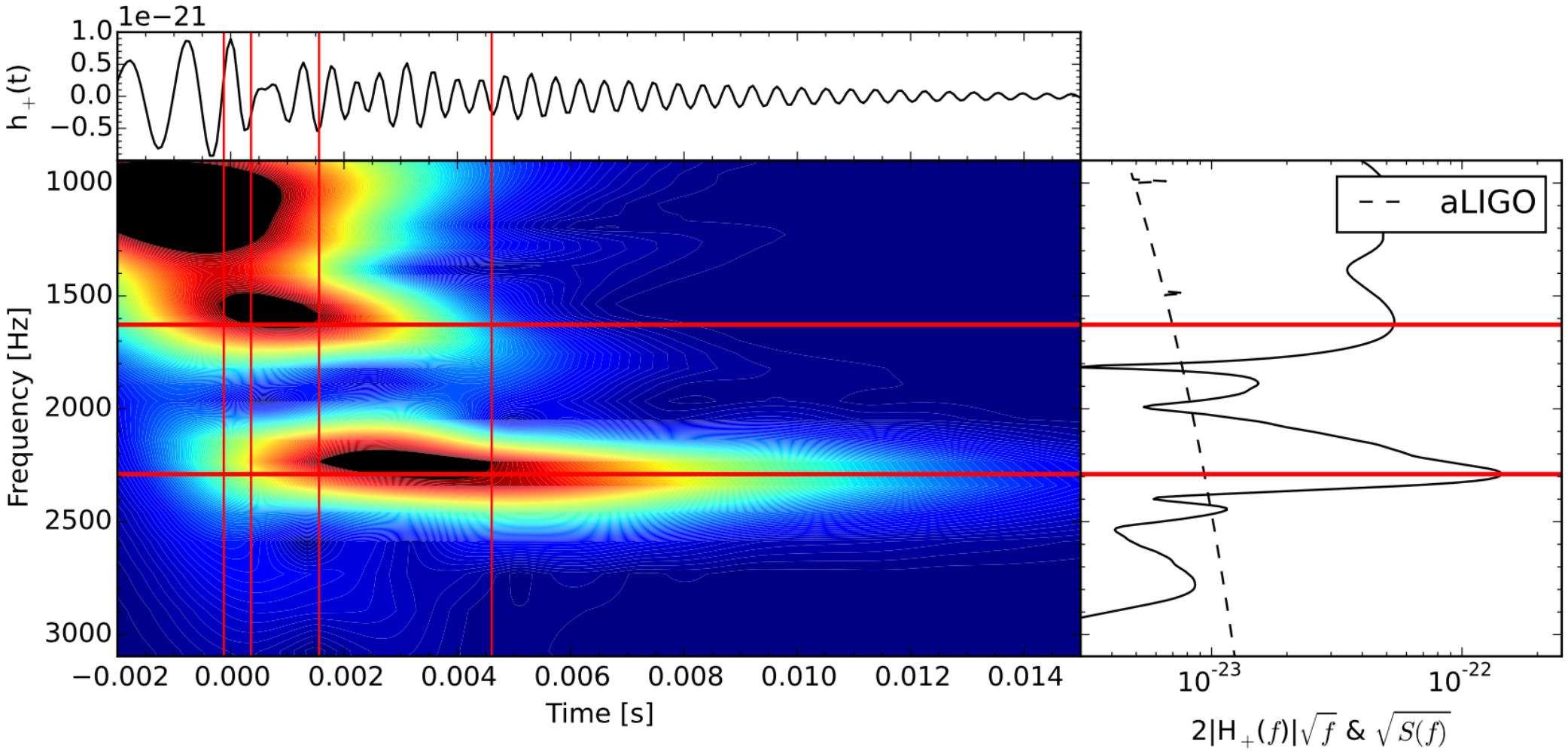

Post-Merger GW Oscillations

Stergioulas et al. (2011)

GRAVITATIONAL WAVES

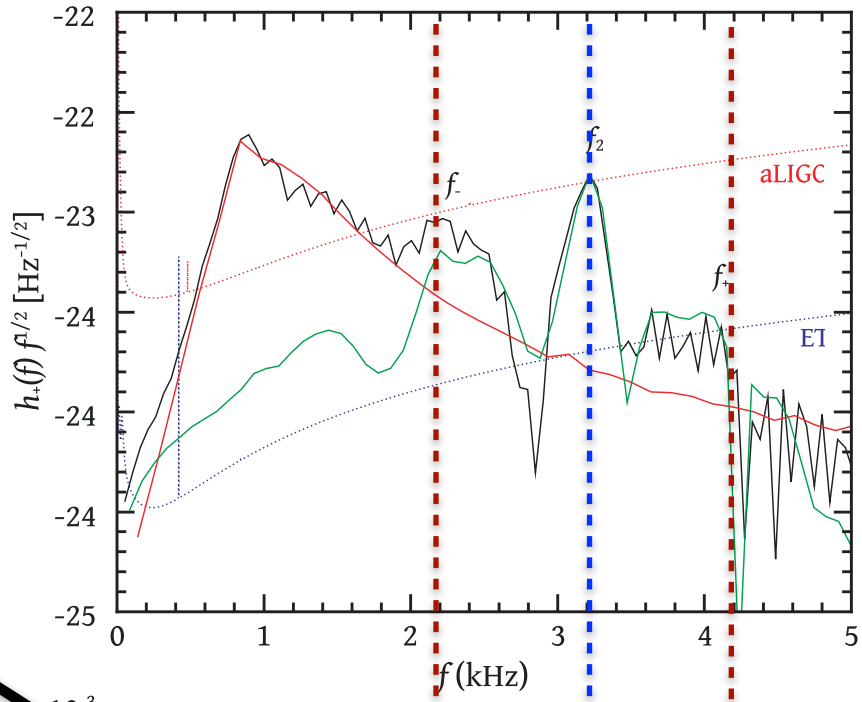

m=0 radial mode

HYDRODYNAMICS

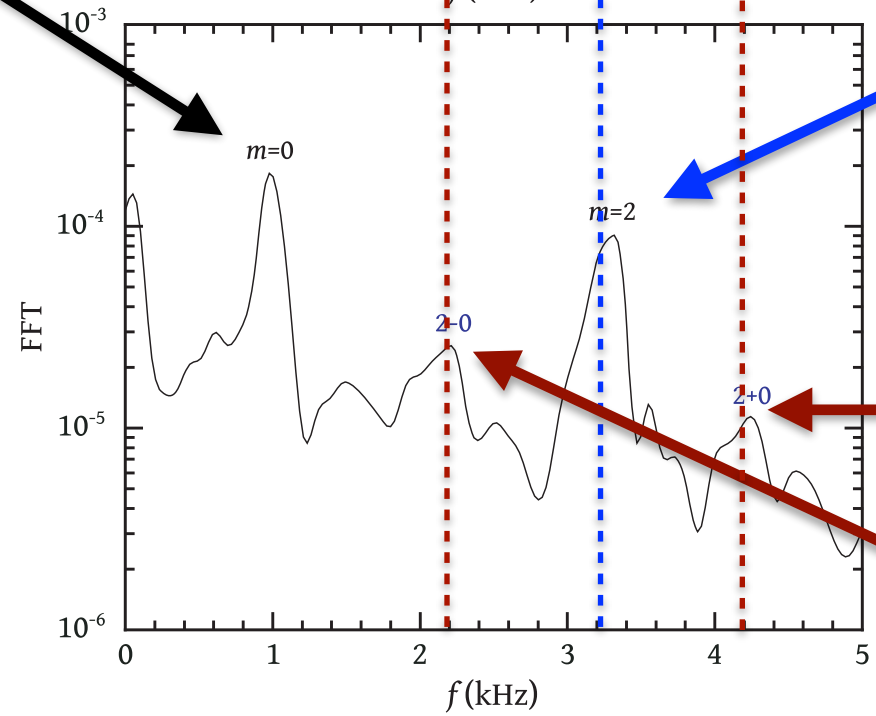

m=2 quadrupole mode

"2-0" and "2+0" quasi-linear combination frequency

Spiral Deformation

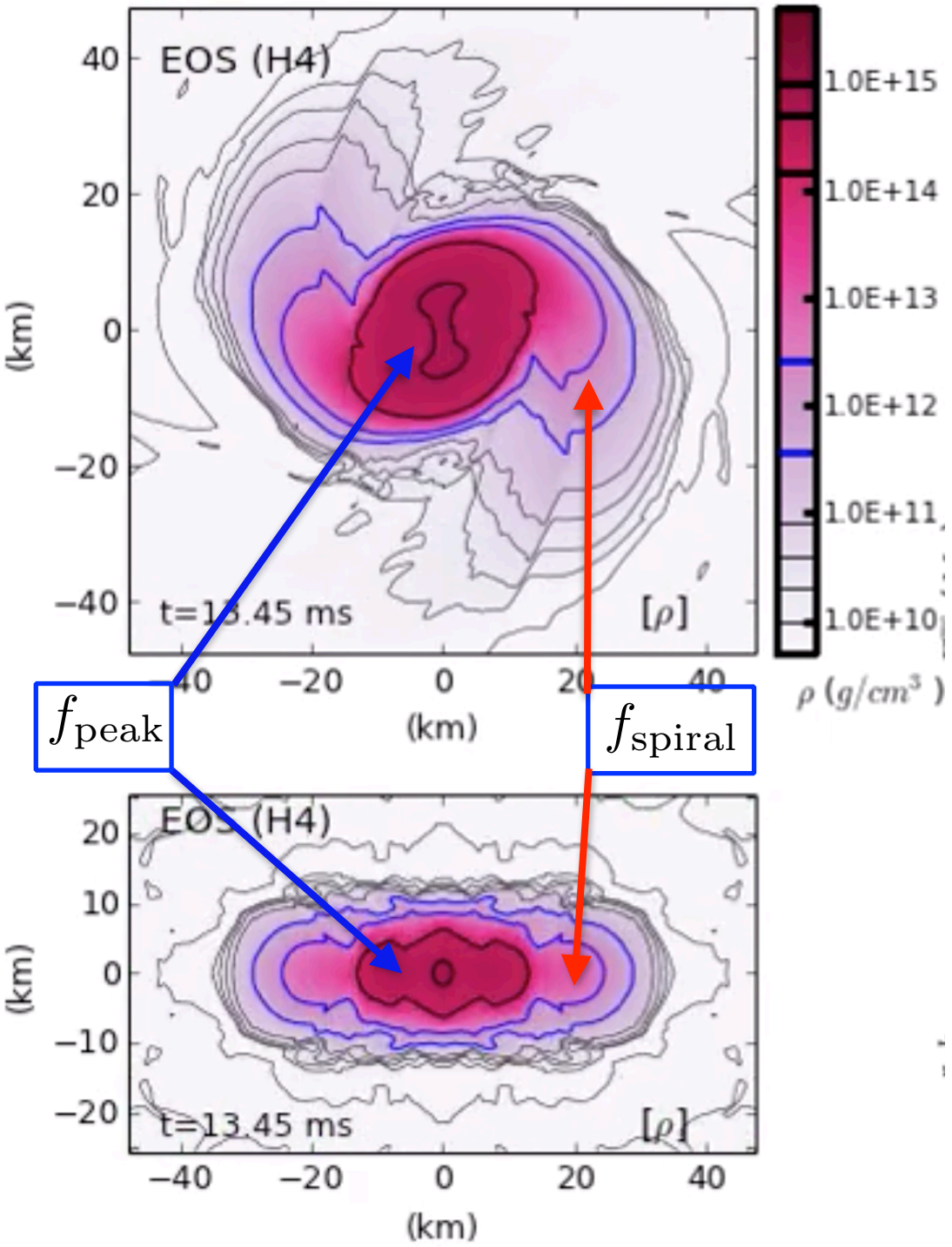

Three Detectable Post-Merger Frequencies

Bauswein & NS (2015)

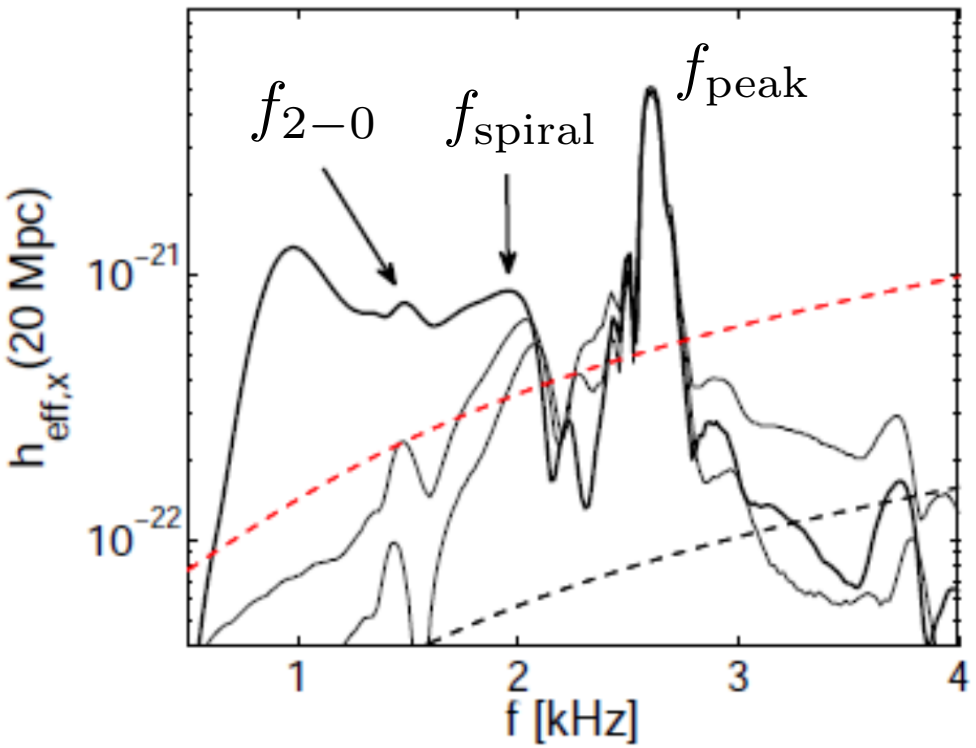

Three Detectable Post-Merger Frequencies

Bauswein & NS (2015)

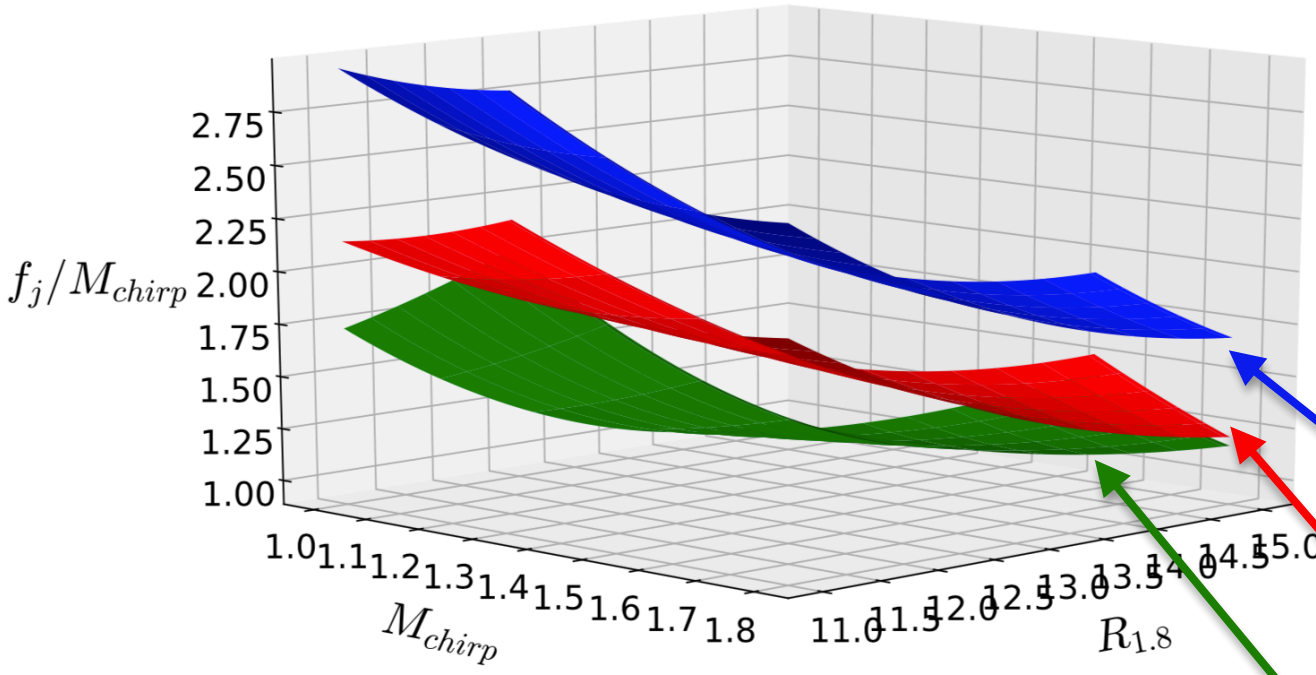

Vretinaris, NS & Bauswein (2019)

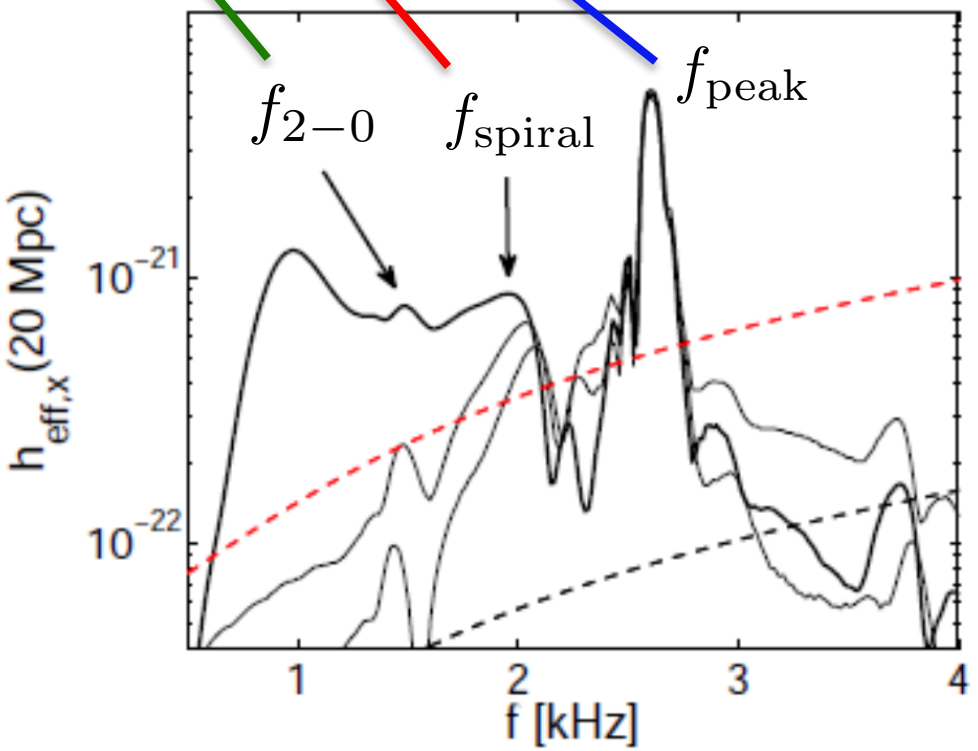

Spectral Classification Scheme

Bauswein & NS (2015)

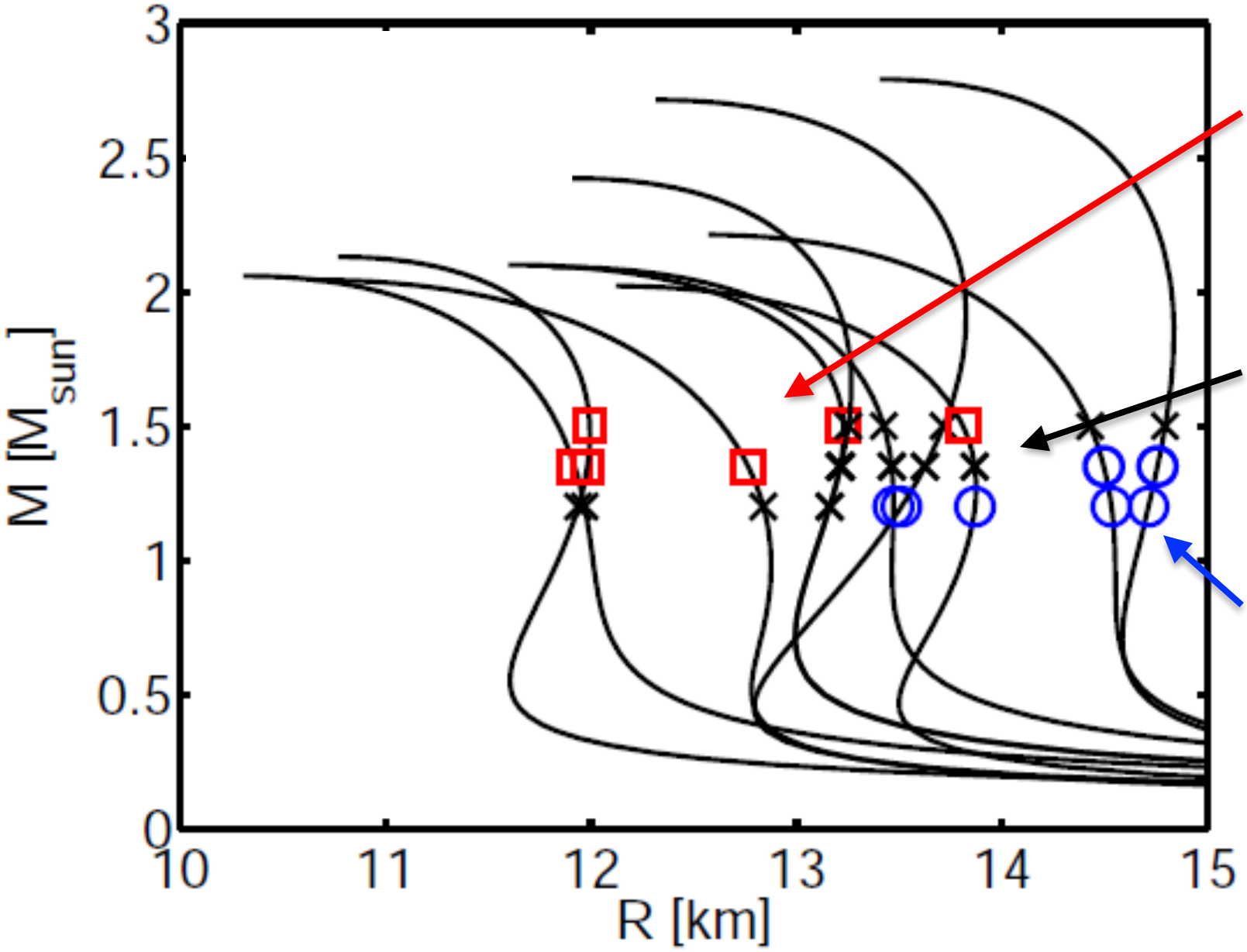

Type I:

$A_{2-0} > A_{\rm spiral}$

Type II:

$A_{2-0} \sim A_{\rm spiral}$

Type III:

$A_{2-0} < A_{\rm spiral}$

Spectral Classification using Machine Learning

Vretinaris, NS & Bauswein (2019)

Clustering: *Affinity Propagation* (Scikit-Learn)
Classification via neural network: *Multi-layer Perceptron (MLP) supervised learning*

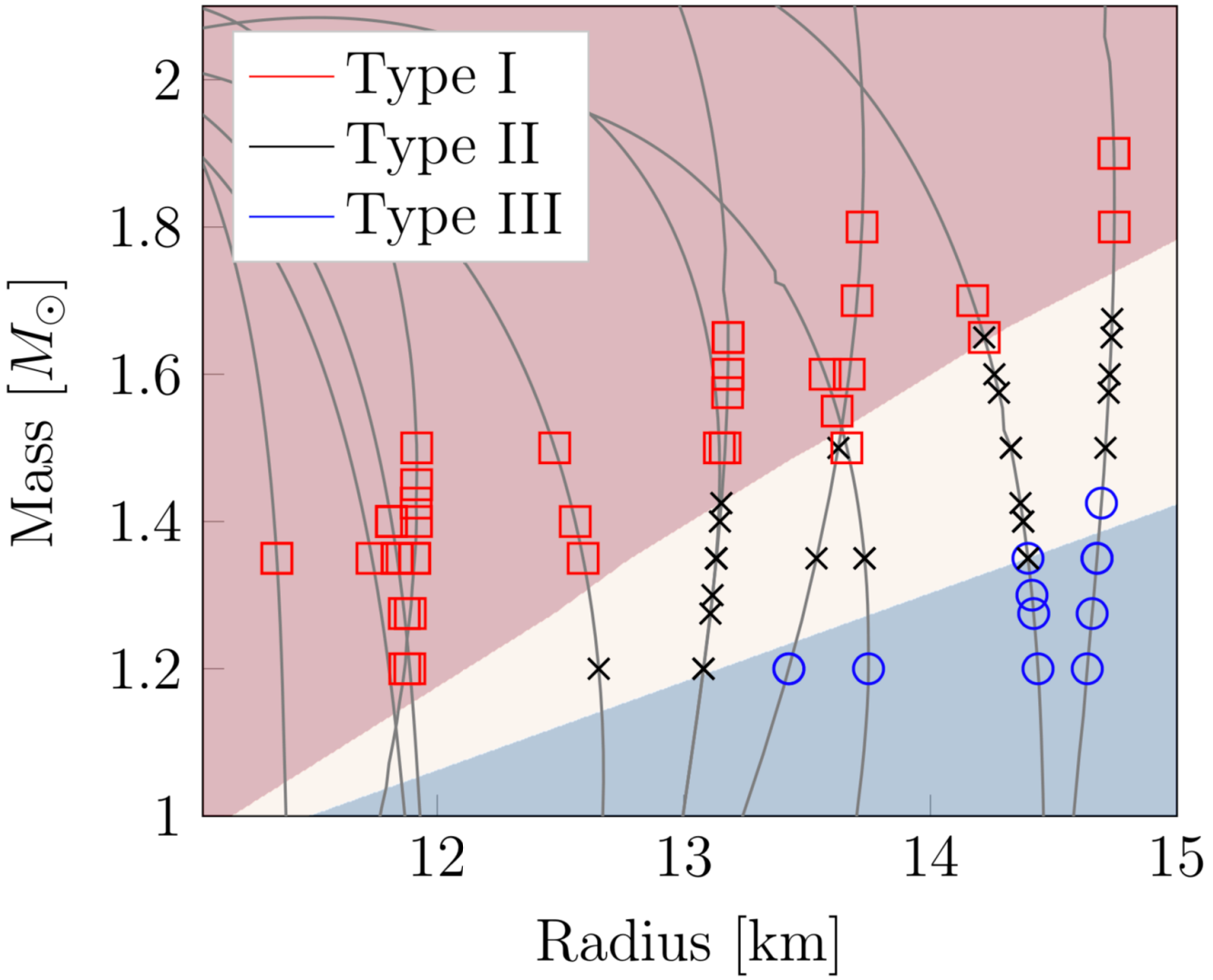

GW Asteroseismology for Isolated Stars

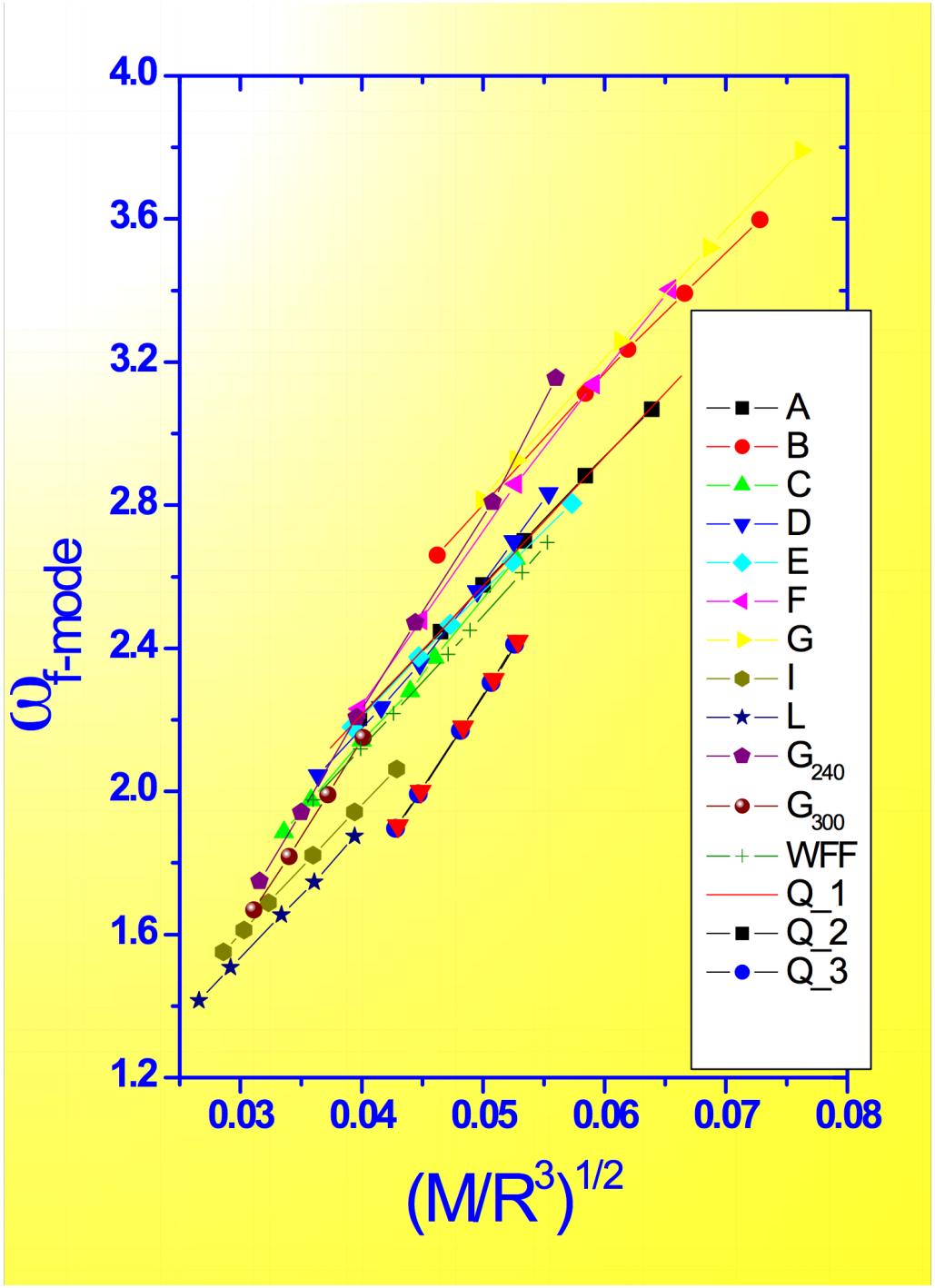

Empirical relations for GW asteroseismology:

$$\omega_f\,(kHz) \approx 0.78 + 1.637\left(\frac{M_{1.4}}{R_{10}^{\ 3}}\right)^{1/2}$$

Andersson & Kokkotas (1998)

Recently extended to fast rotation by Krueger and Kokkotas (2019) !

Radius Determination from Post-Merger Signal

Bauswein et al. (2012)

Bauswein, NS, Janka (2016)

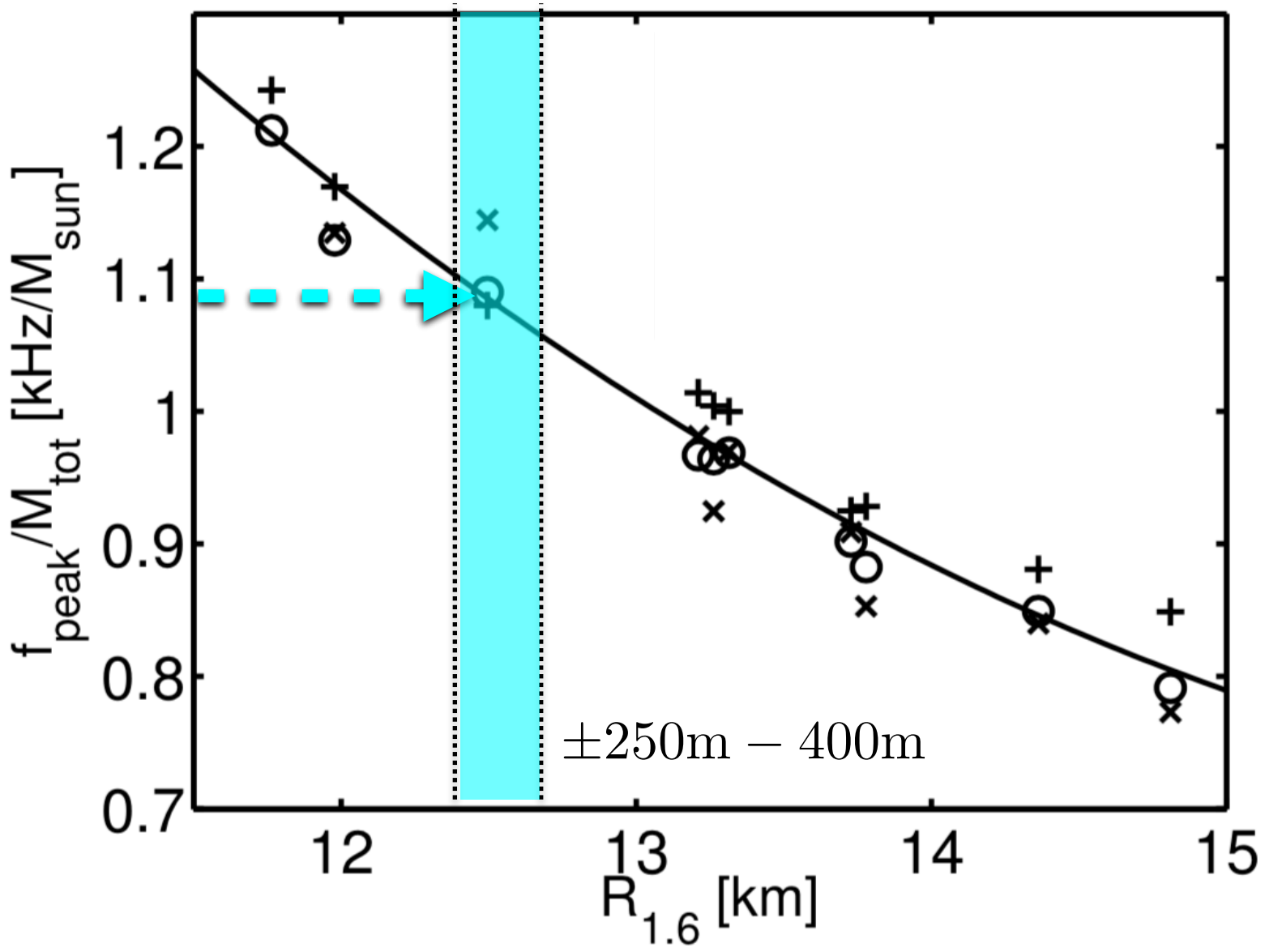

Asymmetric Mergers

Bauswein, NS & Janka (2016)

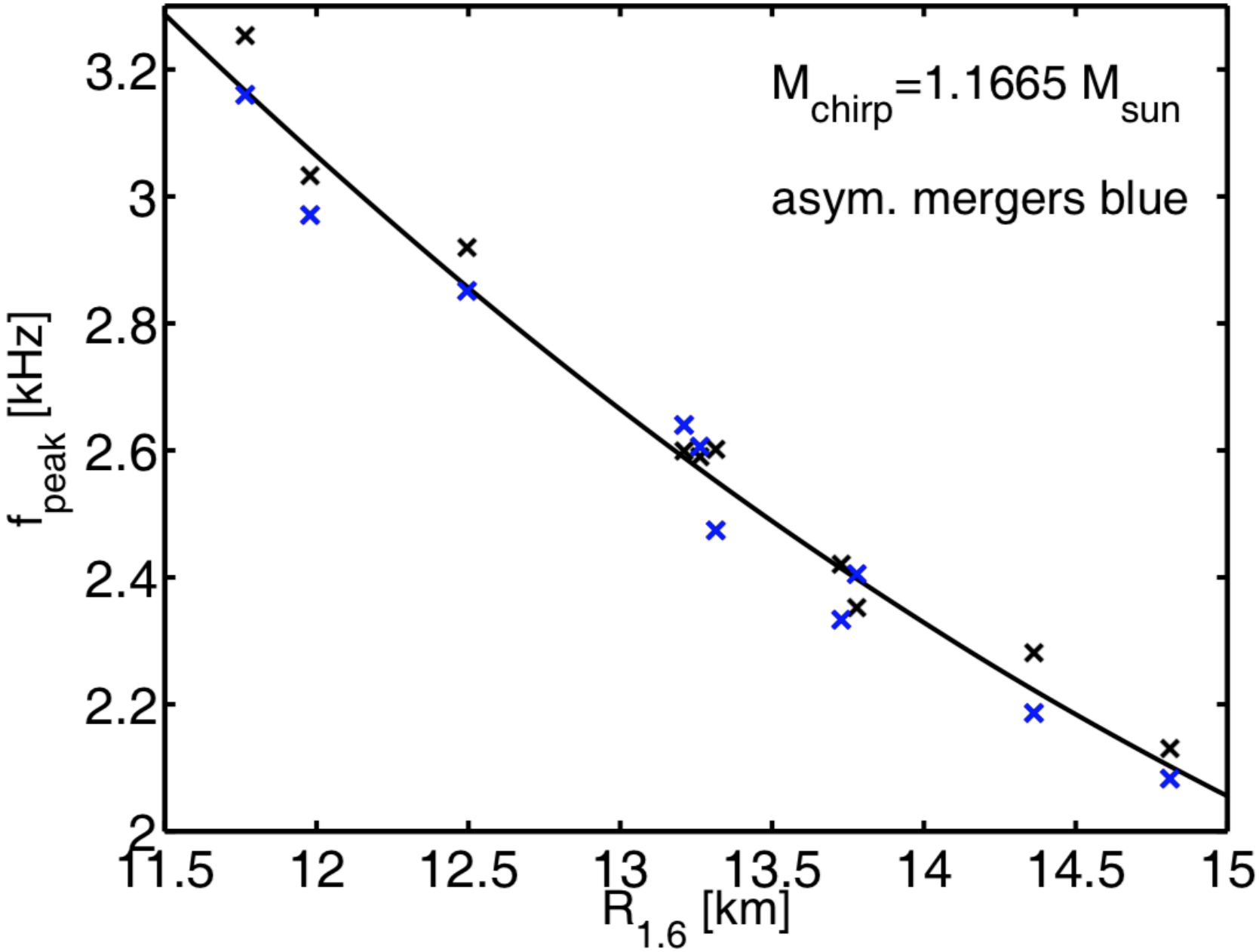

EOS with Strong Phase Transition

Bauswein et al. (2018)

A strong first-order phase transition will have a significant effect on radius extraction.

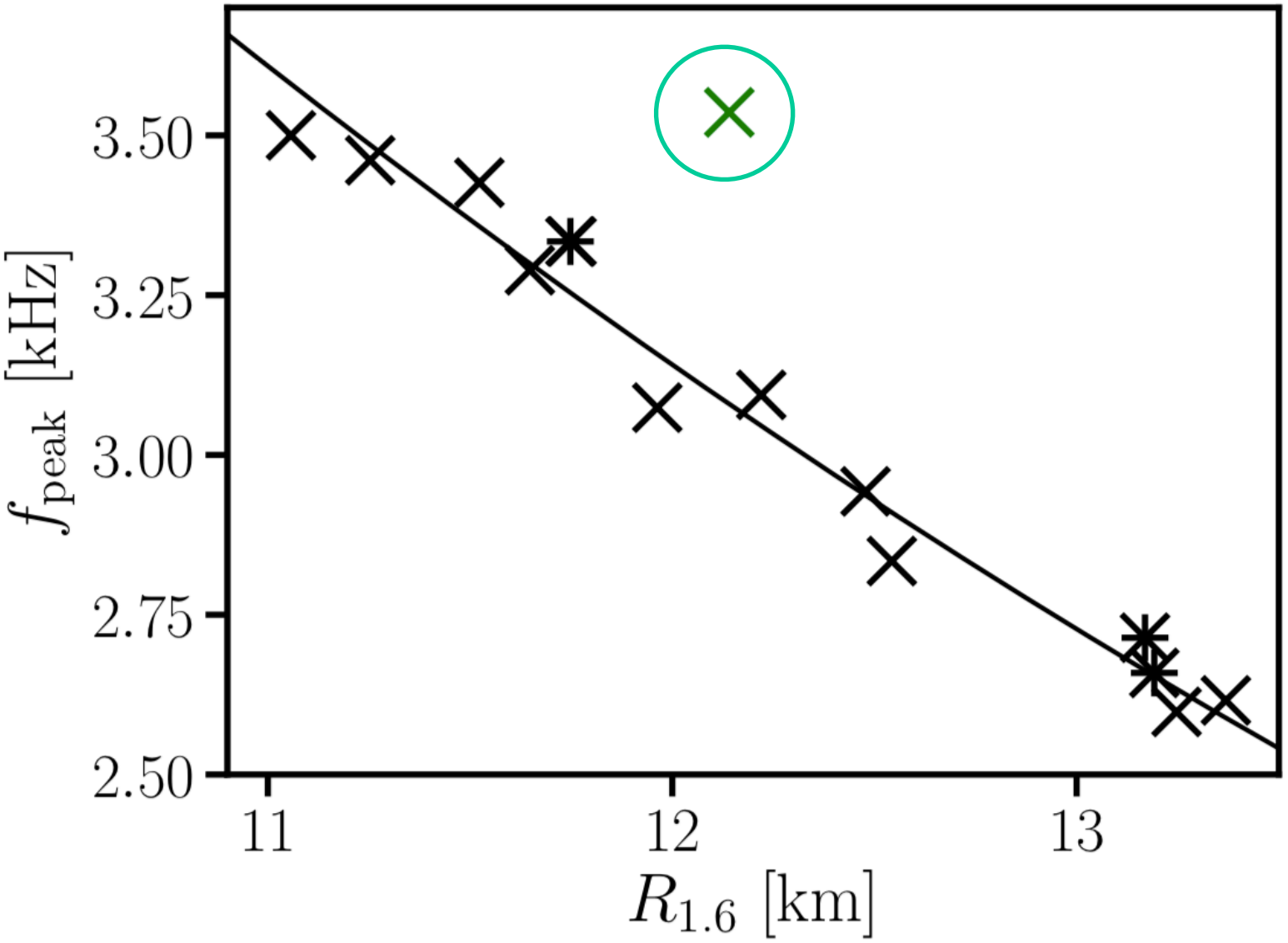

Multi-variate Empirical Relations

Vretinaris, NS & Bauswein (2019)

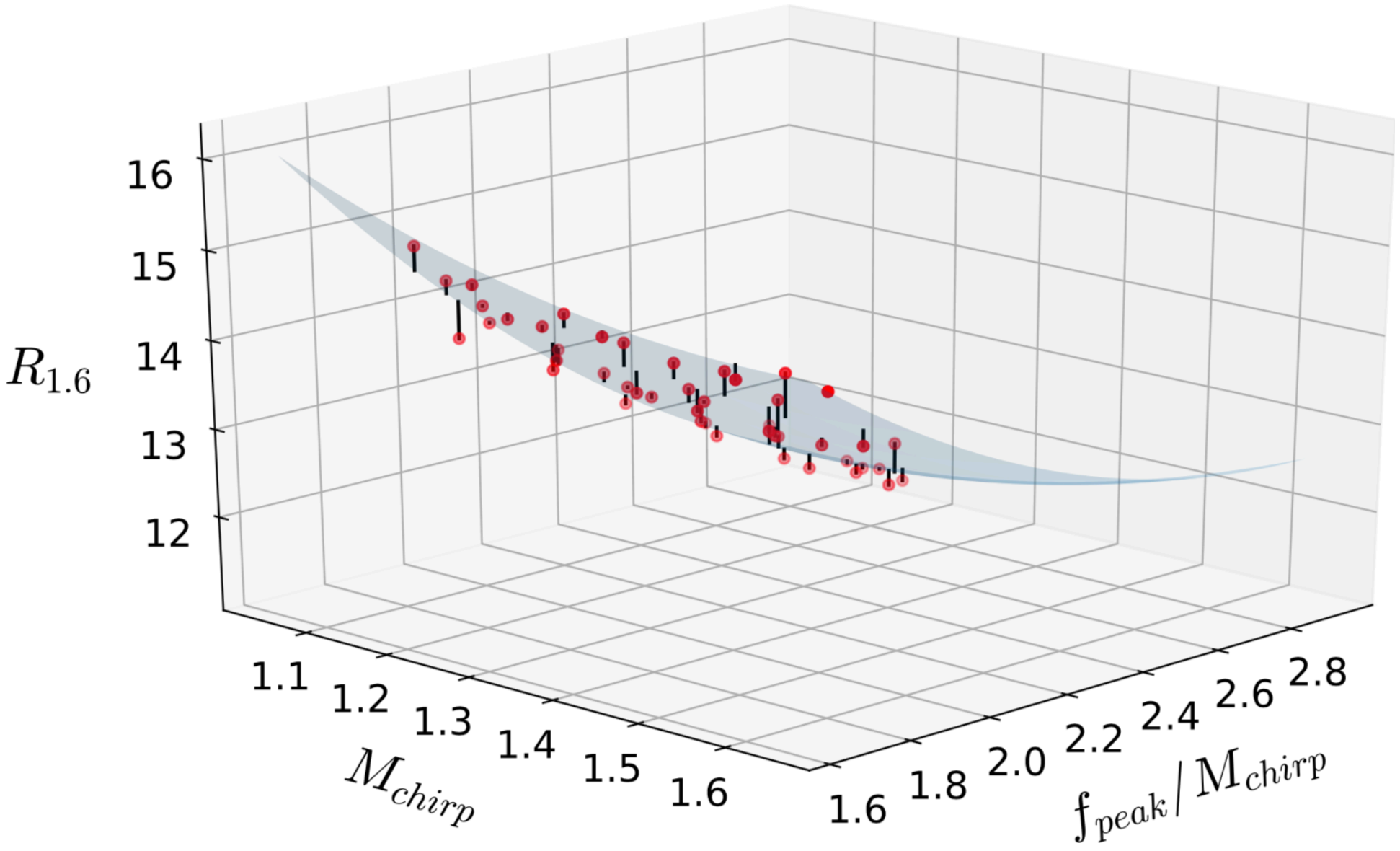

Multi-variate Empirical Relations

Vretinaris, NS & Bauswein (2019)

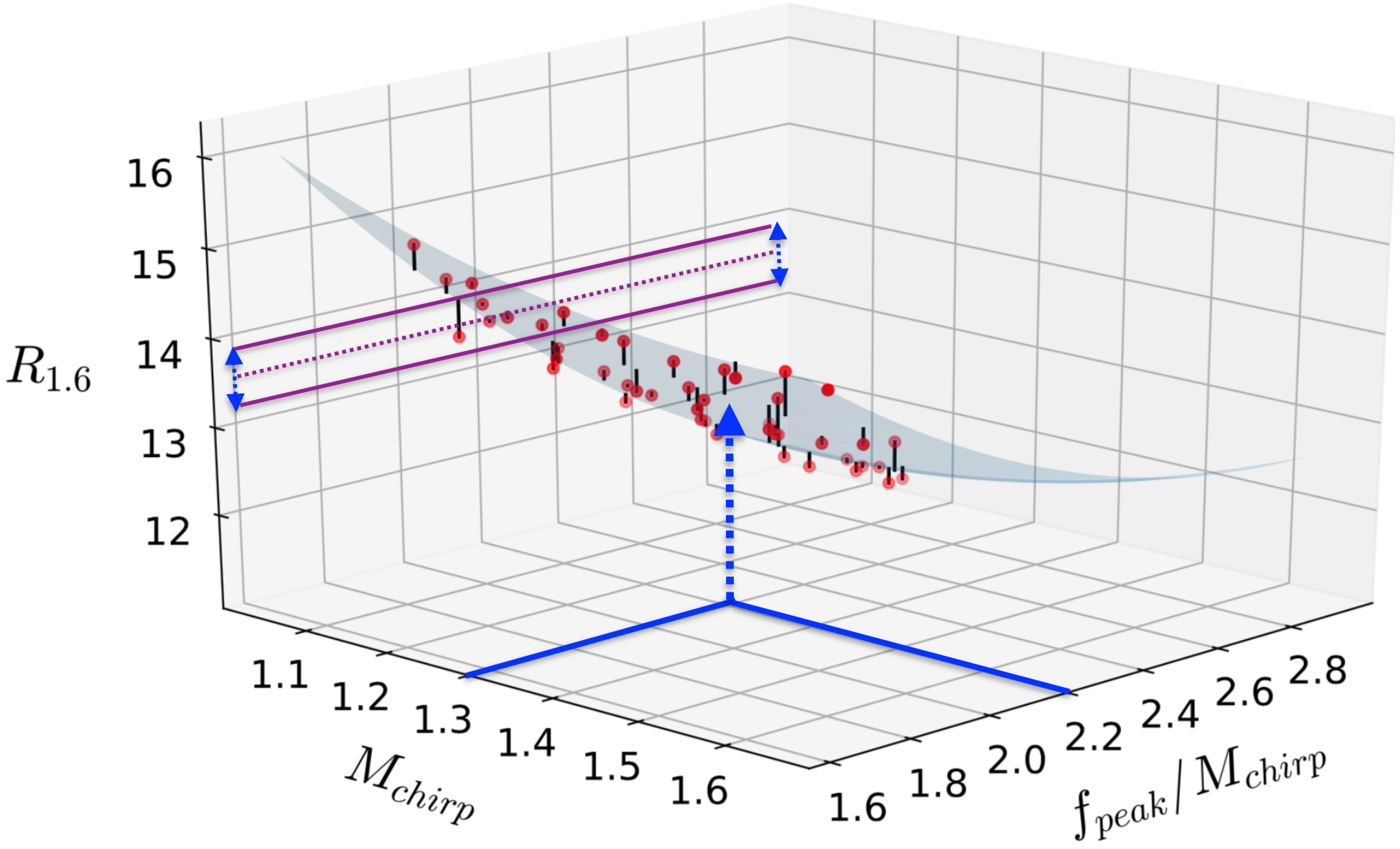

Reconstructing the M-R Diagram

Vretinaris, NS & Bauswein (2019)

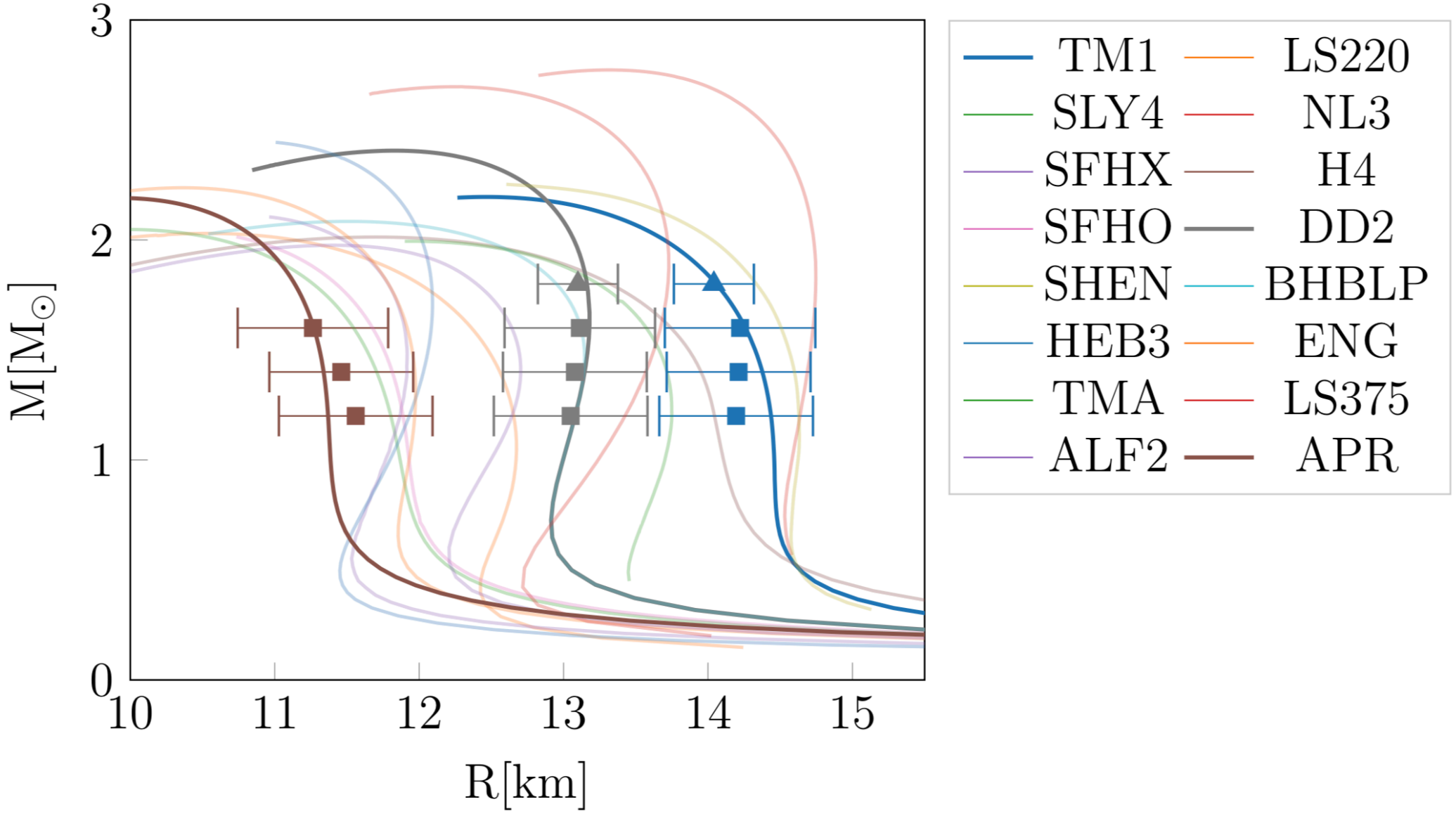

Λ through Post-merger Oscillations

Vretinaris, NS & Bauswein (2019)

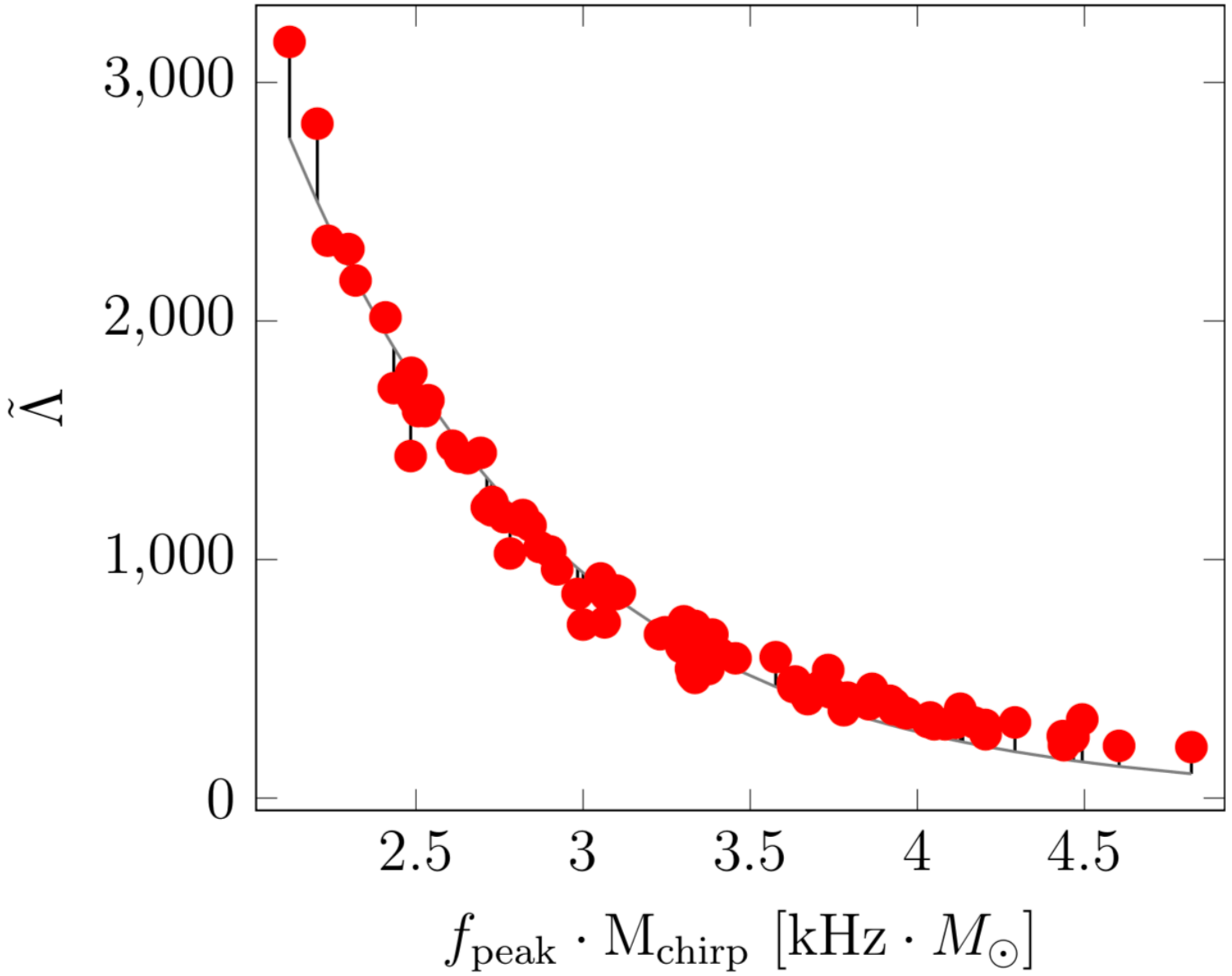

Λ through Post-merger Oscillations

Vretinaris, NS & Bauswein (2019)

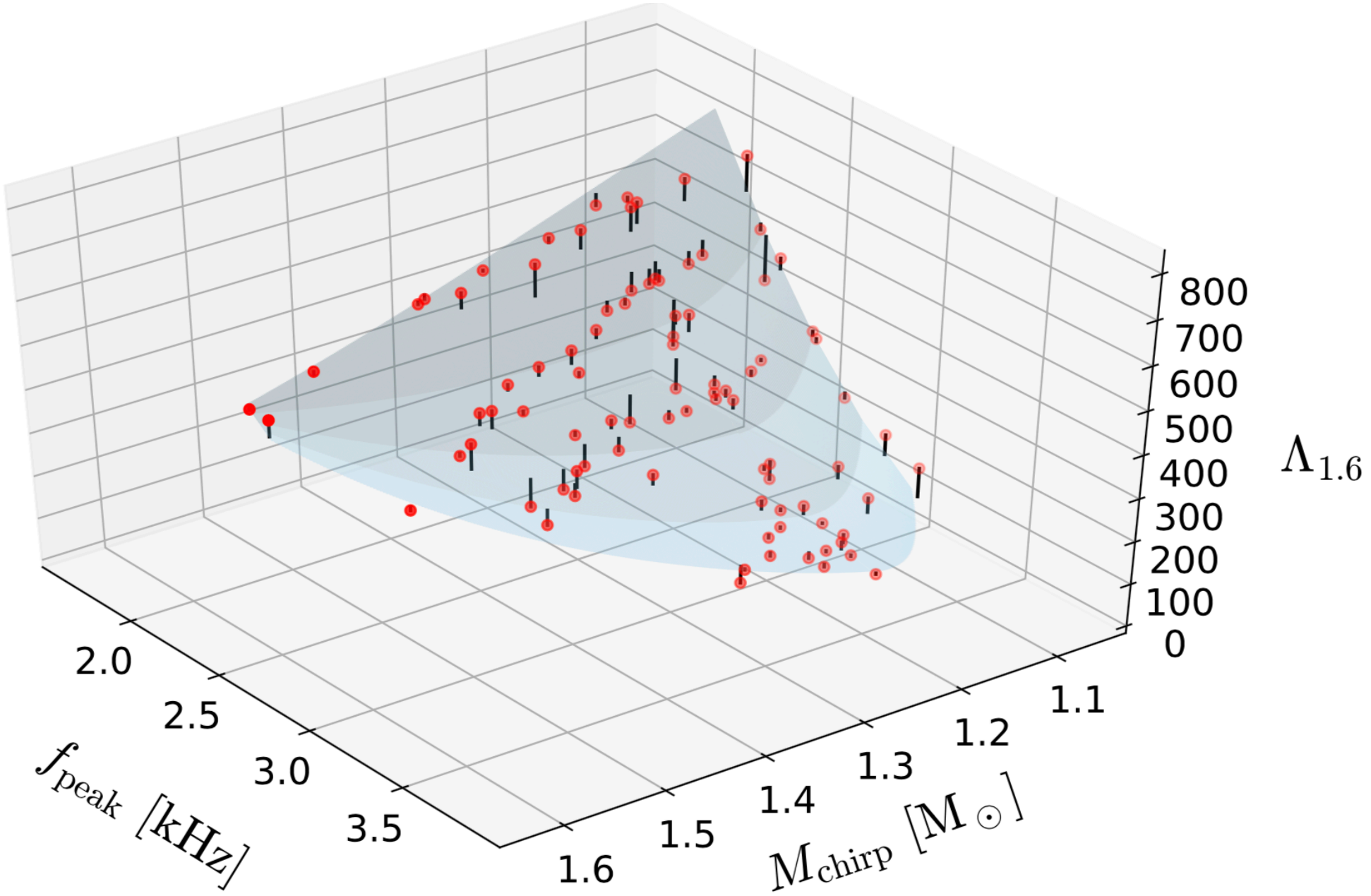

Extrapolating to Larger Masses

Bauswein, NS, Janka (2014)

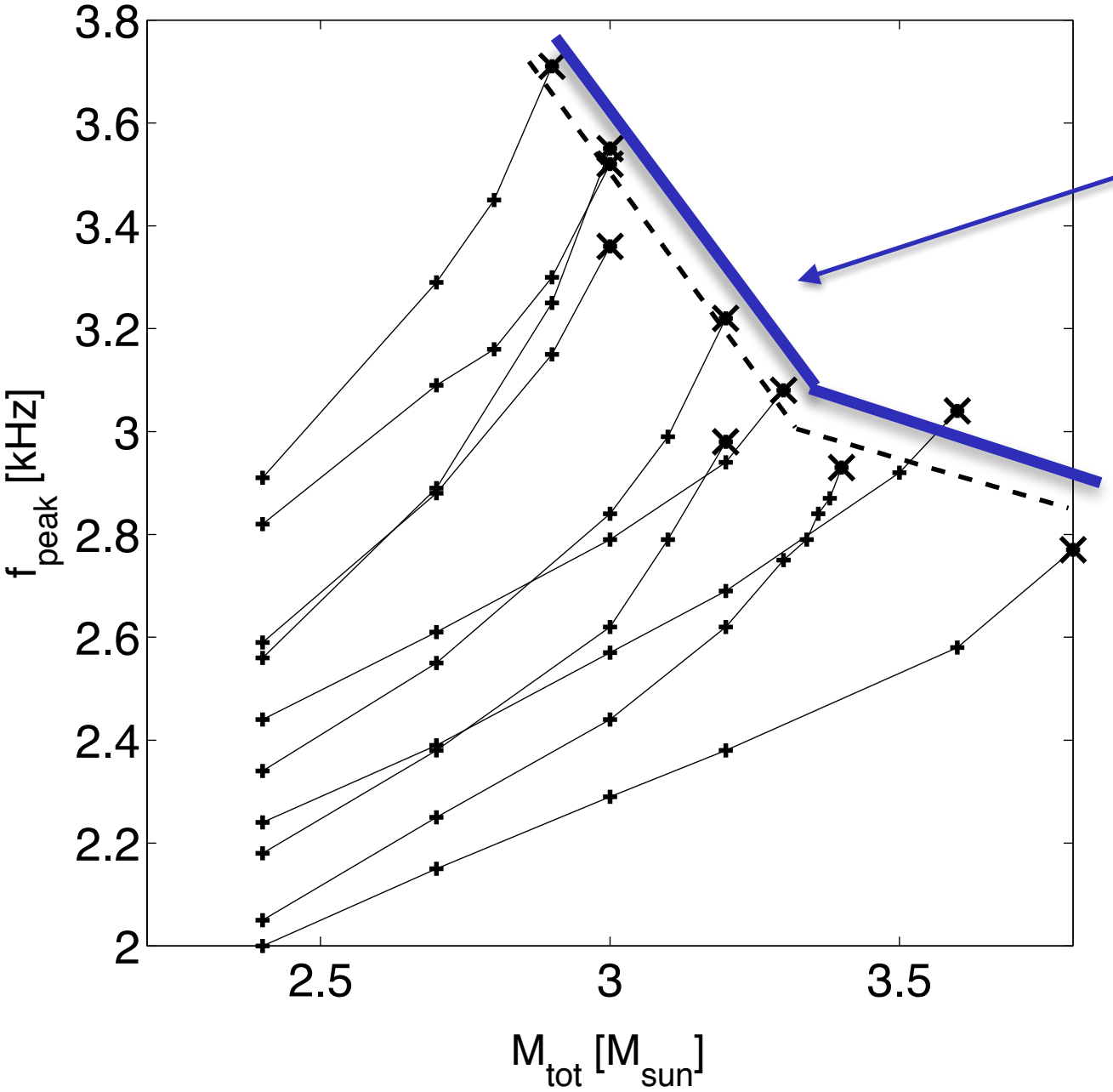

threshold
to collapse

Extrapolating to Larger Masses

Bauswein, NS, Janka (2014)

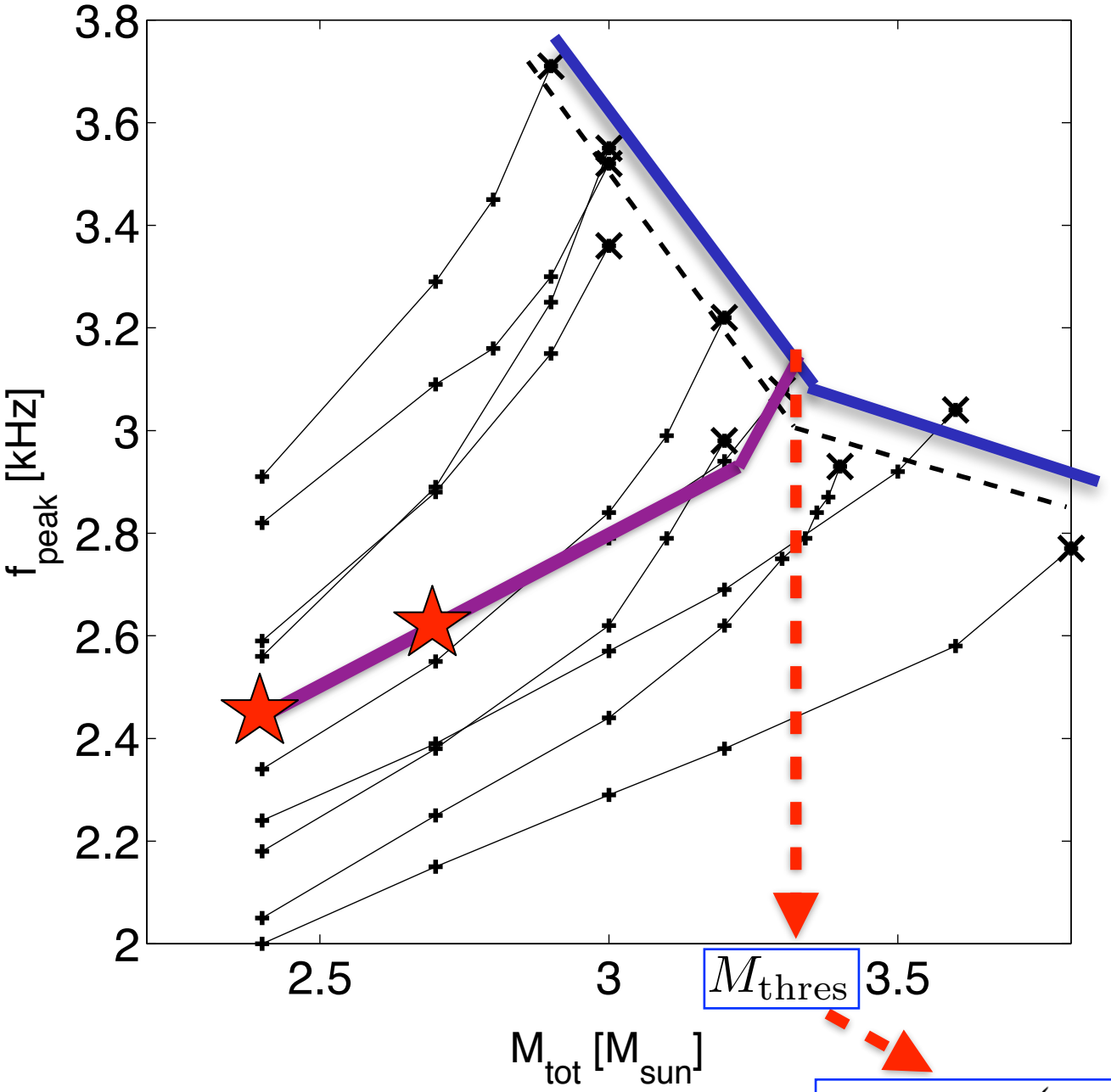

$M_{\rm max}$

$$M_{\rm thres} = \left(-3.606 \frac{G M_{\rm max}}{c^2 R_{1.6}} + 2.38 \right) \cdot M_{\rm max}$$

Extrapolating to Larger Masses

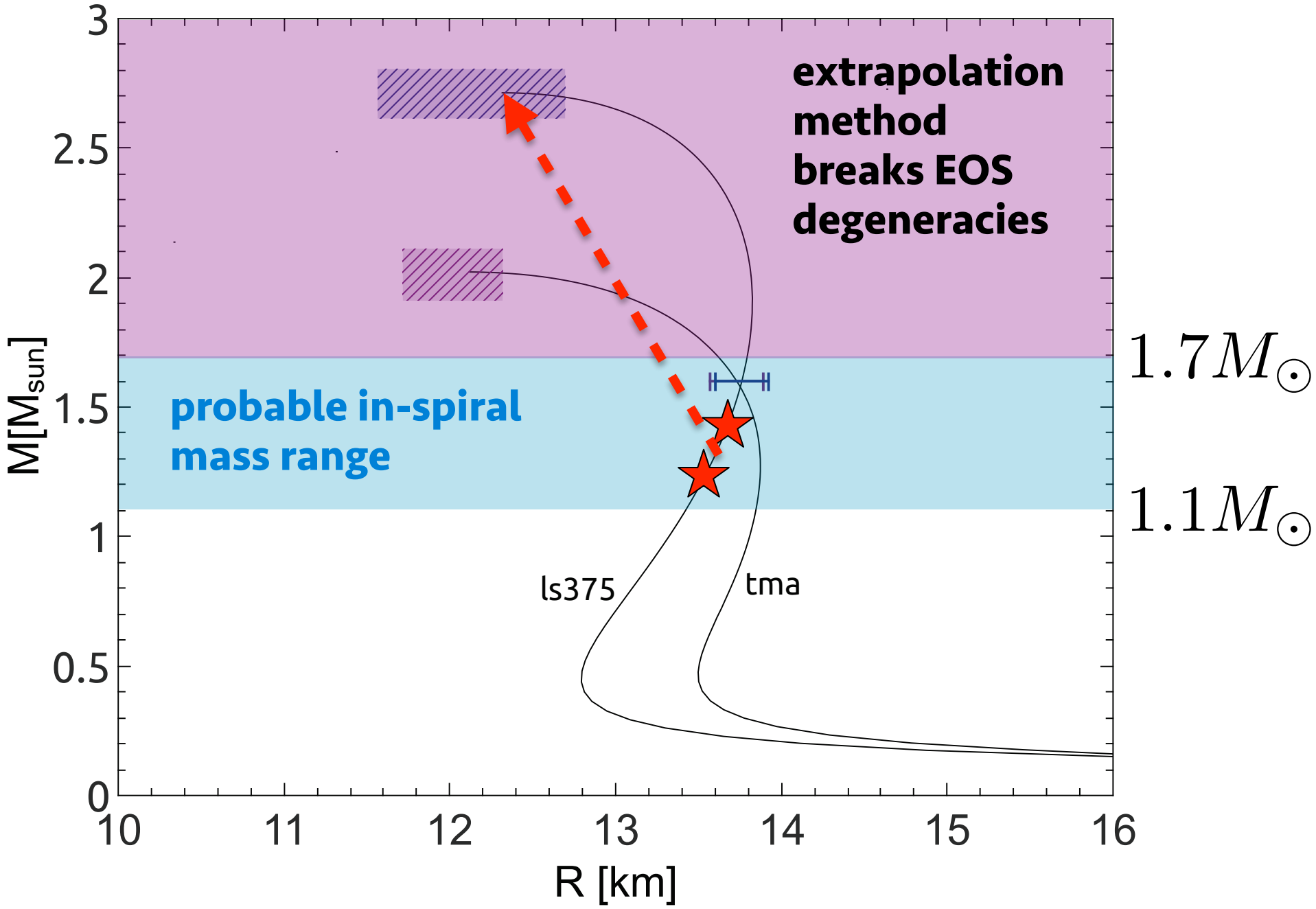

Detectability

Clark, Bauswein, NS, Shoemaker (2016)

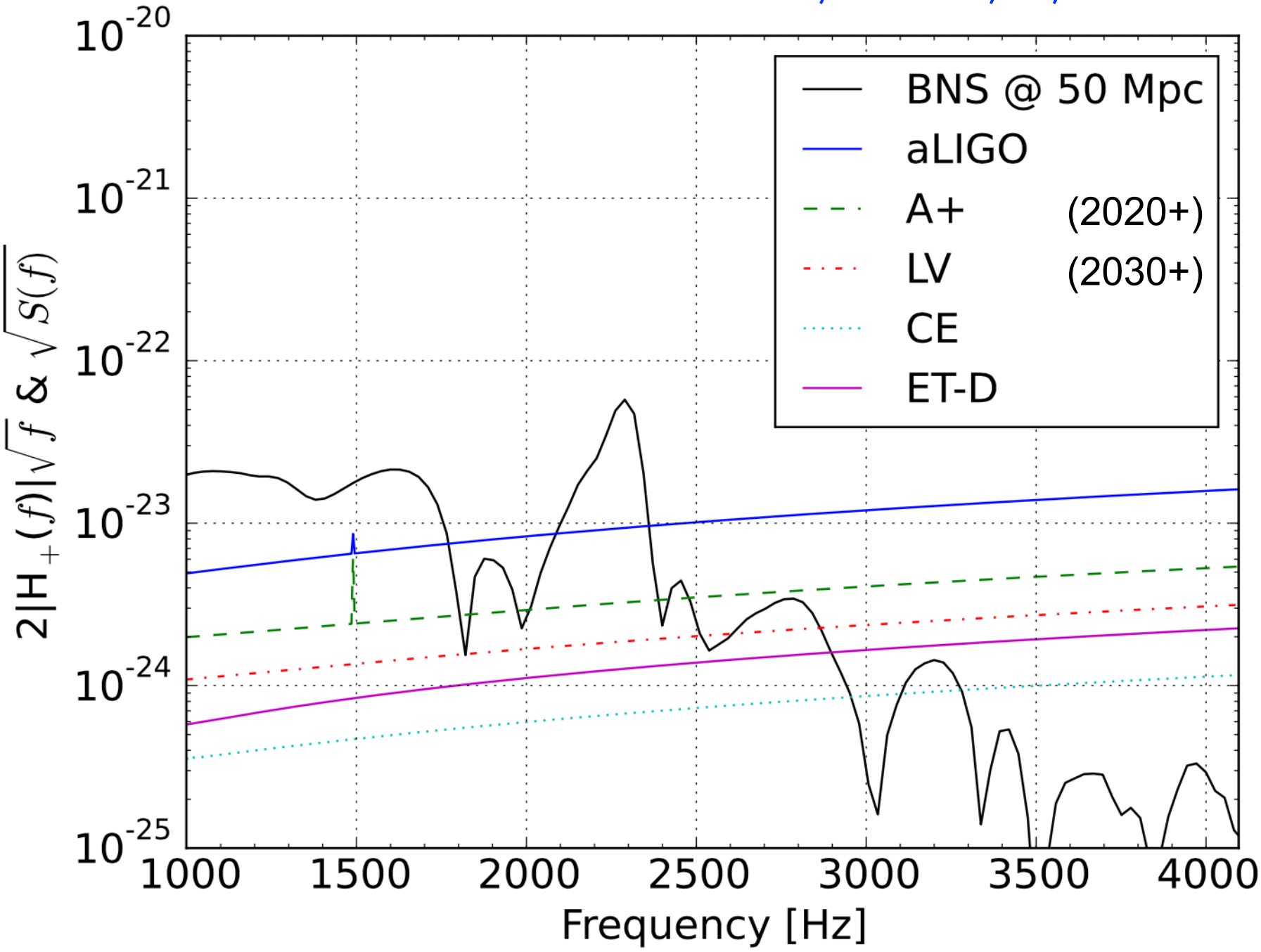

Coherent Wave Burst Analysis

Clark, Bauswein, Cadonati, Janka, Pankow, NS (2014)

A simple burst algorithm only recovers ~40% of the input signal.

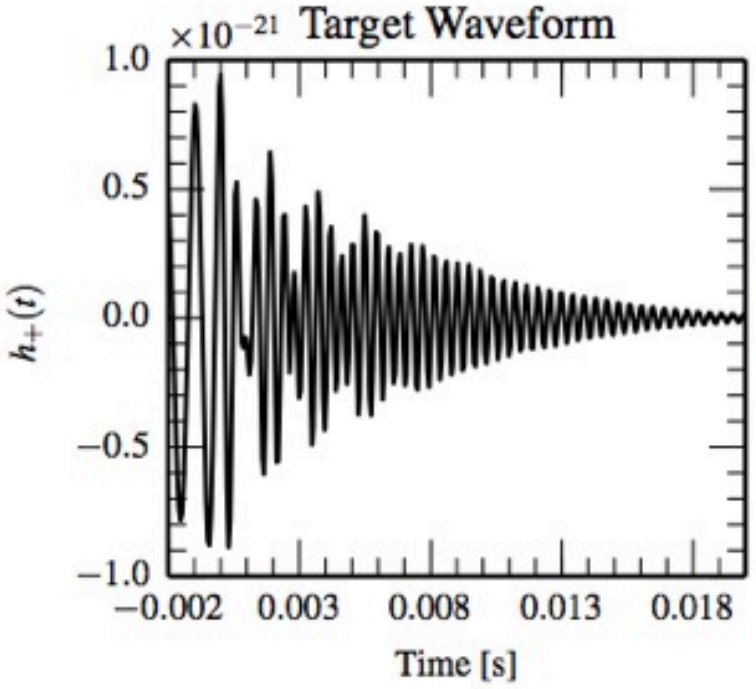

Fit to reconstructed spectrum

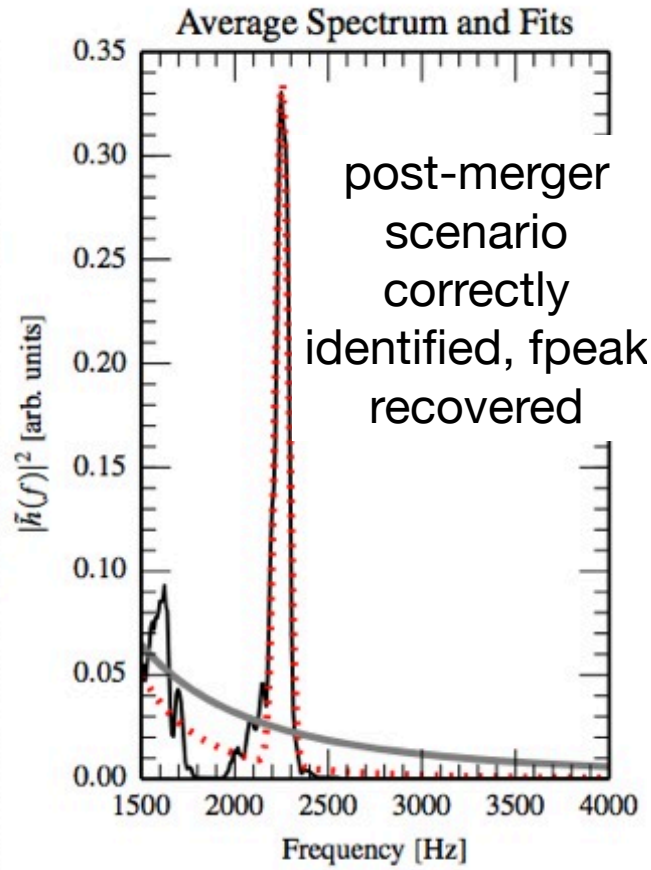

post-merger scenario correctly identified, fpeak recovered

Principal Component Analysis (PCA)

Clark, Bauswein, NS, Shoemaker (2016)

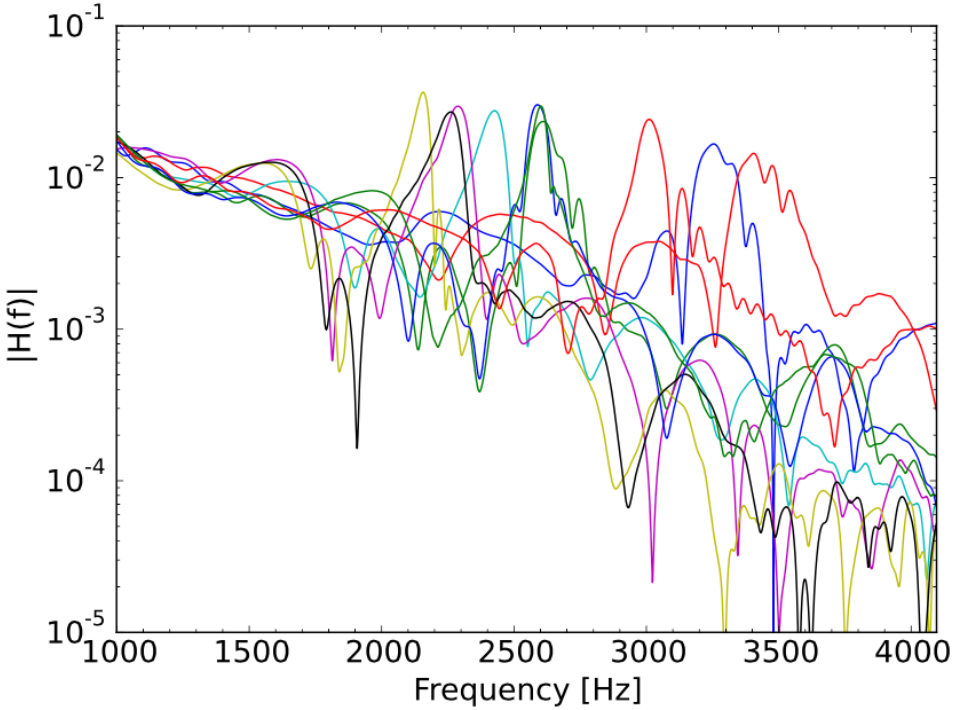

Actual fft's for different models.

Principal Component Analysis (PCA)

Clark, Bauswein, NS, Shoemaker (2016)

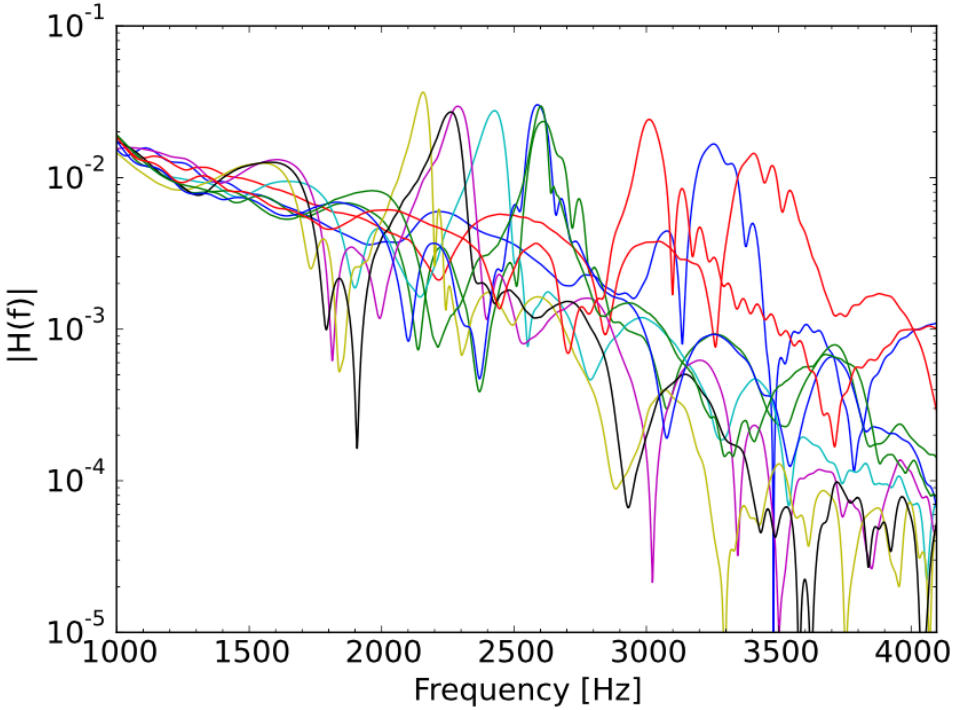

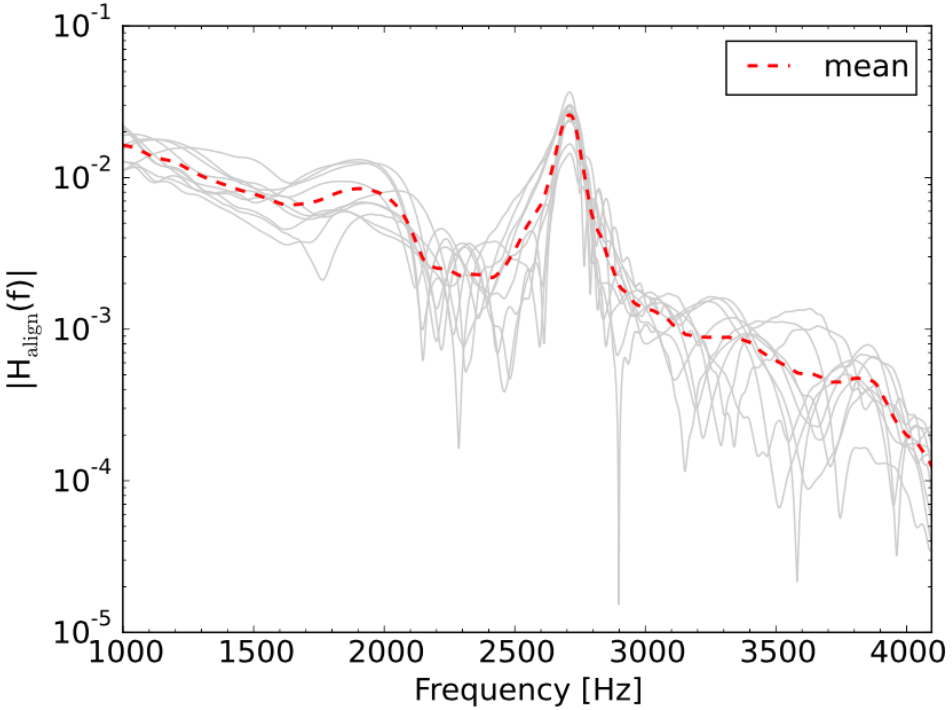

Actual fft's for different models.

Rescaled to common reference model.

Principal Component Analysis (PCA)

Clark, Bauswein, NS, Shoemaker (2016)

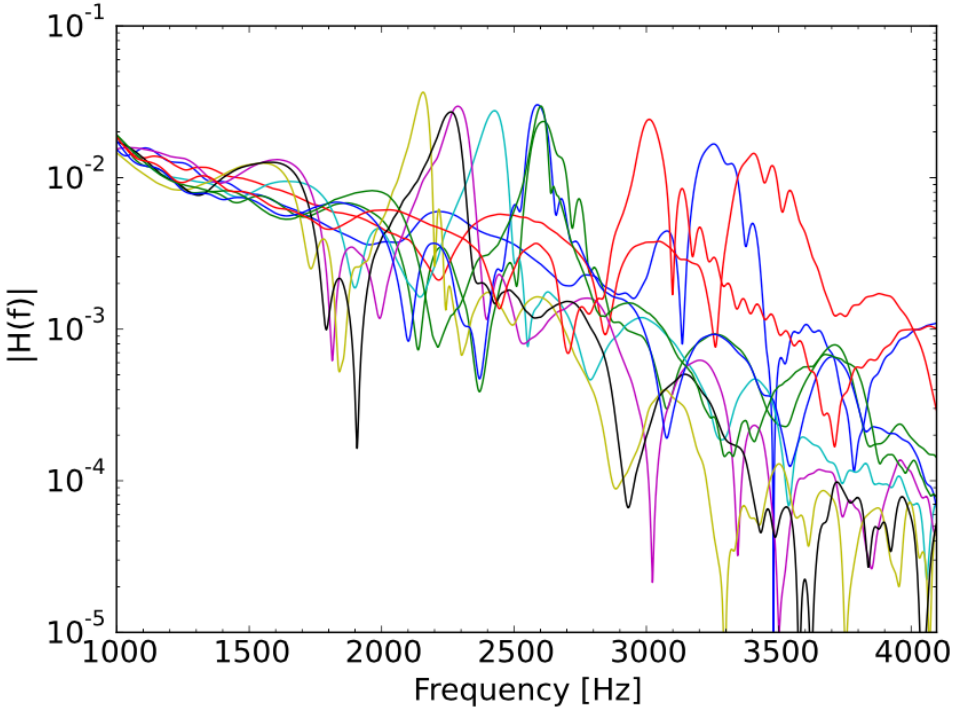

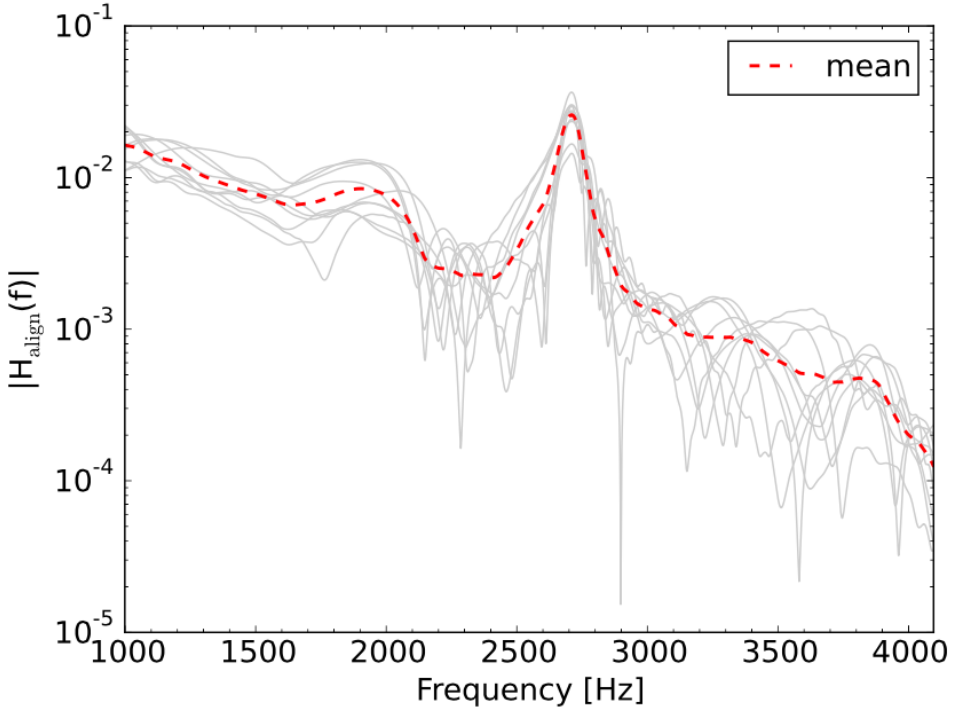

Actual fft's for different models.

Rescaled to common reference model.

The PCA template extracts >90% of signal power compared to only 40% when using simple burst analysis.

PCA Reconstruction of signal

Clark, Bauswein, NS, Shoemaker (2016)

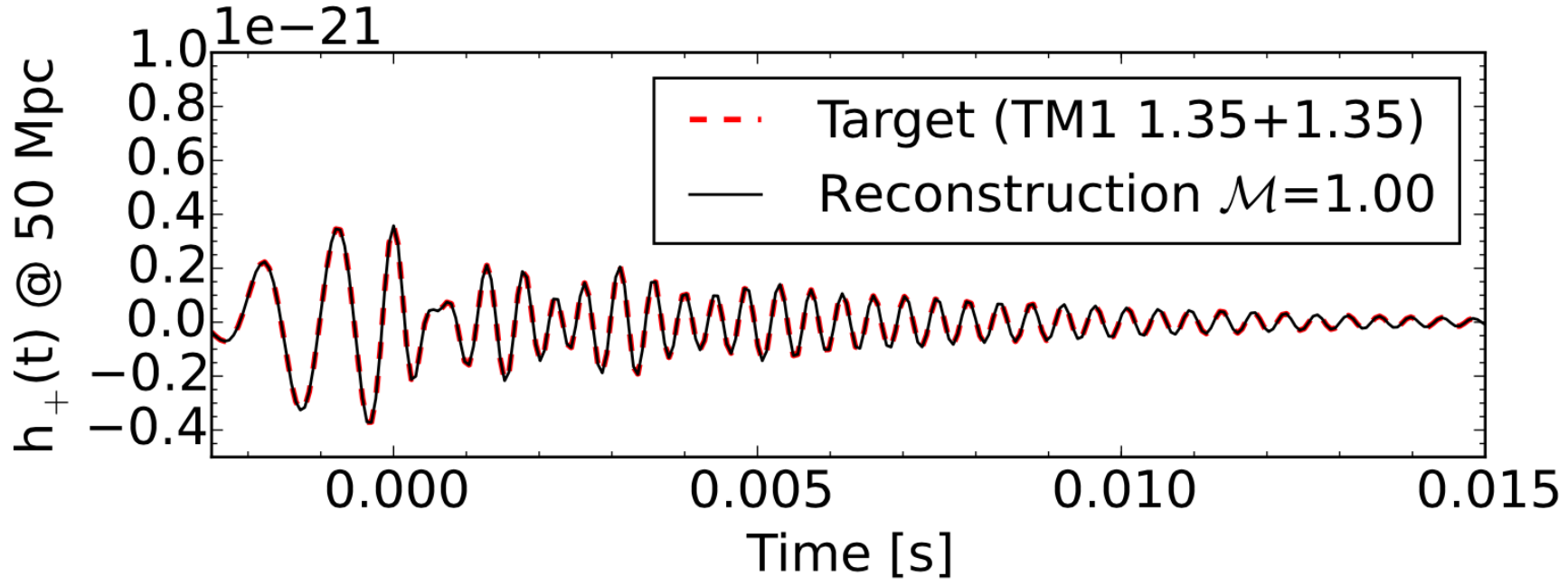

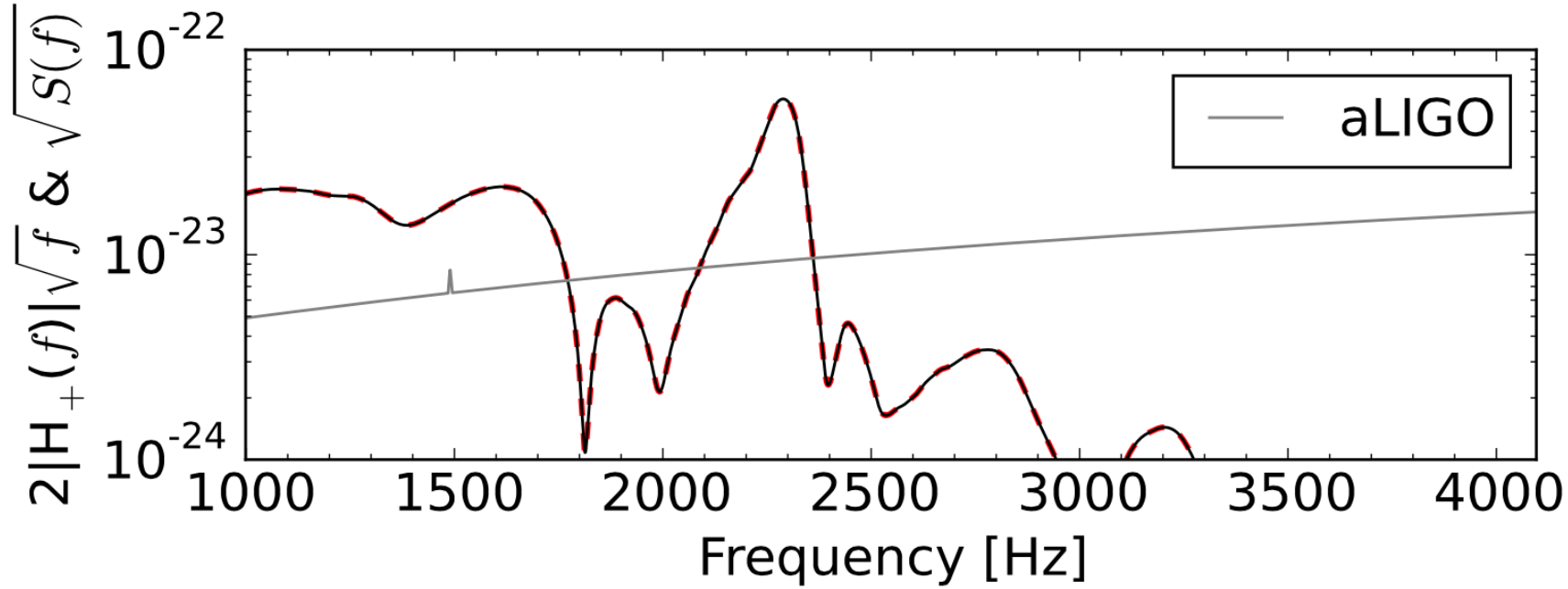

Detectability of Post-Merger GWs

Clark, Bauswein, NS, Shoemaker (2016)

Single-detector detectability (S/N>5, optimal orientation)

Instrument	$\mathrm{SNR}_{\mathrm{full}}$	$\mathrm{SNR}_{\mathrm{post}}$	D_{hor} [Mpc]	$\dot{\mathcal{N}}_{\mathrm{det}}$ [year^{-1}]	
aLIGO	$2.99^{3.86}_{2.37}$	$1.48^{1.86}_{1.13}$	$29.89^{38.57}_{23.76}$	$0.01^{0.03}_{0.01}$	2G
A+	$7.89^{10.16}_{6.25}$	$4.19^{5.35}_{3.26}$	$78.89^{101.67}_{62.52}$	$0.13^{0.20}_{0.10}$	2G+
LVoyager	$14.06^{18.13}_{11.16}$	$7.28^{9.30}_{5.64}$	$140.56^{181.29}_{111.60}$	$0.41^{0.88}_{0.21}$	
ET-D	$26.65^{34.28}_{20.81}$	$12.16^{15.31}_{9.34}$	$266.52^{342.80}_{208.06}$	$2.81^{5.98}_{1.33}$	3G
CE	$41.50^{53.52}_{32.99}$	$20.52^{25.83}_{15.72}$	$414.62^{535.221}_{329.88}$	$10.59^{22.78}_{5.33}$	

Improvements:

- **Network of 5 detectors**
- **Stacking of several detections (e.g. Bose et al. 2018)**
- **Improved templates**

Detectability of GW170817-like Events

Torres-Rivas, Chatziioannou, Bauswein, Clark (2019)

Empirical relations + wavelet-based reconstruction algorithm **BayesWave**

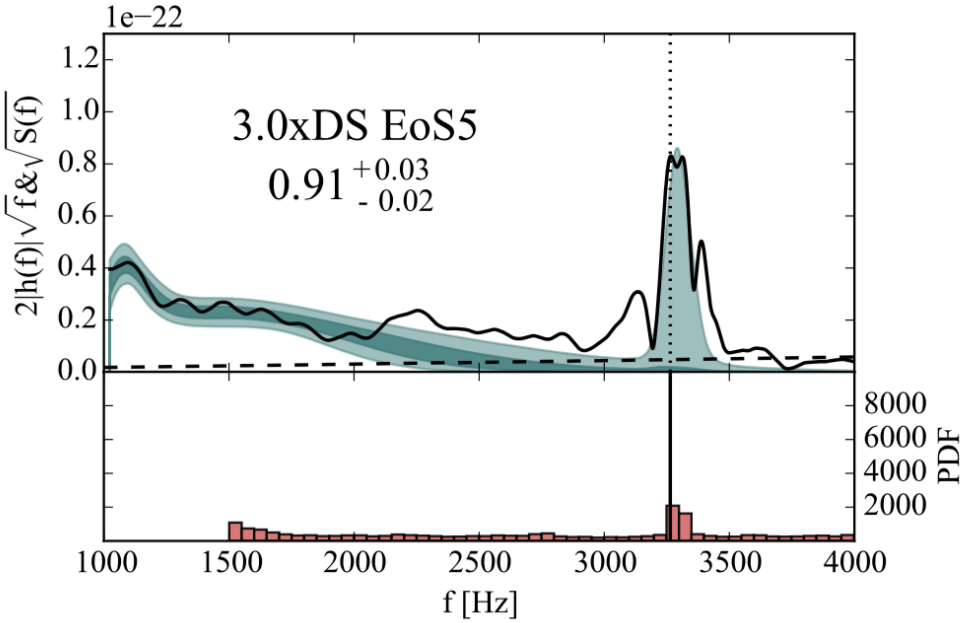

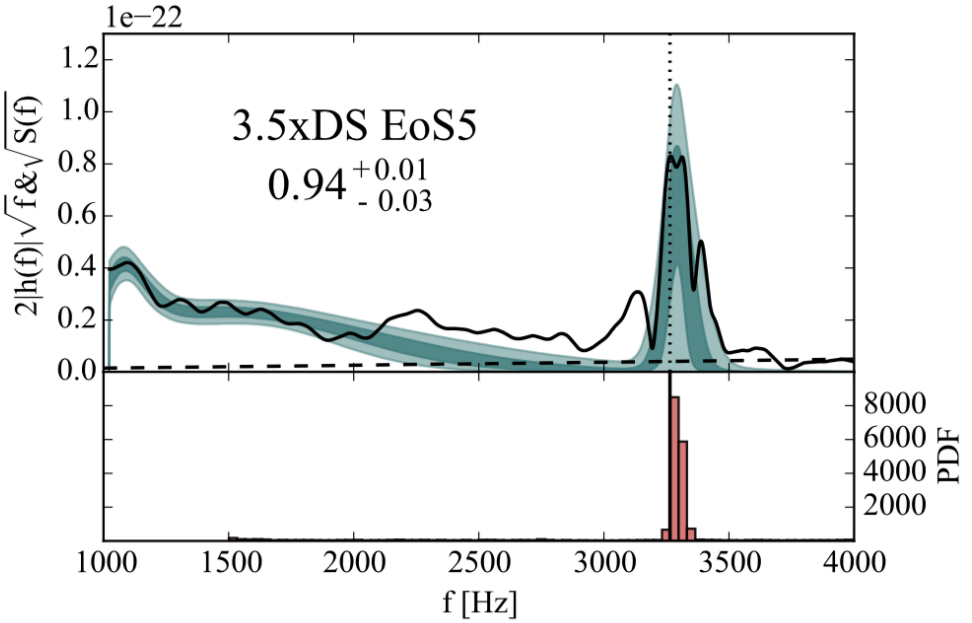

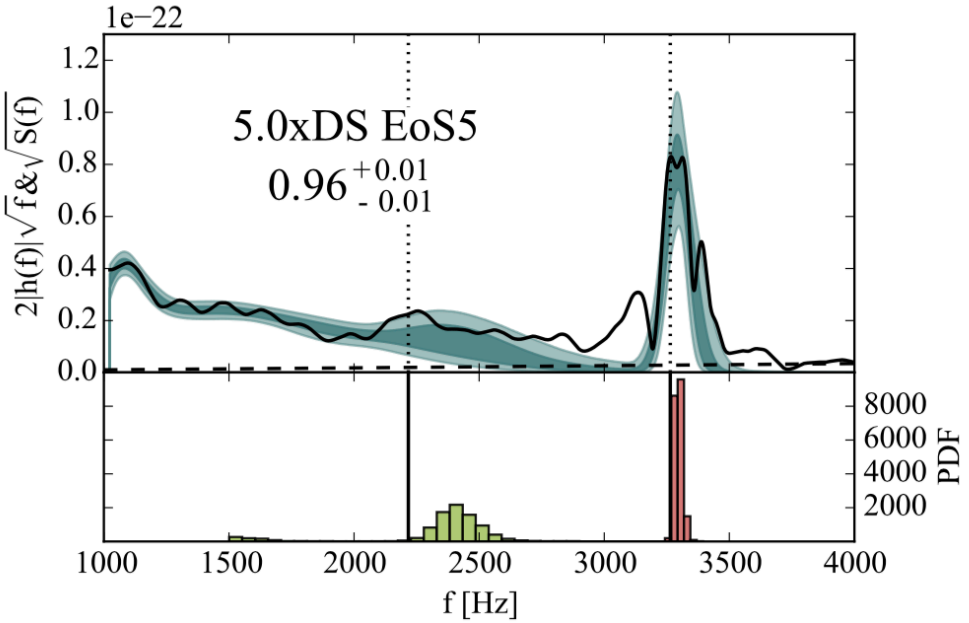

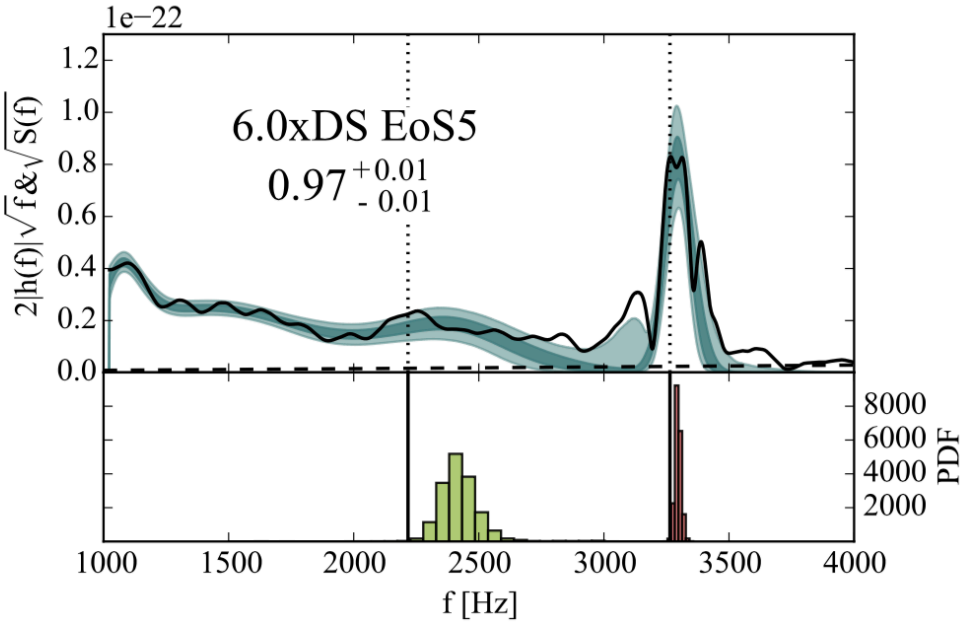

Importance of Secondary Peaks

Torres-Rivas, Chatziioannou, Bauswein, Clark (2019)

Because the detectors a more sensitive at lower frequencies, a broad secondary peak may be detected more easily than the main peak for a very soft EOS.

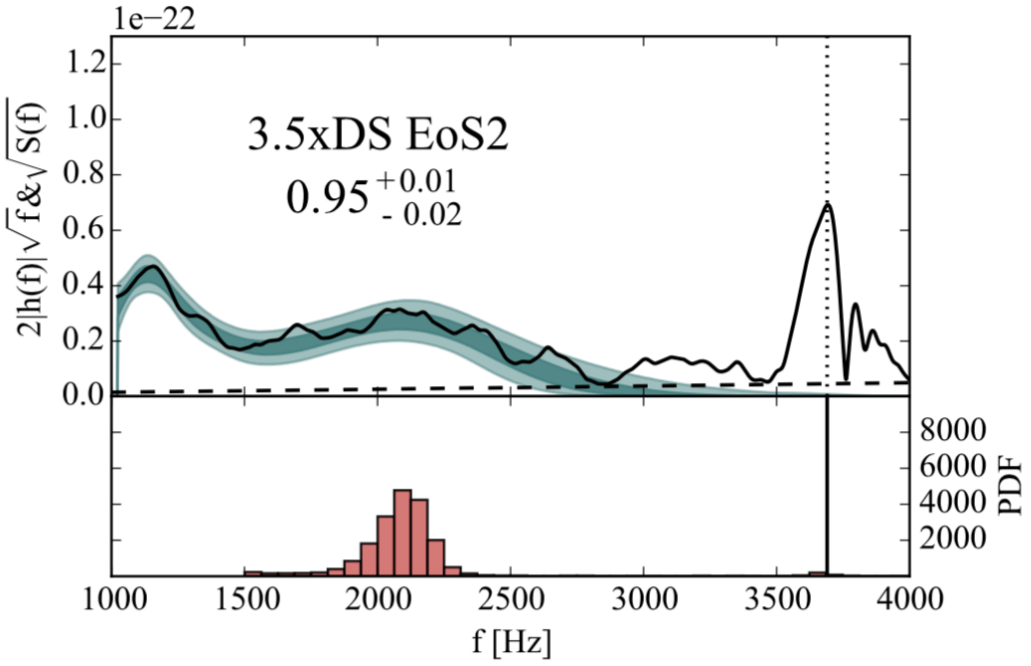

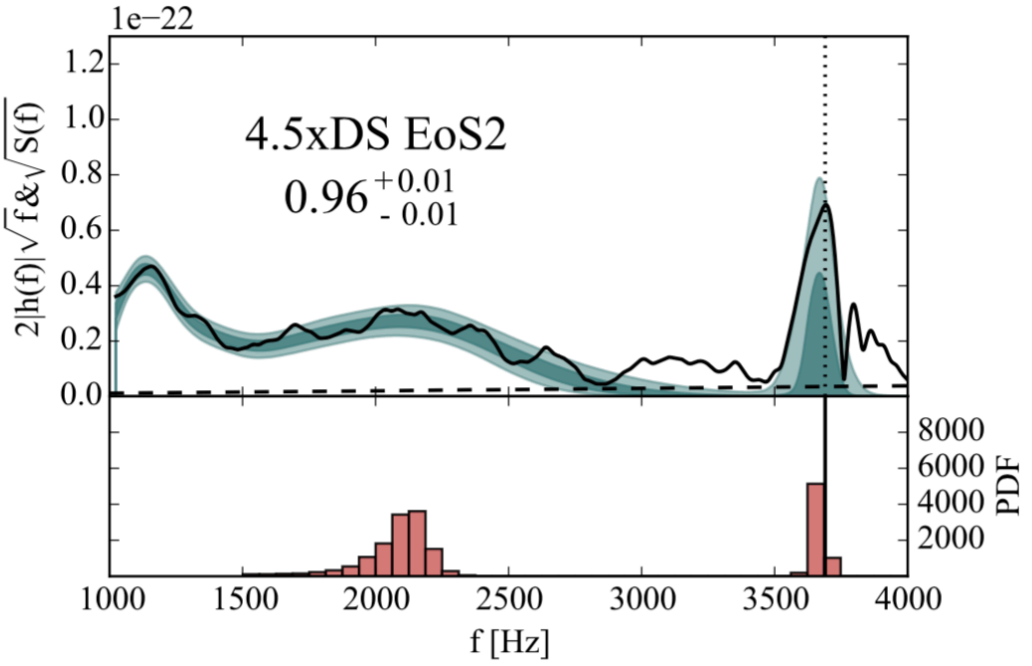

Thermal Structure of BNS Merger Remnant

Parts of the remnant reach temperatures of several tens MeV.

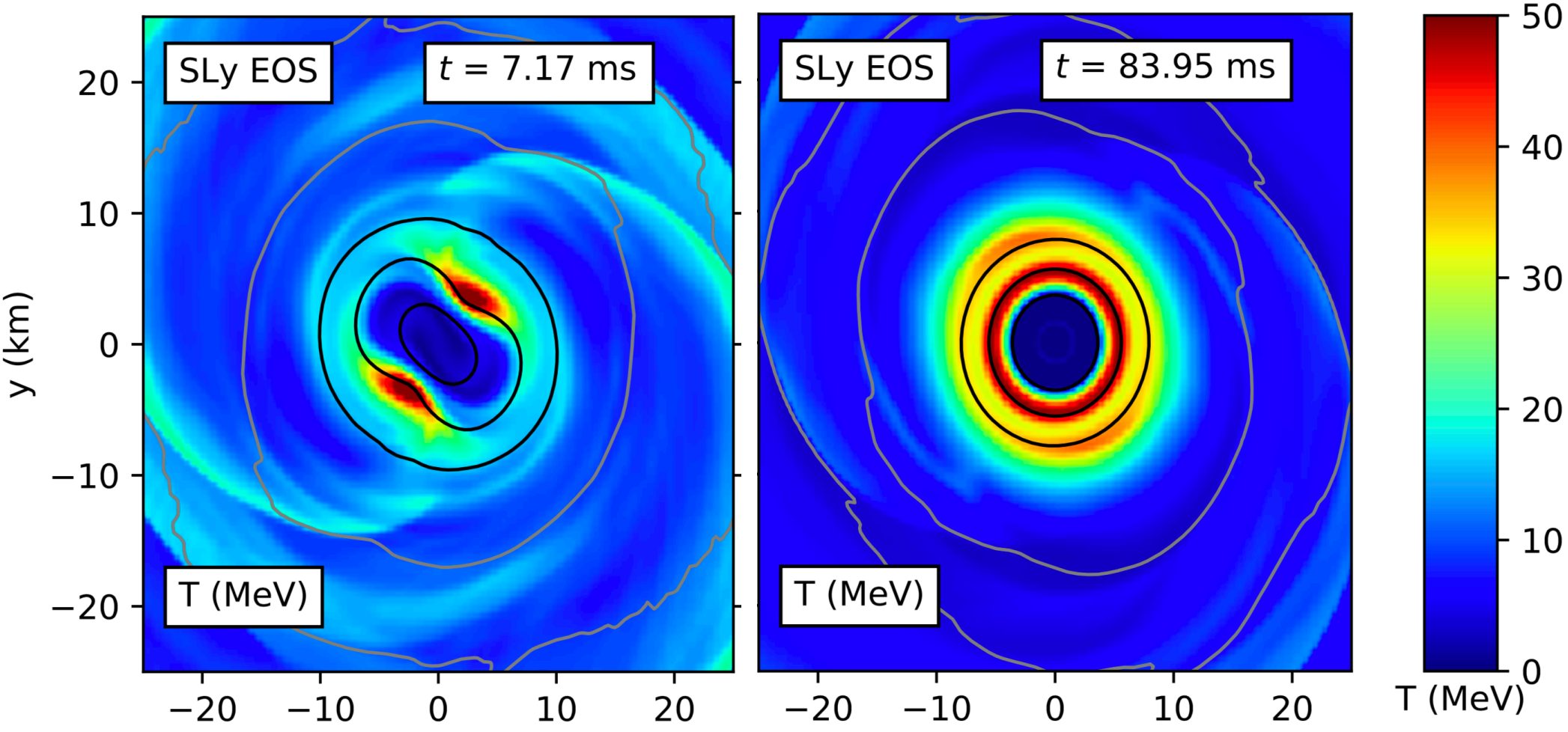

De Pietri et al. (2019)

Inertial Modes!

(Physical Review Letters, 2018)

Convective Excitation of Inertial Modes in Binary Neutron Star Mergers

Roberto De Pietri,[1,2] Alessandra Feo,[3,2] José A. Font,[4,5] Frank Löffler,[6,7] Francesco Maione,[1,2]
Michele Pasquali,[1,2] and Nikolaos Stergioulas[8]

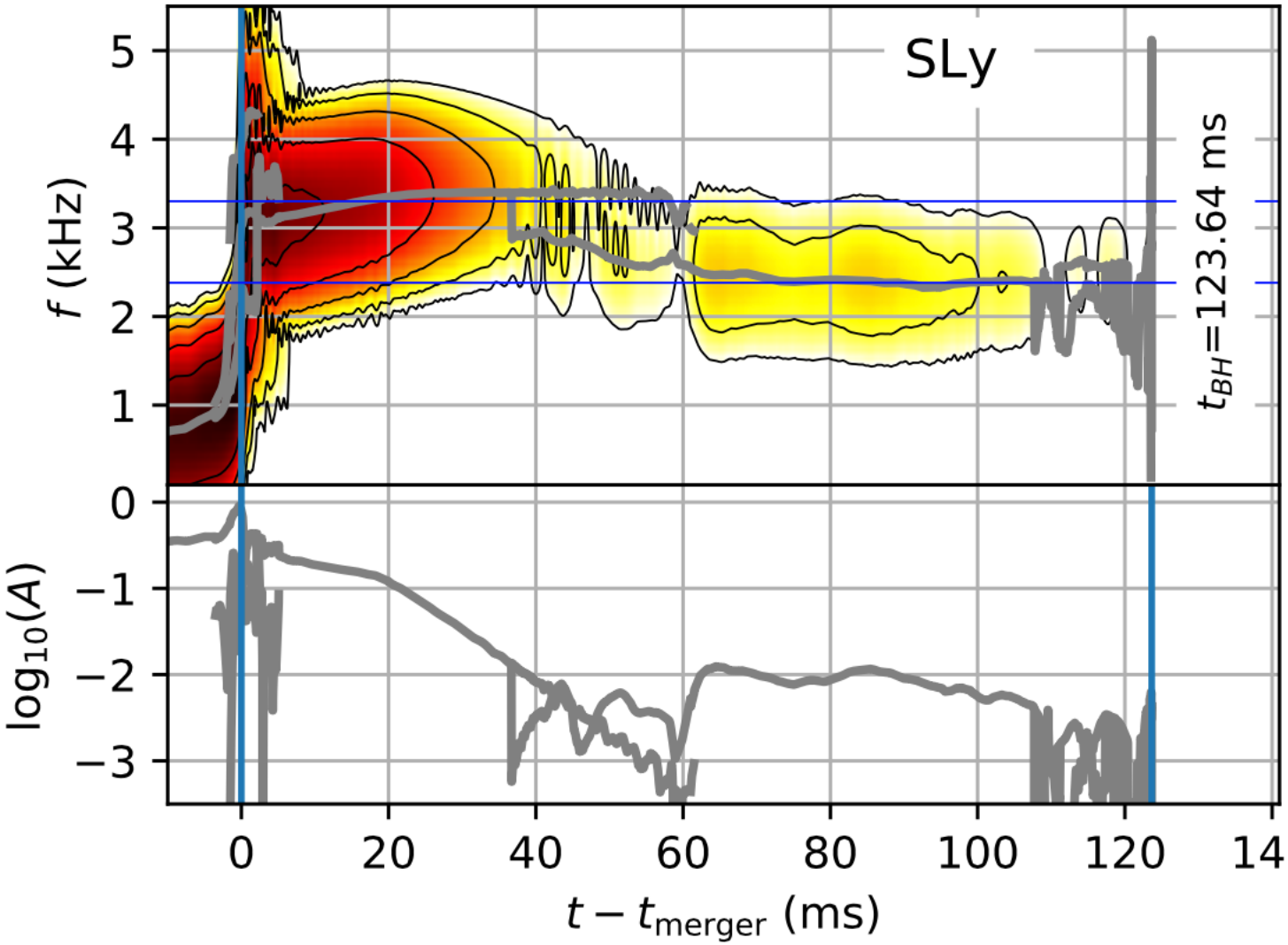

30 million core hours (PRACE)

Convective Instability

The local convective instability depends on the sign of the Schwarzschild discriminant

$$A_\alpha = \frac{1}{\varepsilon + p}\nabla_\alpha \varepsilon - \frac{1}{\Gamma_1 p}\nabla_\alpha p$$

where

$$\Gamma_1 := (\varepsilon + p)/p(dp/d\varepsilon)_s = (d\ln p/d\ln\rho)_s$$

is the adiabatic index.

$A_\alpha < 0$ convective stability

$A_\alpha > 0$ convective instability

For a piecewise-polytropic EOS with a thermal component, we find analytically:

$$\Gamma_1 = \Gamma_{\rm th} + (\Gamma_i - \Gamma_{\rm th})\frac{K_i \rho^{\Gamma_i}}{p}$$

Convective Instability

The sign of A_r in the equatorial plane:

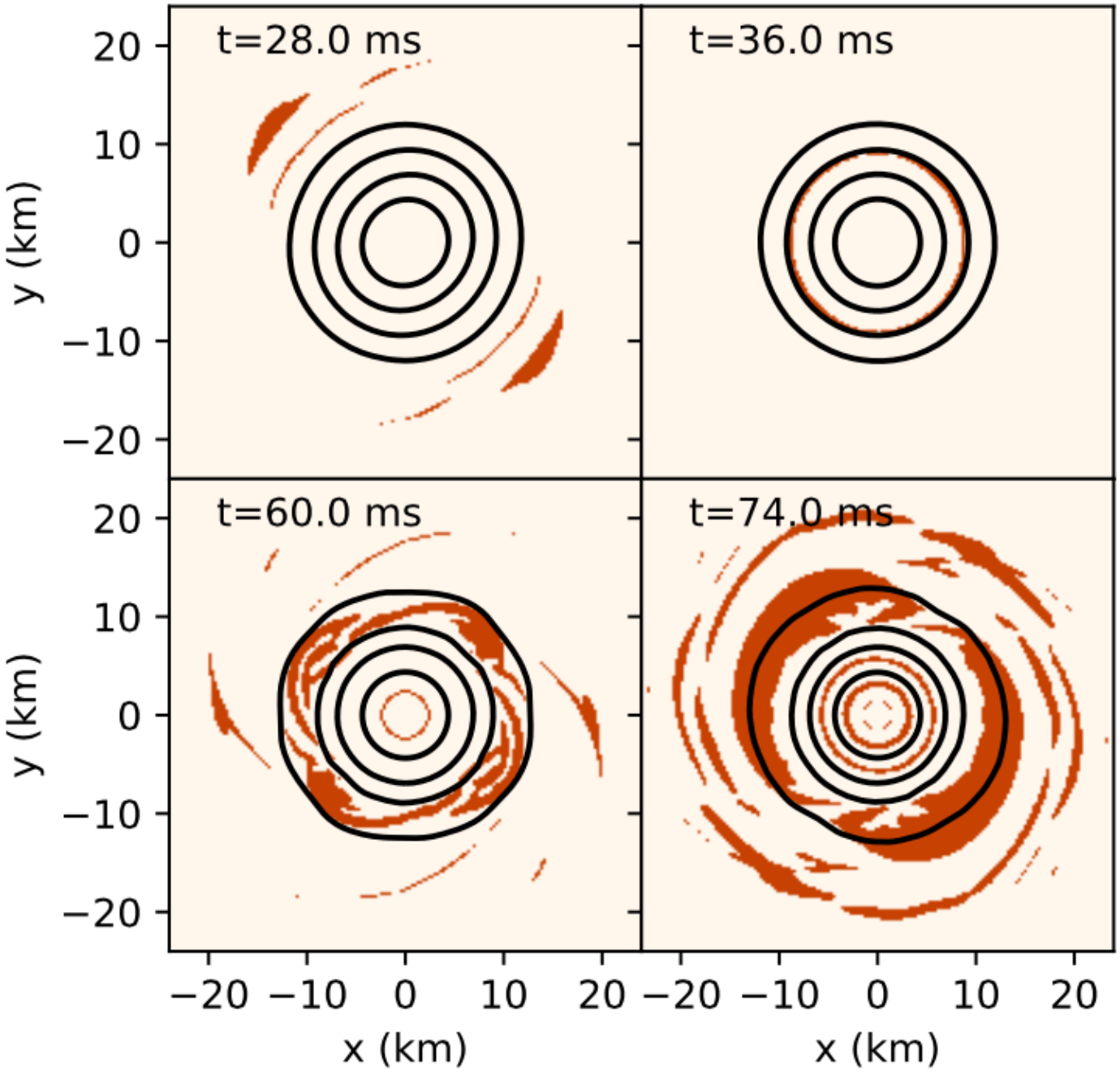

Oscillations

***f*-modes**

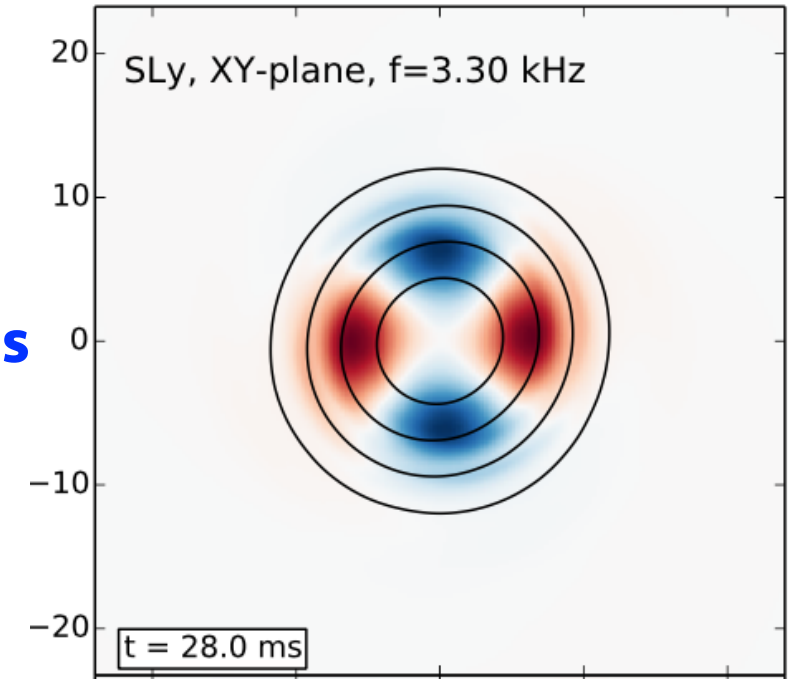

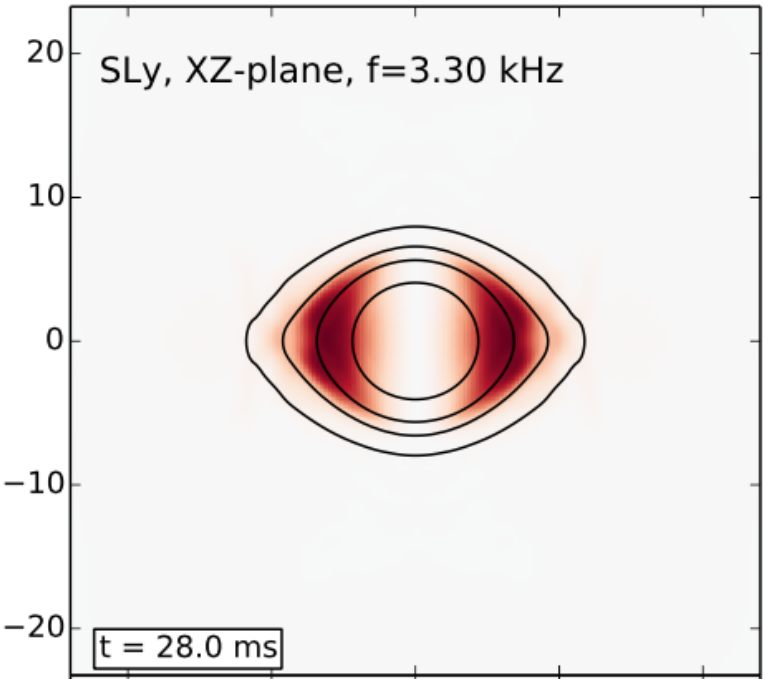

Oscillations

***f*-modes**

***inertial* modes**

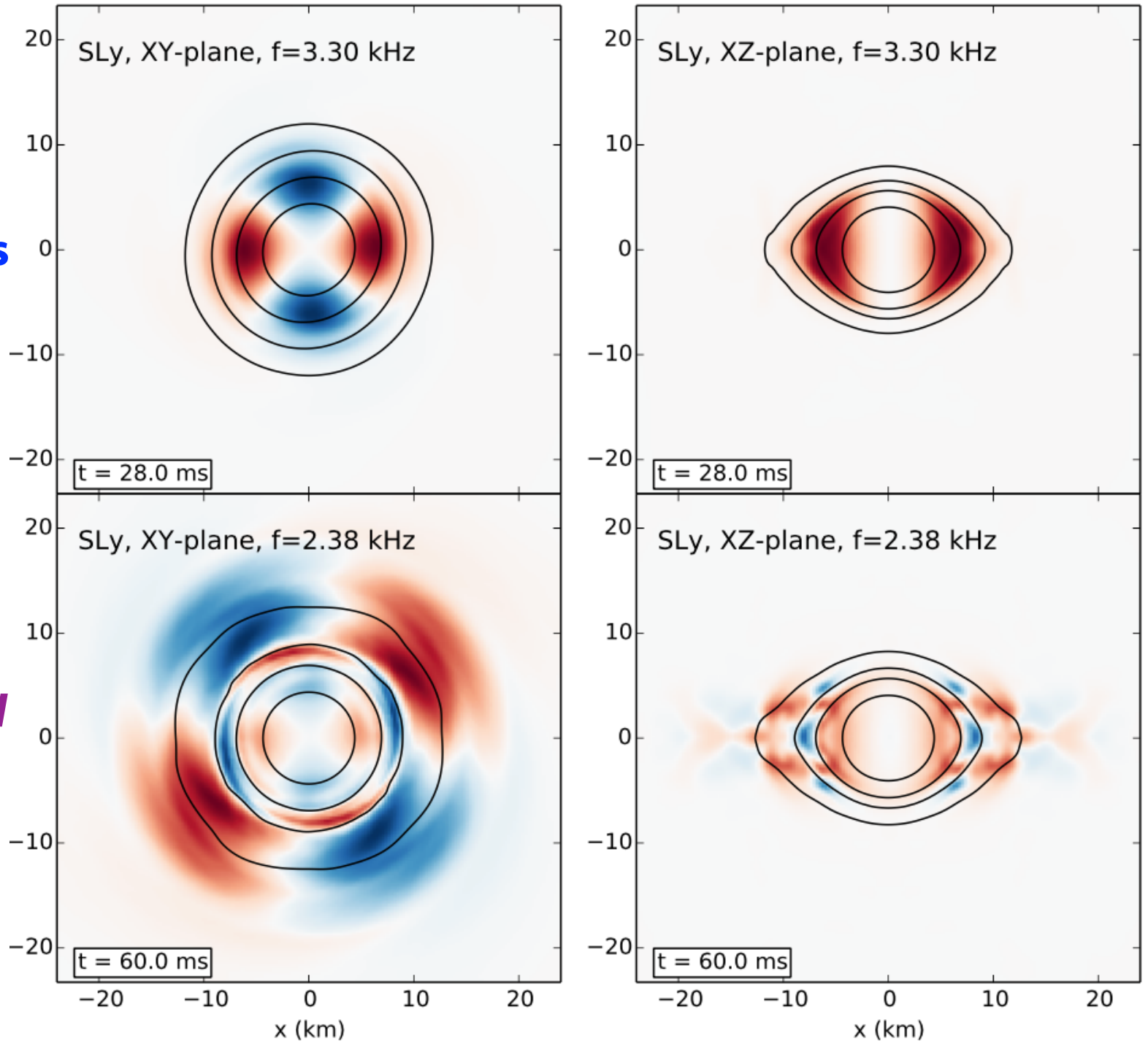

Gravitational Wave Spectrum

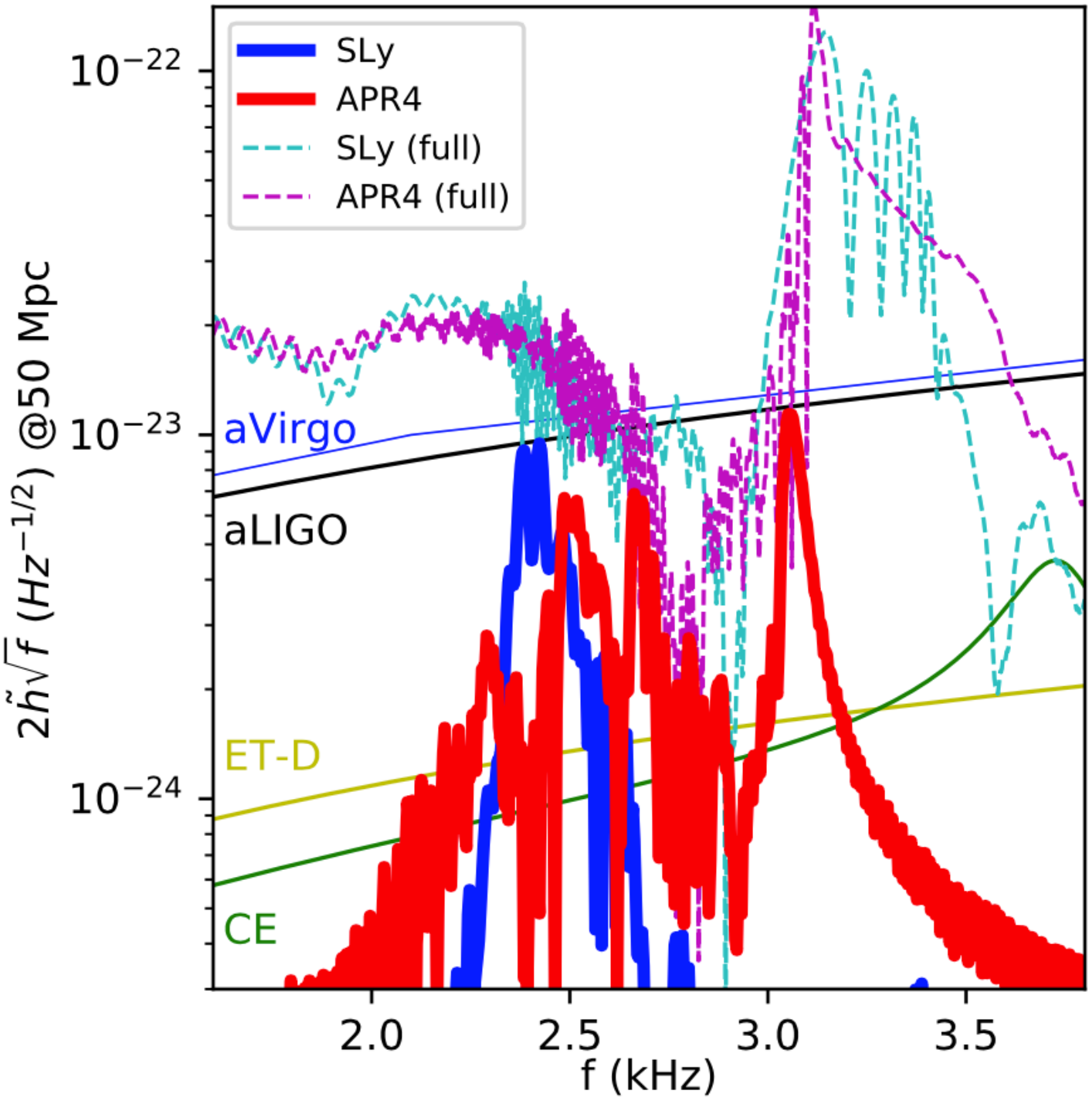

Summary

- Based on a set of minimal assumptions, we set a *strict* lower limit on neutron star radii of 10.7km at $1.6M_{sun}$.
- Gravitational-wave asteroseismology can constrain the neutron star radius to within 0.4km with future observations.
- Principal Component Analysis (PCA) sufficient to reach >90% of optimal signal.
- We discovered *convective instabilities* and *inertial modes* that can probe the thermal part of the EOS.

Supplementary material

Analytic Model with Physical Parameters

Bauswein, NS & Janka (2016)

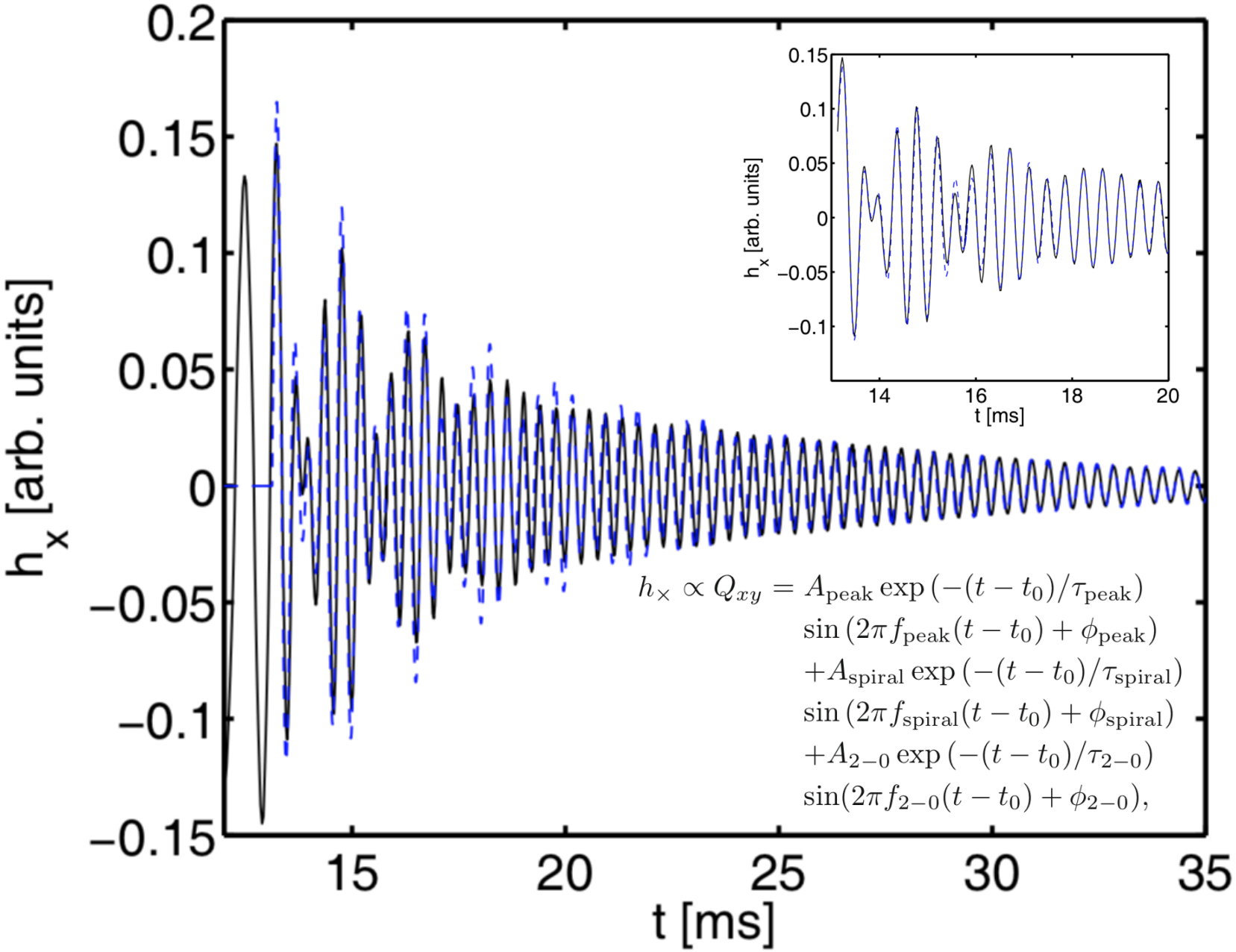

Central Lapse Evolution

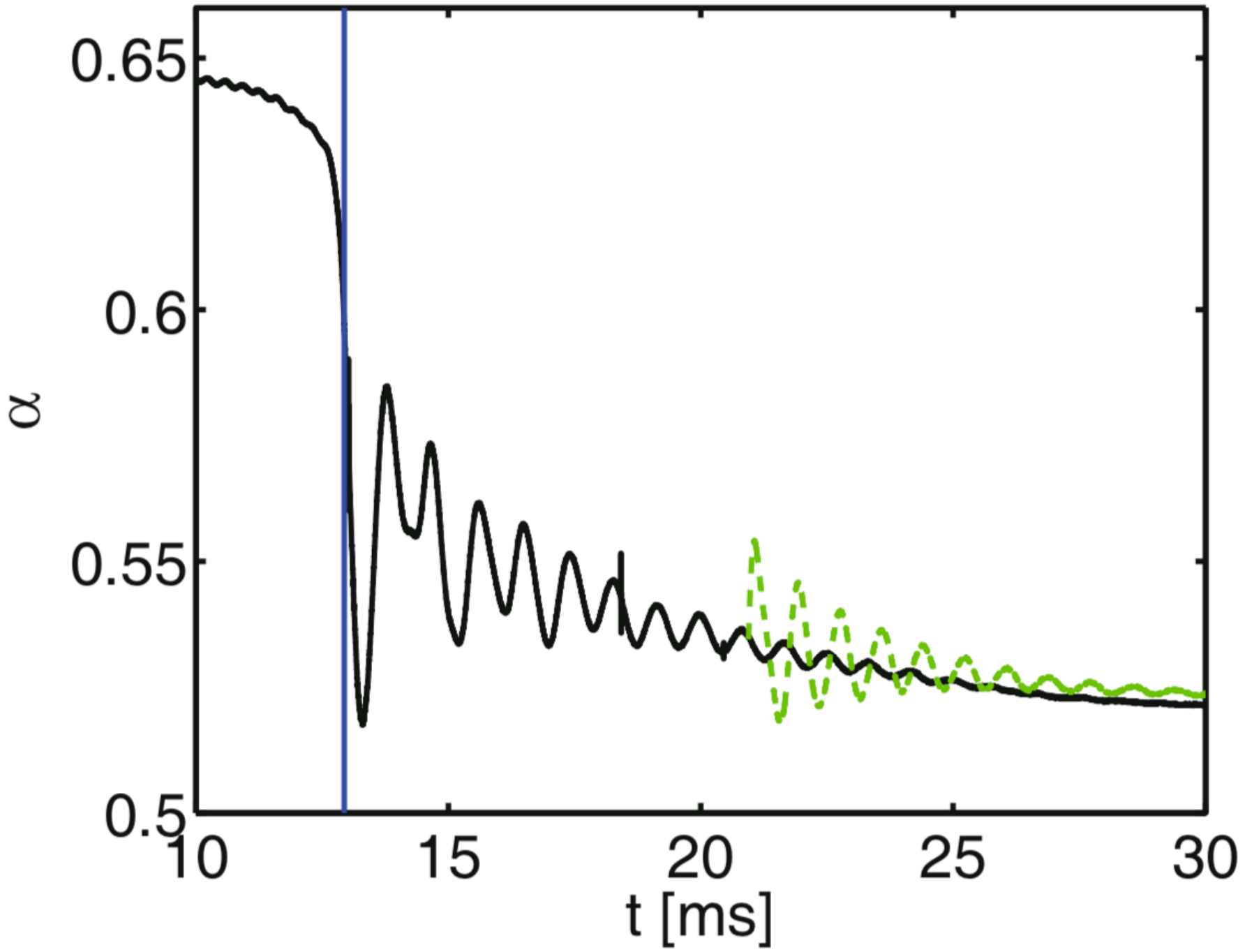

Late-time Excitation of m=2 Mode

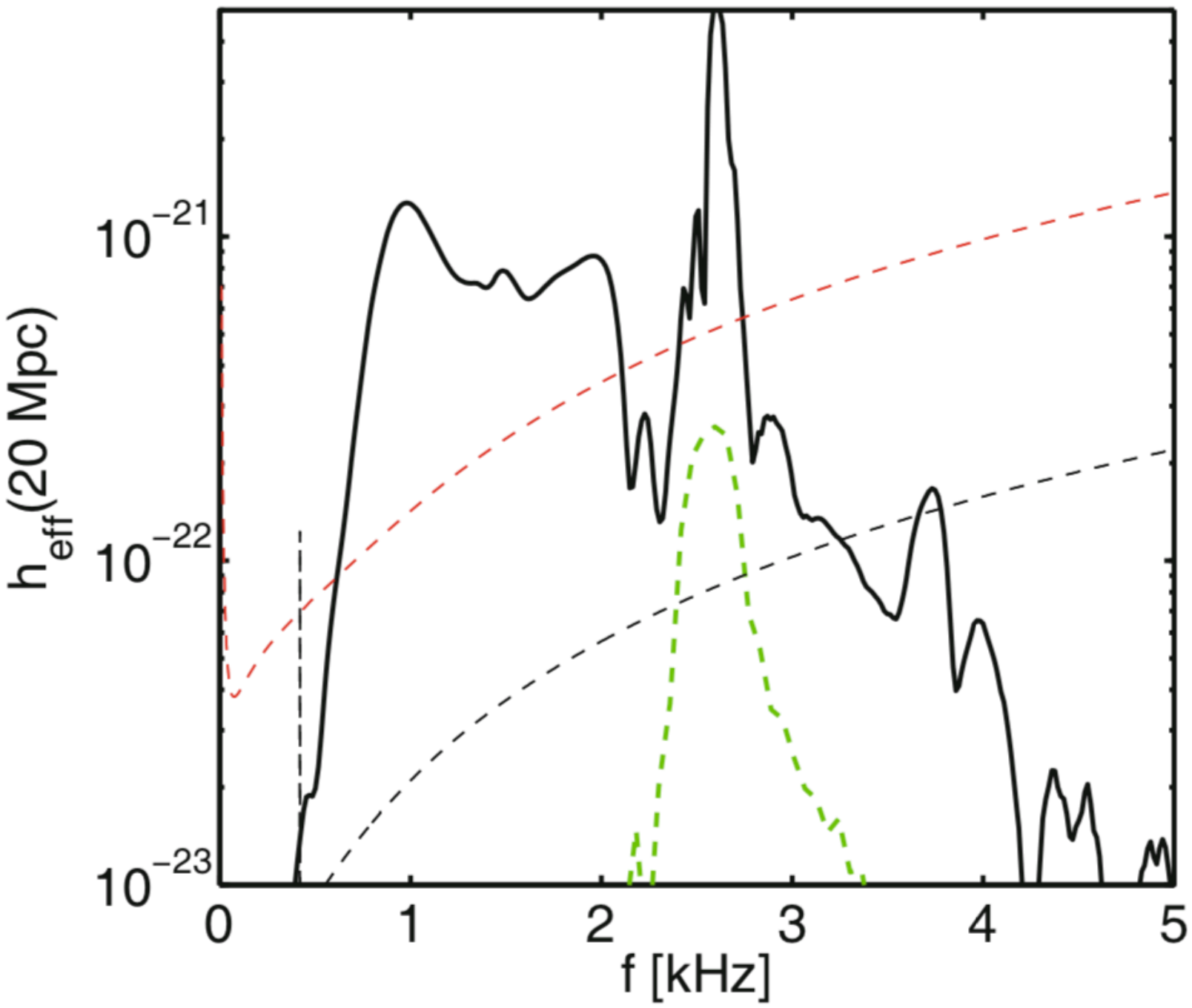

Spacetime Evolution

90´s Nakamura, Oohara, Kojima / Shibata, Nakamura / Baumgarte, Shapiro

Definitions

$$\tilde{\gamma}_{ij} = e^{-4\phi}\gamma_{ij}$$

$$e^{4\phi} = \gamma^{1/3} \equiv \det(\gamma_{ij})^{1/3}$$

$$\tilde{A}_{ij} = e^{-4\phi}A_{ij} \quad A_{ij} = K_{ij} - \frac{1}{3}\gamma_{ij}K,$$

$$\tilde{\Gamma}^i := \tilde{\gamma}^{jk}\tilde{\Gamma}^i_{jk} = -\tilde{\gamma}^{ij}{}_{,j}$$

"1+log" lapse function

$$\partial_t \alpha = -2\alpha A$$

$$\partial_t A = \partial_t K$$

"Gamma-driver" shift condition

$$\partial_t \beta^i = B^i$$

$$\partial_t B^i = \frac{3}{4}\alpha\partial_t\tilde{\Gamma}^i - e^{-4\phi}\beta^i$$

Time evolution

$$\frac{d}{dt}\tilde{\gamma}_{ij} = -2\alpha\tilde{A}_{ij}, \qquad \frac{d}{dt} = \partial_t - \mathcal{L}_\beta$$

$$\frac{d}{dt}\phi = -\frac{1}{6}\alpha K.$$

$$\frac{d}{dt}K = -\gamma^{ij}D_iD_j\alpha + \alpha\left[\tilde{A}_{ij}\tilde{A}^{ij} + \frac{1}{3}K^2 + \frac{1}{2}(\rho + S)\right],$$

$$\frac{d}{dt}\tilde{A}_{ij} = e^{-4\phi}[-D_iD_j\alpha + \alpha(R_{ij} - S_{ij})]^{TF}$$

$$+ \alpha(K\tilde{A}_{ij} - 2\tilde{A}_{il}\tilde{A}^l_j),$$

$$\frac{\partial}{\partial t}\tilde{\Gamma}^i = -2\tilde{A}^{ij}\alpha_{,j} + 2\alpha\left(\tilde{\Gamma}^i_{jk}\tilde{A}^{kj} - \frac{2}{3}\tilde{\gamma}^{ij}K_{,j} - \tilde{\gamma}^{ij}S_j + 6\tilde{A}^{ij}\phi_{,j}\right)$$

$$- \frac{\partial}{\partial x^j}\left(\beta^l\tilde{\gamma}^{ij}{}_{,l} - 2\tilde{\gamma}^{m(j}\beta^{i)}_{,m} + \frac{2}{3}\tilde{\gamma}^{ij}\beta^l_{,l}\right).$$

Radius Determination from Post-Merger Signal

Bauswein, Janka, Hebeler & Schwenk (2012)

f_{peak} correlates very well with the radius @ 1.6 Msun (M_{tot} is known from inspiral).

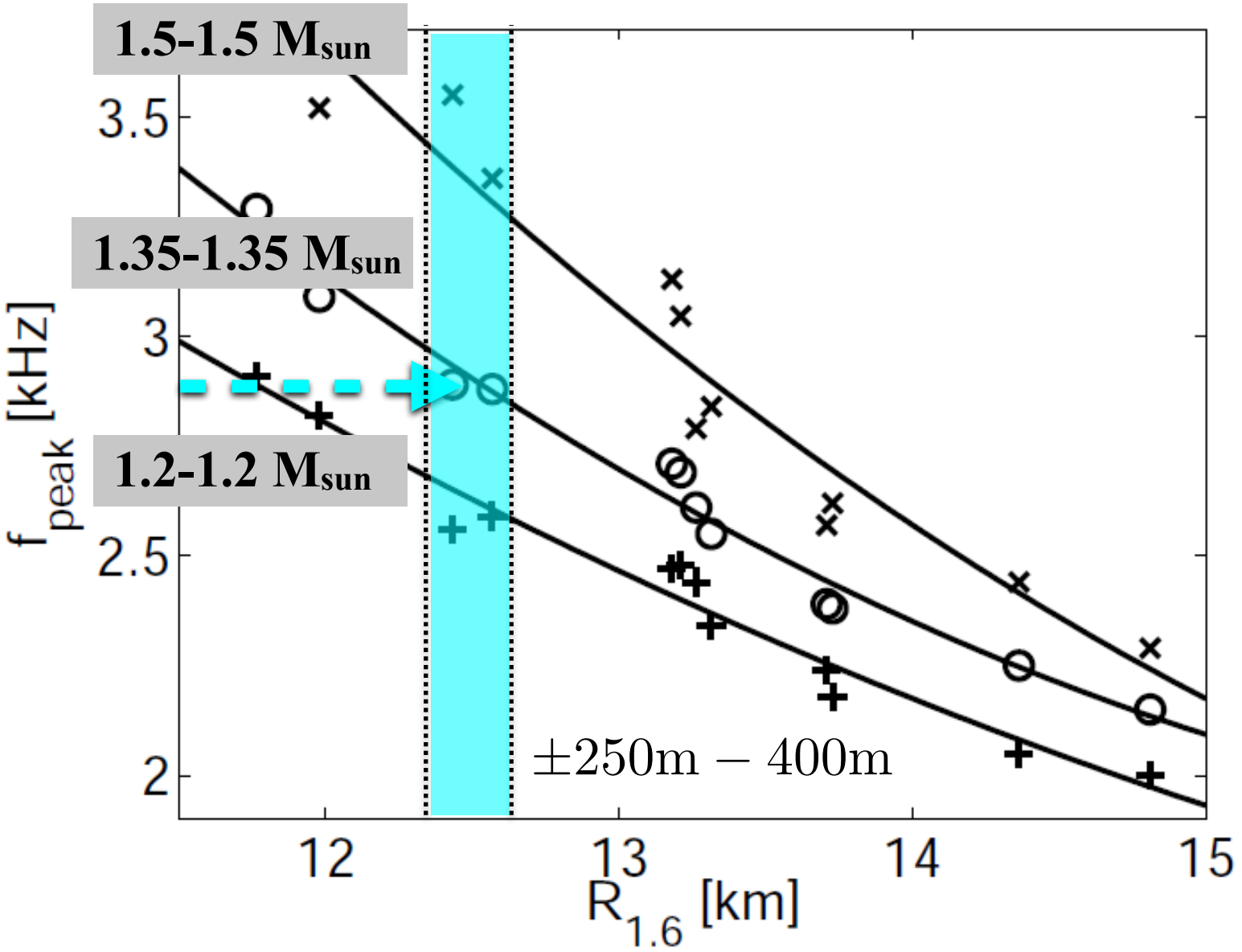

Tidal Deformability

Tidal deformation of NS in the field of a companion:

$$Q_{ij} = -\lambda \mathcal{E}_{ij}$$

Induced quadrupole deformation

Proportionality constant

External tidal field

Dimensionless tidal deformability

$$\Lambda \equiv \frac{\lambda}{M^5} = \frac{2}{3}\kappa_2 \left(\frac{R}{M}\right)^5$$

Quadrupole Love number

Calculating the Tidal Deformability

Assume a spherically symmetric, static background spacetime

$$ds_0^2 = -e^{\nu(r)}dt^2 + e^{\gamma(r)}dr^2 + r^2\left(d\theta^2 + \sin^2\theta d\varphi^2\right)$$

Then

$$\begin{aligned}\Lambda =& \frac{16}{15}(1-2C)^2[2+2C(y(R)-1)-y(R)] \\ & \{2C[6-3y(R)+3C(5y(R)-8)] \\ & +4C^3\left[13-11y(R)+C(3y(R)-2)+2C^2(1+y(R))\right] \\ & +3(1-2C)^2[2-y(R)+2C(y(R)-1)]\ln(1-2C)\}^{-1}\end{aligned}$$

where

$$C \equiv M/R$$

and

$$\frac{dy}{dr} = \frac{4\left(m+4\pi r^3 p\right)^2}{r(r-2m)^2} + \frac{6}{r-2m} - \frac{y^2}{r} - \frac{r+4\pi r^3(p-\rho)}{r(r-2m)}y - \frac{4\pi r^2}{r-2m}\left\{5\rho+9p+\frac{\rho+p}{(dp/d\rho)}\right\}$$

Empirical Relation for Λ @ Specific Mass

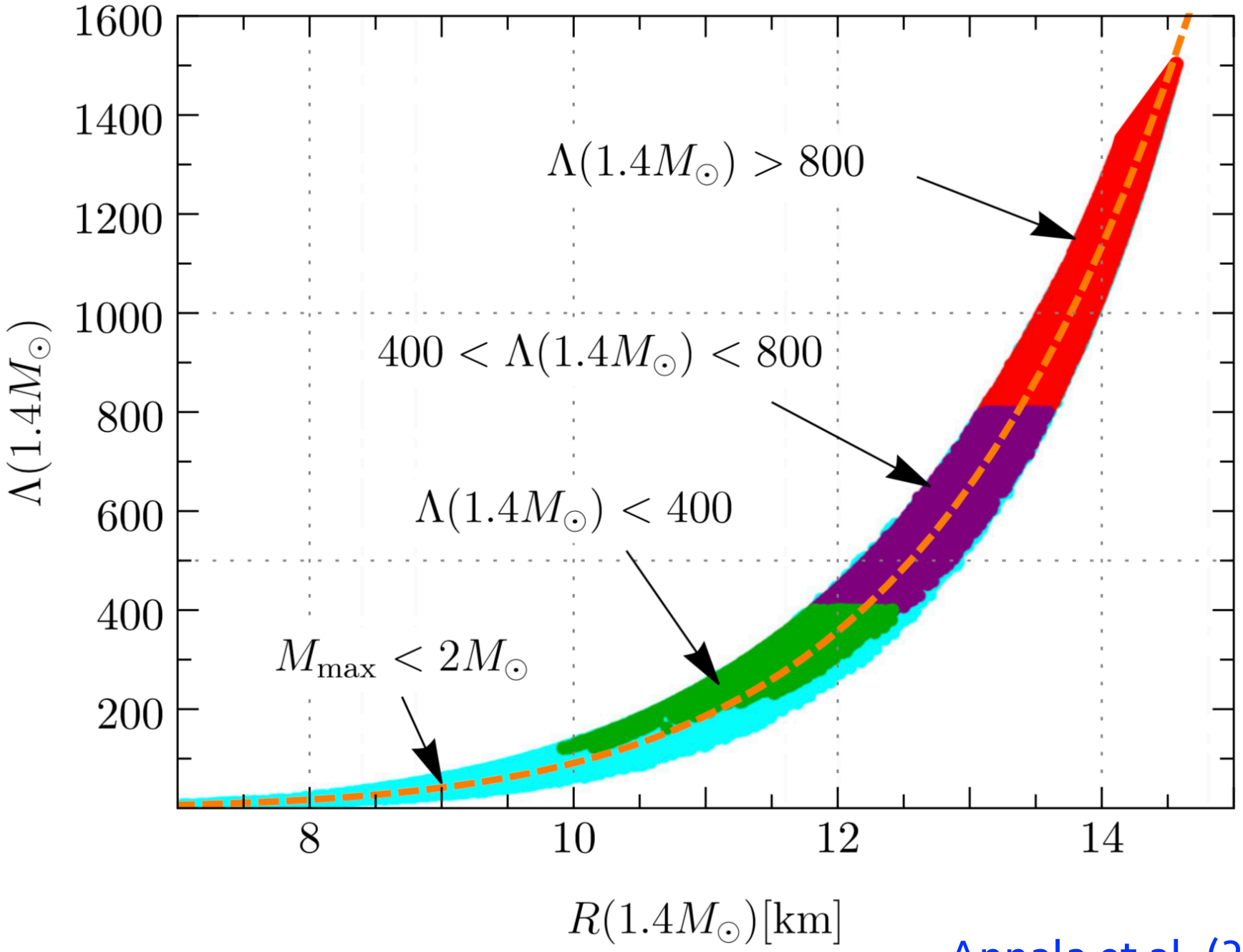

Annala et al. (2018)

EOS Constraints

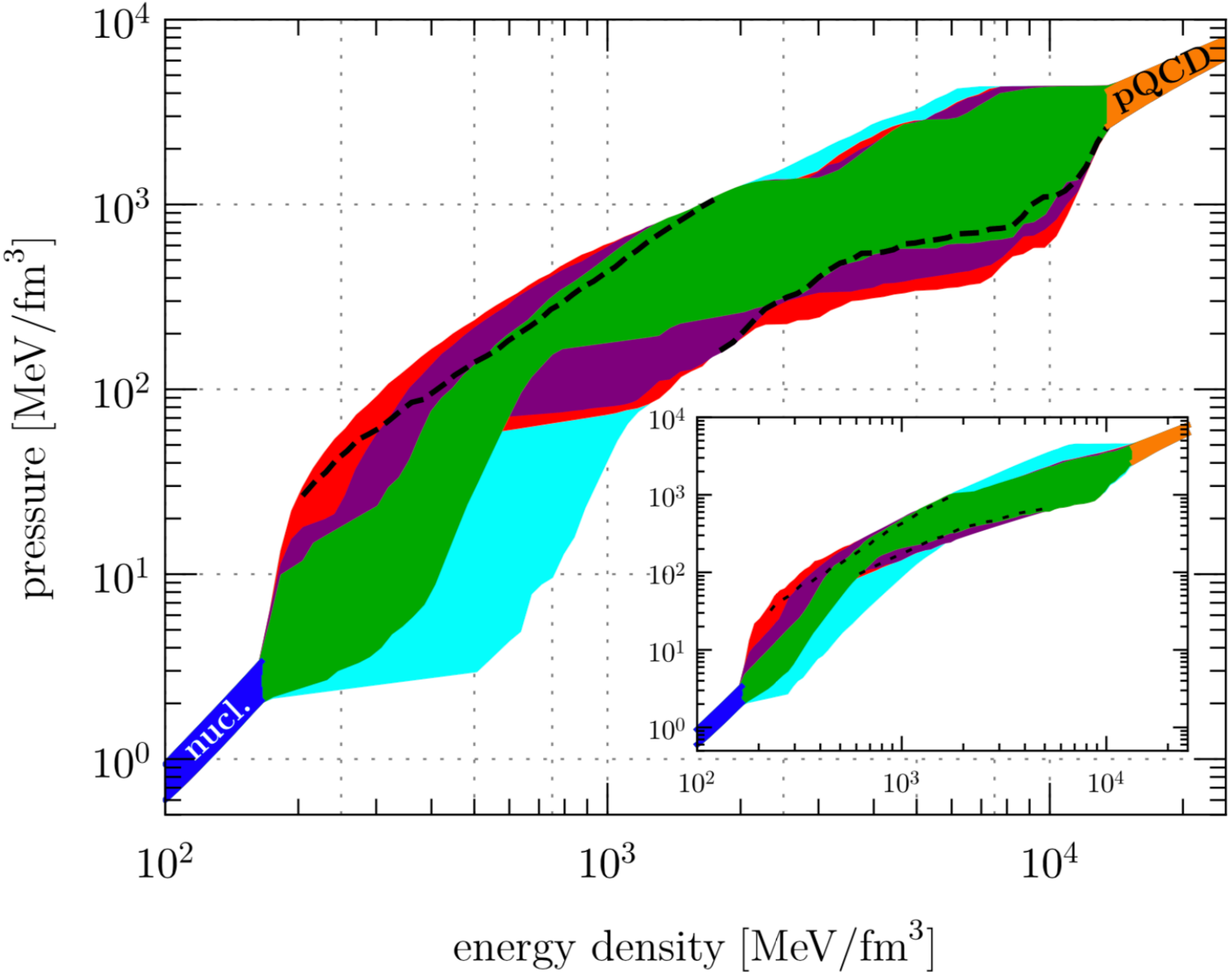

Annala et al. (2018)

Radius uncertainties before GW170817

Bauswein, Janka, Hebeler & Schwenk (2012)

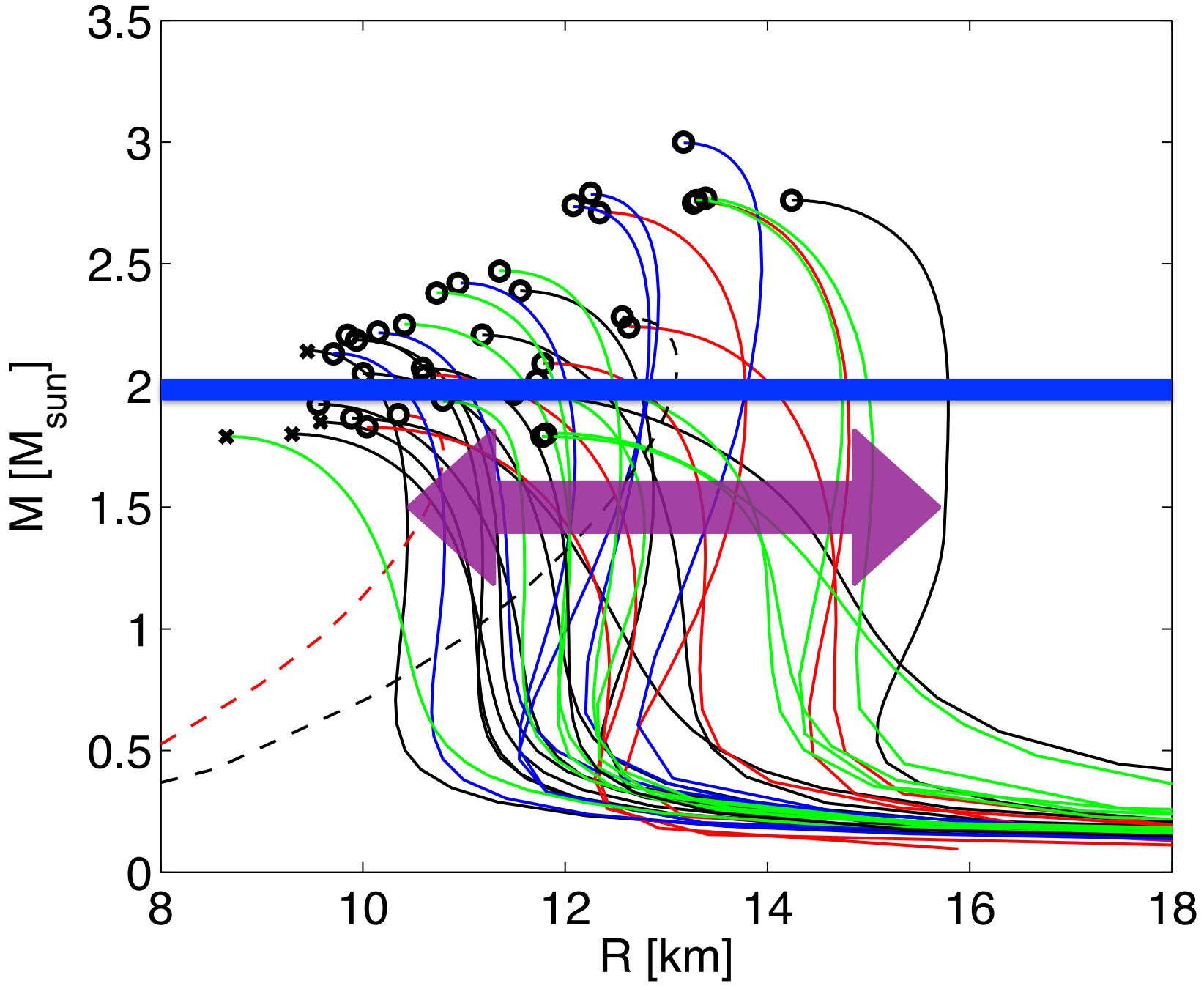

PCA Reconstruction of signal

Clark, Bauswein, NS, Shoemaker (2016)

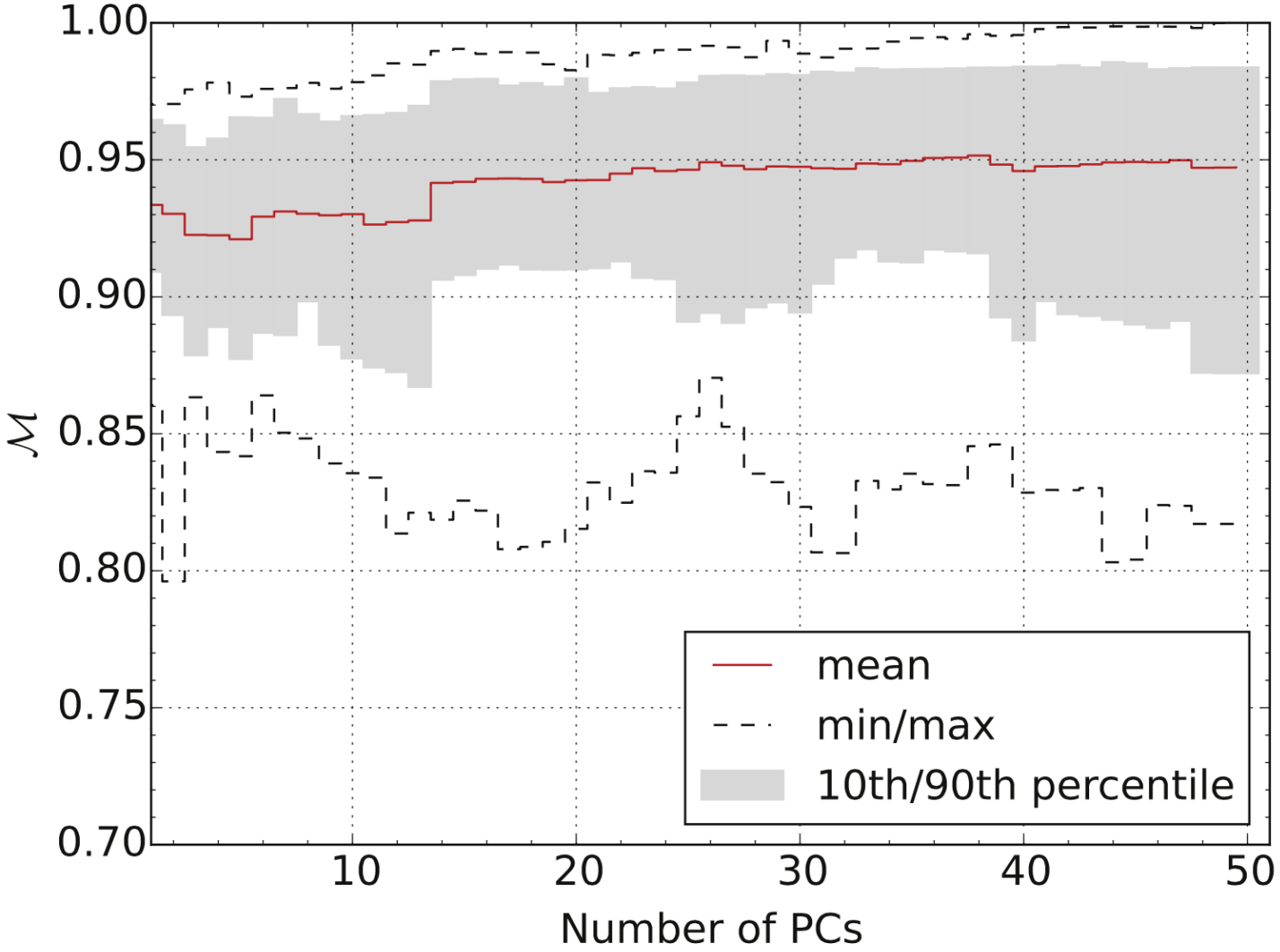

Our PCA template extracts >90% of input signal. Even with mean+1 PC, it is >80% (compared to 40% for a burst analysis).